UNIVERSITEIT VAN PRETORIA
UNIVERSITY OF PRETORIA
YUNIBESITHI YA PRETORIA

Jost-matrix analysis of nuclear scattering data

by

Paul Vaandrager

Submitted in partial fulfilment of the requirements for the degree

Philosophiae Doctor

Department of Physics
Faculty of Natural and Agricultural Sciences
University of Pretoria
Pretoria

August 2020

Abstract

Jost-matrix analysis of nuclear scattering data

by

Paul Vaandrager

Supervisor: Professor S.A. Rakitianski

Degree: *Philosophiae Doctor* (Physics)

The analysis of scattering data is usually done by fitting the S-matrix at real experimental energies. An analytic continuation to complex and negative energies must then be performed to locate possible resonances and bound states, which correspond to poles of the S-matrix. Difficulties in the analytic continuation arise since the S-matrix is energy dependent via the momentum, k and the Sommerfeld parameter, η, which makes it multi-valued. In order to circumvent these difficulties, in this work, the S-matrix is written in a semi-analytic form in terms of the Jost matrices, which can be given as a product of known functions dependent on k and η, and unknown functions that are entire and singled-valued in energy. The unknown functions are approximated by truncated Taylor series where the expansion coefficients serve as the data-fitting parameters. The proper analytic structure of the S-matrix is thus maintained. This method is successfully tested with data generated by a model scattering potential. It is then applied to α^{12}C scattering, where resonances of ^{16}O in the quantum states $J^\pi = 0^+$, 1^-, 2^+, 3^-, and 4^+ are located. The parameters of these resonances are accurately determined, as well as the corresponding S-matrix residues and Asymptotic Normalisation Coefficients, relevant to astrophysics. The method is also applied to $d\alpha$ scattering to determine the bound and resonance state parameters, corresponding S-matrix residues and Asymptotic Normalisation Coefficients of ^{6}Li in the 1^+, 2^+, 3^+, 2^-, and 3^- states.

Samevatting

Jost-matriks analise van atoomkern-botsingsdata

deur

Paul Vaandrager

Studieleier:	Professor S.A. Rakitianski
Graad:	*Philosophiae Doctor* (Fisika)

Die analise van botsingsdata vereis gewoonlik die passing van die S-matriks by reële eksperimentiële energiewaardes. Om moontlike resonansies en gebonde toestande te bepaal moet die analitiese voortsetting van die S-matriks dan na komplekse en negatiewe energiewaardes uitgevoer word. Hierdie resonansies en gebonde toestande stem ooreen met die pole van die S-matriks. Aangesien die S-matriks via die momentum, k, en die Sommerfeld parameter, η, afhanklik is van die energie, is dit meerwaardig in energie. Probleme in die analitiese voortsetting kan dus ontstaan. Om hierdie probleme te omseil, word die S-matriks in die huidige werk in 'n semi-analitiese vorm in terme van die Jost matrikse geskryf. Die Jost matrikse kan as die produkte van bekende funksies afhanklik van k en η, en onbekende, eenduidige, eenwaardige funksies van energie gegee word. Die onbekende funksies word benader deur eindige terme van Taylor reekse. Die uitbreidingskoëffisiënte van hierdie reekse dien as die passingsparameters. Die korrekte analitiese struktuur van die S-matriks bly dus behoue. Hierdie passingsmetode word suksesvol getoets met data wat deur 'n modelpotensiaal gegenereer is. Dit word dan op α^{12}C botsingsdata toegepas en resonansies van ^{16}O in die $J^{\pi} = 0^{+}$, 1^{-}, 2^{+}, 3^{-}, en 4^{+} kwantum-toestande word bepaal. Die parameters van die resonansies word akkuraat bereken, asook die ooreenstemmende S-matriksresidu waardes en Asimptotiese Normalisasiekoëffisiënte, relevant tot astrofisika. Die metode word ook op $d\alpha$ botsingsdata toegepas om die parameters van die gebonde toestand en resonansies, ooreenstemmende S-matriksresidu waardes en Asimptotiese Normalisasiekoëffisiënte vir ^{6}Li in die 1^{+}, 2^{+}, 3^{+}, 2^{-}, en 3^{-} toestande te bepaal.

UNIVERSITEIT VAN PRETORIA
UNIVERSITY OF PRETORIA
YUNIBESITHI YA PRETORIA

Declaration

I, Paul Vaandrager, declare that this thesis, which I hereby submit in partial fulfilment of the requirements for the degree *Philosophiae Doctor* at the University of Pretoria, was written by me, that the work contained herein is my own except where explicitly stated otherwise in the text and that this work has not been submitted for any other degree at this or any other tertiary institution.

Signature:	.....
	Paul Vaandrager
Student number:	27155375
Date:	6th August 2020

Acknowledgements

I wish to extend my sincere gratitude to the following people for their massive contribution to this thesis:

- My supervisor, Professor S.A. Rakitianski, for his guidance and continued patience in the many years we have worked together.
- My family and friends for their encouragement, positive attitude and faith in my abilities.
- The staff and students of the Department of Physics of the University of Pretoria, for creating a constructive and pleasant work environment.
- My father, Maarten Vaandrager, for his encouragement in pursuing my dreams as well as the years of financial support.

Financial Support

Financial support provided by the National Research Foundation (NRF)[1] in respect of the costs of the study is hereby acknowledged.

[1]Disclaimer: Any opinion, findings and conclusions or recommendations in this material are those of the author(s) and therefore the NRF do not accept any liability in regard thereto.

Dedications

I dedicate this thesis to the memory of my mother, Leonie Vaandrager, who taught me to approach any problem with logic, enthusiasm and perseverance.

"In the realm of ideas everything depends on enthusiasm...

in the real world all rests on perseverance."

- Johann Wolfgang von Goethe

Contents

Chapter 1

Introduction

Nuclear and atomic systems can be studied by extracting scattering parameters from fitting experimental data. In such studies the scattering matrix, or S-matrix, is used in the form of a phenomenological function depending on some free parameters. These parameters are adjusted to fit the measured scattering cross-sections or phase-shifts. When the S-matrix is found from the fitting, it is used to determine bound and resonance state parameters.

Historically, one of the most widely-used methods of analysing scattering data to determine resonance parameters in particular, is the Breit-Wigner parameterisation, introduced in Ref. [1] in 1936. Resonance energies are complex, given by $E_r - i\Gamma/2$, where E_r is the collision energy at which this state can be excited and Γ is the total resonance width, related to the lifetime of the decaying resonance state. For a multi-channel system, the total width is the sum of the partial channel widths, $\Gamma = \Gamma_1 + \Gamma_2 + \cdots$. The relative probability of decaying into the n^{th} channel is given by Γ_n/Γ.

Within the Breit-Wigner method, the scattering cross-section is approximated in terms of the resonance parameters themselves; E_r, Γ, Γ_1, Γ_2 and so forth. These parameters are treated as the fitting parameters and are the varied quantities in the fitting procedure. Variations of this method are still in use [2, 3]. It is also the prime example of a group of methods where the resonance parameters are the fitting parameters. In general, the methods of this group use some parametric expression for the

S-matrix, scattering amplitude or directly for the cross-section, where the resonance singularities (or the zigzags of the cross-section) are embedded into the parametric expression by hand [4]. The methods of this group only differ in the method of parameterisation and in the approximations made in the derivation of the parametric expression. A limitation of these methods is the requirement that the number of resonances are fixed in the fitting from the outset. It is also particularly difficult to determine the parameters of wide, short-lived resonances. Furthermore, by the nature of the fitting parameters, it is also impossible to directly determine bound state energies from such fittings.

In a second distinct group of fitting methods, bound and resonance state parameters are determined by finding the poles of the *S*-matrix in an appropriate domain of the Riemann surface of energy. Bound states correspond to negative energy poles on the physical sheet of the Riemann surface of energy and resonances correspond to *S*-matrix poles at complex energies, $\mathcal{E}_i = E_r - i\Gamma/2$, on the unphysical sheet of the energy Riemann surface.

For the methods in this second group, the *S*-matrix is written in a more general form in terms of adjustable parameters that do not necessarily coincide with bound or resonance state parameters. The number of bound or resonance states is furthermore unknown, if any exist at all. Such methods then allow unknown, difficult-to-find states to be located. After fitting the data at real, experimental scattering energies to construct the *S*-matrix, it is analytically continued onto the appropriate Riemann sheet where its poles are located to determine bound and resonance state parameters. The Padé approximation of the *S*-matrix (see Ref. [2], for example) and the Laurent-Pietarinen series expansion of the scattering amplitude (see Ref. [5]) are typical examples of such methods [4]. The method used in this thesis, where the *S*-matrix is written in terms of a semi-analytic expression for the Jost matrix, also belongs to this second group.

The main idea of the proposed method of analysis was inspired by the effective-range expansion fitting method [4, 6]. The effective-range expansion fitting method also falls within the second group of fitting methods and is widely used in nuclear

and atomic physics, often in conjunction with methods like the Padé approximation. The effective-range parameters are an extension of scattering parameters from Classical Physics, which explains the historic significance of effective range methods. With these methods, a certain function of the scattering phase-shift is expanded in the power series of the collision energy. The power-series expansion coefficients are used as the adjustable parameters to fit experimental data. The traditional effective-range parameterisation is limited to low energies and is furthermore difficult to apply to multi-channel processes. Technically the scattering phase-shift is also only defined for real, positive energies, which causes complications in the analytic continuation to locate bound and resonance states. Further complications also arise when considering the scattering of charged particles.

As will be shown, these complications and limitations are all addressed by considering a more fundamental scattering quantity: the Jost matrix. While all texts on scattering theory mention the Jost matrix, or Jost function for single-channel scattering (see [3], for example), it is usually not considered useful in practical calculations. However, there is a convenient relationship between the Jost matrix and bound and resonance states, as will be shown. The S-matrix can furthermore be defined as the "ration" of the Jost matrices. If the Jost matrices can be determined from fitting experimental data by using a suitable expansion, the corresponding expansion of the S-matrix can be derived. This allows the phase-shift, scattering cross-section or any other quantity of importance for any number of channels, as well as bound and resonance state parameters, to be determined.

However, the Jost matrices are multi-valued, since they depend on energy via the channel momenta, k_n. This causes square-root branching in the energy Riemann surface at each channel threshold energy. For the scattering of charged particles, the Jost matrices also depend on the energy via the Sommerfeld parameter for each scattering channel, η_n. As will be shown, this causes further logarithmic branching of the Riemann surface at each channel threshold energy.

The Jost matrices must be analytically continued onto the correct sheet of the energy Riemann surface in order to obtain correct bound and resonance state parameters. To

ensure that the continuation is always onto the correct sheet, the fitted Jost matrices are used in a semi-analytic form. In this form, the factors dependent on k_n and η_n are factorised explicitly. The remaining factors are entire and single-valued in energy, and can then be approximated by truncated Taylor series. The expansion coefficients then serve as the fitting parameters. Since the factors dependent on k_n and η_n are written explicitly, the appropriate sheet can always be chosen correctly when the Jost matrices are analytically continued. The correct analytic structure of the Jost matrices (and so also the S-matrix) will be maintained, irrespective of the approximation used for the unknown functions.

In this thesis, this method using the Jost matrices will be implemented to extract bound and resonance state parameters from experimental data of the scattering of two charged particles. This method is tested for a non-physical, model scattering system to show its reliability. It is then successfully applied to two nuclear scattering problems: the scattering of the α-particle (^{4}He) by the carbon-twelve nucleus (α^{12}C scattering) and the scattering of d, the deuteron (^{2}H) by the α-particle ($d\alpha$ scattering). These two scattering problems are of particular importance in astrophysics.

In the remainder of this chapter, the Jost matrices will be defined for the multi-channel scattering of neutral particles with zero spin. The properties of the Jost matrices with respect to bound, resonance and scattering sates will be considered in particular. In Chapter 2, the discussion will be extended to particles with charge as well as the scattering of particles with non-zero spin.

Chapters 1 and 2 provide the required mathematical background to introduce the method of extracting scattering parameters from experimental data of charged particles, which will be discussed in Chapter 3. The method will further be tested for the model system in Chapter 3, which is based on Ref. [4]. A small detour to some of the introductory concepts of astrophysics follows in Chapter 4, where the Asymptotic Normalisation Coefficients and their relation to the Jost matrices are of particular importance. The Jost method of analysis is applied to α^{12}C scattering data in Chapter 5, which is based on Ref. [7]. In Chapter 6, based on Ref. [8], the method is used to analyse $d\alpha$ scattering data. The thesis concludes with Chapter 7.

1.1 Two-body quantum scattering

Numerous complicated scattering systems can be modelled by a two-body system. Consider, for example, the ^{16}O nucleus, the energy levels of which will be determined in Chapter 5. In its ground state it can be viewed as a bound state of the α-particle and the ^{12}C nucleus [9]. The α-particle has a binding energy of ~ 28 MeV and is the most tightly bound of the light nuclei. For energies below this binding energy, the α-particle cluster should be present within the composite ^{16}O nucleus. For the non-relativistic energies under consideration, the ^{12}C cluster should similarly be present, as it has an even larger binding energy of ~ 90 MeV. Even for excited states of ^{16}O, these two clusters would still be distinguishable within the ^{16}O nucleus. If two-body α^{12}C scattering is considered, as is done in Chapter 5, the bound and resonance state parameters of ^{16}O can reliably be determined.

Mathematically, the two-body scattering problem is also well-understood, since it reduces to an equivalent single-body scattering problem. Although much progress has recently been made in extending the Jost method to a three-body problem (see for example Ref [10]), it is beyond the scope of this thesis.

First consider a general quantum system in the Schrödinger picture, which is fully described by a state vector, $|\mathbf{\Psi}_a(t)\rangle$ at a time, t. It is determined by a full set of conserving quantum numbers, $a = \{\alpha_1, \alpha_2, ..., \alpha_N, \}$, which are the eigenvalues of a set of Hermitian, commuting operators.

The state vector is also orthogonal and is normalised to unity:

$$\langle \mathbf{\Psi}_a(t) | \mathbf{\Psi}_{a'}(t) \rangle = \delta_{aa'}, \tag{1.1}$$

where δ_{ij} is the Kronecker Delta. The Schrödinger equation governs the time-evolution of the state vector:

$$i\hbar \frac{d}{dt} |\mathbf{\Psi}_a(t)\rangle = \hat{H} |\mathbf{\Psi}_a(t)\rangle, \tag{1.2}$$

where $\hat{H}$ is the Hamiltonian operator.

Provided that the Hamiltonian is time-independent (which corresponds with a conservation of energy), the state vector can be written in terms of an exponential time-evolution operator acting on a time-independent vector [11]:

$$|\mathbf{\Psi}_a(t)\rangle = e^{-i(t-t_0)\hat{H}/\hbar}|\mathbf{\Psi}_a(t_0)\rangle, \tag{1.3}$$

where t_0 is a reference time, usually chosen $t_0 = 0$. The reduced Planck constant is given by $\hbar$. For most calculations in atomic and nuclear psychics, including the calculations of this work, the units are chosen such that $\hbar = c = 1$. The time-independent equation,

$$\hat{H}|\psi_a\rangle = E|\psi_a\rangle, \tag{1.4}$$

results from the fact that the eigenvalues of the Hamiltonian are the discrete set of possible energies of the system, and $|\mathbf{\Psi}_a(t_0)\rangle = |\psi_a\rangle$.

The Hamiltonian is the sum of the kinetic energy operator (which corresponds to the free-particle Hamiltonian, $\hat{H}^0$ of the two-body system) and the potential energy operator, which includes the spatially dependent interaction potential, $\hat{U}(\mathbf{r})$ as well as the potential due to the internal dynamics of the particles in the moving system, $\hat{h}$. For two particles with masses m_1 and m_2 and positions $\mathbf{r}_1$ and $\mathbf{r}_2$, relative to a specific reference frame, the two-body Hamiltonian is given by [3]:

$$\hat{H} = \hat{H}_1^0 + \hat{H}_2^0 + \hat{U}(\mathbf{r}_1 - \mathbf{r}_2) + \hat{h} \tag{1.5}$$

with

$$\hat{H}_i^0 = \frac{\hat{\mathbf{p}}_i^2}{2m_i}, \qquad i = 1,2, \tag{1.6}$$

where $\hat{\mathbf{p}}$ is the momentum operator. Assuming that the centre-of-mass frame of reference is stationary relative to the laboratory frame, an expression for the two-body Hamiltonian identical to that of a single particle in a central potential can be obtained [11]:

$$\hat{H} = \frac{\hat{\mathbf{p}}^2}{2\mu} + \hat{U}(\mathbf{r}) + \hat{h}, \tag{1.7}$$

with the relative position and reduced mass given by:

$$\mathbf{r} = \mathbf{r}_1 - \mathbf{r}_2 \tag{1.8}$$

$$\mu = \frac{m_1 m_2}{m_1 + m_2} \tag{1.9}$$

The eigenvalues of the two-body Hamiltonian correspond to the bound state energy spectrum of the two interacting particles. The Scattering matrix, or S-matrix, is introduced in the next section and is related to the bound, resonance and scattering states.

1.2 The S-matrix

In the scattering of particles, it is experimentally impossible to observe the evolution of the state vector in the interaction region. This is because the size of this region is in the order of 1-100 fm for nuclear scattering, which corresponds with an average nuclear radius. For atomic scattering, the interaction region magnitude is in the order of the average atomic radius of $0.1 - 10$ nm.

In general, the incoming state can be prepared explicitly: the orientation, energy and polarisation of an incoming beam of particles is known. Furthermore, experimentally measurable quantities related to the outgoing state (the scattering cross-section, for example) can be measured. The state vector will then be written in terms of these incoming and outgoing states.

The state vector in terms of the time-evolution operator acting on a time-independent state, is given by Eq. (1.3): $|\Psi_a(t)\rangle = e^{-it\hat{H}/\hbar}|\psi_a\rangle$, with $t_0 = 0$ representing the reference time when the interaction commences.

In a scattering experiment, at a time well before and well after the interaction, the state vector behaves like a free particle, where the two-body Hamiltonian of Eq. (1.7)

reduces to a simple free-body Hamiltonian:

$$\hat{H}^0 = \frac{\hat{\mathbf{p}}^2}{2\mu}. \tag{1.10}$$

The incoming and outgoing states can then be given in terms of the incoming and outgoing time-independent asymptotic states, represented by $|\psi_a^{\text{in}}\rangle$ and $|\psi_{a'}^{\text{out}}\rangle$:

$$|\mathbf{\Psi}_a(t)\rangle = e^{-it\hat{H}/\hbar)}|\psi_a\rangle \xrightarrow[r\to-\infty]{} e^{-it\hat{H}_0/\hbar}|\psi_a^{\text{in}}\rangle, \tag{1.11}$$

$$|\mathbf{\Psi}_{a'}(t)\rangle = e^{-it\hat{H}/\hbar)}|\psi_{a'}\rangle \xrightarrow[r\to\infty]{} e^{-it\hat{H}_0/\hbar}|\psi_{a'}^{\text{out}}\rangle. \tag{1.12}$$

The set of quantum numbers describing the outgoing state may differ from the incoming state. They are therefore distinguished by a and a'. Equations (1.11) and (1.12) represent the *Asymptotic Condition* [3], which can be proven for the nuclear, short-ranged part of the interaction potentials under consideration in this work. As discussed in Ref. [3], the following three conditions are applicable for such potentials:

I $|U(r)| \leq c|r|^{-3-\varepsilon}$ as $r \to \infty$ (for some $\varepsilon > 0$ and constant, c)

II $|U(r)| \leq c|r|^{-2+\varepsilon}$ as $r \to 0$ (for some $\varepsilon > 0$ and constant, c)

III $U(r)$ is continuous for $0 < r < \infty$, except at a finite number of possible finite discontinuities.

These conditions hold for nuclear, short-ranged potentials, but do not hold for the Coulomb potential, which will be discussed in Chapter 2. Furthermore, while these conditions are specifically applicable to spherically central potentials, the *Asymptotic Condition* can also be proven for non-central potentials [3].

The time-independent state vectors before and after the collision can then be represented in terms of the asymptotic time-independent states:

$$|\psi_a\rangle = \hat{\Omega}^{(+)}|\psi_a^{\text{in}}\rangle, \tag{1.13}$$

$$|\psi_{a'}\rangle = \hat{\Omega}^{(-)}|\psi_{a'}^{\text{out}}\rangle, \tag{1.14}$$

with the Møller operators, $\hat{\Omega}^{(\pm)}$, defined as follows:

$$\hat{\Omega}^{(\pm)} \equiv \lim_{t\to+\infty} e^{\mp it(\hat{H}-\hat{H}^0)/\hbar}. \tag{1.15}$$

It is mathematically important to indicate that equations (1.13), (1.14) and (1.13) are to be understood within the strong operator topology, for the limits to have meaning [12].

The probability that a initial state $|\psi_a\rangle$ will evolve into a final state $|\psi_{a'}\rangle$ is then given by:

$$\langle\psi_{a'}|\psi_a\rangle = \left\langle \psi_{a'}^{\text{out}} \middle| \left(\hat{\Omega}^{(-)}\right)^{\dagger} \hat{\Omega}^{(+)} \middle| \psi_a^{\text{in}} \right\rangle = \hat{S}_{a'a}, \tag{1.16}$$

where $\hat{S}$ is the scattering operator. In the energy representation, this becomes the S-matrix (see Ref. [3], for example).

Depending on the energy, E, the outgoing wave is in a bound, resonance or scattering state. The S-matrix allows the energy of the outgoing state to be determined. Furthermore, the S-matrix can be constructed in terms of the Jost matrices - in fact, the S-matrix will be defined in terms of the Jost matrices. To define the Jost matrices, the asymptotic behaviour of the regular solution to the radial Schrödinger equation must be considered. The system of coupled radial equations for multi-channel scattering will therefore be derived.

1.3 Multi-channel scattering

Return to the two-body Hamiltonian (1.7), which is a general result and is applicable to single-channel and multi-channel scattering. But what is meant by *channels*? In the two-body scattering of hypothetical particles A and B, depending on the available energy, there could be numerous resulting reactions; the first of which being $A + B \to A + B$. This is elastic scattering and is always the first available channel, with threshold energy usually fixed by $E_1 = 0$ as reference.

The threshold energies are the eigenvalues of the internal dynamics operator, $\hat{h}$, of

the particles in the system. Each internal state of a two-body system corresponds with a different channel of the scattering process. Other channels may open at larger threshold energies. For example, one might have $A+B \rightarrow C+D$ or $A+B \rightarrow E+F$. This would be the second and third channel, with threshold energies E_2 and E_3 determined relative to E_1 and $E_1 < E_2 < E_3$.

There are infinitely many possible internal states, which corresponds with an infinite number of channels. All the eigenstates of $\hat{h}$ are given by:

$$\hat{h}|n\rangle = E_n|n\rangle, \qquad n = 1,2,3,...,\infty. \tag{1.17}$$

The operator $\hat{h}$ can then be approximated by:

$$\hat{h} \approx \sum_{n=1}^{N} |n\rangle E_n \langle n|, \tag{1.18}$$

where an exact expression would be obtained if $N \rightarrow \infty$. It is assumed the first N states are most probable, hence the approximation.

Using $\hat{\mathbf{p}}^2 = -\hbar^2\Delta_{\mathbf{r}}$, the matrix representation of the Hamiltonian (1.7) is then given by:

$$\begin{aligned}
\langle n|\hat{H}|n'\rangle &= \langle n|\hat{H}^0|n'\rangle + \langle n|\hat{U}(\mathbf{r})|n'\rangle + \langle n|\hat{h}|n'\rangle \\
\therefore \hat{H}_{nn'} &= \delta_{nn'}\frac{\langle n|\hat{\mathbf{p}}^2|n'\rangle}{2\mu_n} + U_{nn'}(\mathbf{r}) + \sum_{n=1}^{N}\langle n||n\rangle E_n\langle n||n'\rangle \\
\therefore \hat{H}_{nn'} &= -\delta_{nn'}\frac{\hbar^2}{2\mu_n}\Delta_{\mathbf{r}} + U_{nn'}(\mathbf{r}) + E_n\delta_{nn'},
\end{aligned} \tag{1.19}$$

where μ_n is the reduced mass in the channel, n. Implementing this multi-channel two-body Hamiltonian in the time-independent Schrödinger equation (1.4), results in the following system of coupled differential equations in the position representation:

$$\left[\frac{\hbar^2}{2\mu_n}\Delta_{\mathbf{r}} + (E - E_n)\right]\psi_n(E,r) = \sum_{n'=1}^{N} U_{nn'}(\mathbf{r})\psi_{n'}(E,r), \tag{1.20}$$

where n is the channel number with $n = 1,2,...,N$ and $\psi_n(E,\mathbf{r})$ is the time-independent wave-function for the channel, n.

The scattering problem is then uniquely determined by the interaction potential, $U_{nn'}(\mathbf{r})$, which is a $N \times N$ matrix. The full wave-function for such a multi-channel scattering problem is the linear combination of all the channel wave-functions, which can also be represented as a column matrix comprised of the channel wave-functions:

$$\Psi_a(E,\mathbf{r}) = \begin{pmatrix} \psi_1(E,\mathbf{r}) \\ \psi_2(E,\mathbf{r}) \\ \vdots \\ \psi_n(E,\mathbf{r}) \end{pmatrix}. \tag{1.21}$$

The channels are not only characterised by the threshold energies, but also by the complete set of channel quantum numbers, $a = \{\alpha_1, \alpha_2, ..., \alpha_N, \}$. This means that states with different spin or angular momentum also become new channels. Any states of a system that differ by at least one quantum number are then considered as different channels, even if the threshold energies for these states are the same [3]. Such channels with the same threshold energy will be referred to as degenerate channels, as they are degenerate in energy.

In a multi-channel scattering experiment, the multi-channel mathematical formalism describes all the channels in the scattering simultaneously. To explain the notation used to distinguish between the scattering data for the various channels, $n \to n'$, consider the following two-channel scattering problem:

$$A + B \to \begin{cases} A + B \\ \\ C + D \end{cases}.$$

The first channel would be the elastic scattering: $A + B \to A + B$, and will be indicated by $1 \to 1$. The second channel also represents elastic scattering, but of the second pair of particles: $C + D \to C + D$. The first transition channel, indicated by $1 \to 2$, represents the reaction: $A + B \to C + D$. The second transition channel, indicated by

$2 \rightarrow 1$, then represents the reaction: $C + D \rightarrow A + B$.

The notation is similar for degenerate channels. For the scattering of particles where only one threshold energy is open, but the quantum numbers of the scattered particles differ, the value of the changing quantum number will typically replace n and n' in the expression for the channel, $n \rightarrow n'$. In Chapter 6, for example, the channels are defined by ℓ_J. For channels defined by $J = 1$, the transition channel of an S-wave (where $\ell = 0$) transforming into a D-wave (where $\ell = 2$), will be indicated by $S_1 \rightarrow D_1$.

In a scattering experiment, information on all the channels are often unavailable, depending on the particles that are scattered. It is, however, possible to gain information on the unknown channels from suitable fittings of the data from the known channels. This will be discussed in detail, with a suitable example, in Chapter 3.

1.4 Multi-channel radial equation

For a system with zero spin, the two conserving quantum numbers for each channel are the magnetic quantum number, m, with corresponding orbital angular momentum quantum number, ℓ. The quantity, ℓ appears explicitly in the radial Schrödinger equation when a separation of polar configuration variables into a radial and polar-angle part is performed [11].

They are related to the eigenvalues of the total angular momentum operator for the two-body system, $\hat{\boldsymbol{\ell}} = \hat{\mathbf{r}} \times \hat{\mathbf{p}}$, and the component of this operator, $\hat{\ell}_z$, usually chosen as the z-component in an arbitrary Cartesian coordinate system. The operators $\hat{\boldsymbol{\ell}}$ and $\hat{\ell}_z$ do not commute. However, $\hat{\boldsymbol{\ell}}^2$ and $\hat{\ell}_z$ do commute, thus they share a set of eigenvectors, $|\ell m\rangle$. The eigenvalues of these operators are:

$$\hat{\boldsymbol{\ell}}^2|\ell m\rangle = \ell(\ell+1)\hbar^2|\ell m\rangle, \tag{1.22}$$

$$\hat{\ell}_z|\ell m\rangle = m\hbar|\ell m\rangle. \tag{1.23}$$

The eigenvectors that describe a specific space-configuration (the eigenvectors of the position operator) are given, in polar coordinates, by:

$$|\mathbf{r}\rangle = |r,\theta,\varphi\rangle. \tag{1.24}$$

Projecting $|\ell m\rangle$ on the spherical-angle part of the configuration eigenvectors results in the well-known Spherical Harmonics:

$$\langle\theta,\varphi|\ell m\rangle = Y_{\ell m}(\theta,\varphi), \tag{1.25}$$

which can be written in terms of the Associated Legendre polynomials, $P_{\ell m}(z)$ [11]:

$$Y_{\ell m}(\theta,\varphi) = (-1)^m \sqrt{\frac{(2\ell+1)(\ell-m)!}{(4\pi)(\ell+m)!}} P_{\ell m}(\cos\theta) e^{im\varphi}. \tag{1.26}$$

This then allows one to show that the spherical harmonics are orthonormal:

$$\int Y^*_{\ell m} Y_{\ell' m'} d\Omega = \int_0^{2\pi}\int_0^{\pi} Y^*_{\ell m} Y_{\ell' m'} \sin\theta \; d\theta d\varphi = \delta_{\ell\ell'}\delta_{mm'}. \tag{1.27}$$

Consequently, the eigenvectors, $|\ell m\rangle$ form an orthonormal basis.

It can further be shown from Eq. (1.22), (1.23) and (1.25) that:

$$\hat{\boldsymbol{\ell}}^2 Y_{\ell m}(\theta,\varphi) = \ell(\ell+1) Y_{\ell m}(\theta,\varphi), \tag{1.28}$$

$$\hat{\ell}_z Y_{\ell m}(\theta,\varphi) = m Y_{\ell m}(\theta,\varphi). \tag{1.29}$$

The time-independent channel wave-functions in configuration space, $\psi_n(E,\mathbf{r})$, are the set of projections of the time-independent wave-vector on the basis of configuration vectors, $|\mathbf{r}\rangle$:

$$\langle\mathbf{r}|\psi_n\rangle = \psi_n(E,r,\theta,\varphi) \tag{1.30}$$

The channel wave-vectors are also eigenvectors of the operators $\hat{\boldsymbol{\ell}}^2$ and $\hat{\ell}_z$ and are therefore distinguished by the quantum numbers ℓ and m for each channel. Expand-

ing Eq. (1.30) over the orthonormal basis of eigenvectors, $|\ell_n m_n\rangle$, of each channel, n, gives:

$$\begin{aligned}\psi_n(E,\mathbf{r}) &= \sum_{\ell_n m_n} \langle r,\theta,\varphi|\ell_n m_n\rangle\langle \ell_n m_n|\psi_n\rangle \\ &= \sum_{\ell_n m_n} \langle \theta,\varphi|\ell_n m_n\rangle\langle r,\ell_n m_n|\psi_n\rangle \\ &= \sum_{\ell_n m_n} Y_{\ell_n m_n}(\theta,\varphi)\langle r,\ell_n m_n|\psi_n\rangle \end{aligned} \tag{1.31}$$

Now the radial wave-function for each channel is defined by:

$$u_{\ell_n}(E,r) \equiv r\langle r,\ell_n m_n|\psi_n\rangle. \tag{1.32}$$

Substituting this definition into Eq. (1.31) then gives the time-independent channel wave-functions as the product of a radially dependent part and the angular dependent spherical harmonics:

$$\psi_n(E,r,\theta,\varphi) = \sum_{\ell_n m_n} \frac{u_n(E,r)}{r} Y_{\ell_n m_n}(\theta,\varphi). \tag{1.33}$$

Without loss of generality, it can further be assumed that the relative motion in each channel has a single value of ℓ_n and m_n [13]. If there is a difference in the quantum numbers of a specific energy channel, another degenerate channel (with the same threshold energy but differing in quantum numbers) can be opened. In general, specific partial wave-functions distinguished by ℓ for each channel will be considered.

This simplifies the notation considerably, since it is no longer required to sum over all possible values of ℓ_n and m_n:

$$\psi_n(E,r,\theta,\varphi) = \frac{u_n(E,r)}{r} Y_{\ell_n m_n}(\theta,\varphi). \tag{1.34}$$

The Laplacian operator, $\Delta_{\mathbf{r}}$ in polar coordinates, is also given in terms of the orbital

angular momentum operator, $\hat{\boldsymbol{\ell}}$, by [11]:

$$\Delta_{\mathbf{r}} = \frac{1}{r^2}\partial_r\left(r^2\partial_r - \frac{\hat{\boldsymbol{\ell}}^2}{\hbar^2 r^2}\right). \tag{1.35}$$

Keeping in mind that each radial wave-function is in a particular ℓ_n state, and using Eq. (1.35) with (1.28) and the separation (1.34) in the time-independent Schrödinger equation (1.20), the following is obtained:

$$\left[\partial_r^2 + k_n^2 - \frac{\ell_n(\ell_n+1)}{r^2}\right] u_n(E,r)Y_{\ell_n m_n}(\theta,\varphi)(E,r)$$
$$= \sum_{n'=1}^{N} U_{nn'}(r)u_{n'}Y_{\ell_{n'}m_{n'}}(\theta,\varphi)(E,r)$$

with the channel wave-momenta defined by:

$$k_n^2 \equiv \frac{2\mu_n}{\hbar^2}(E - E_n). \tag{1.36}$$

Multiplying by $Y^*_{\ell_n m_n}(\theta,\varphi)$, integrating over the solid angle Ω and implementing the orthonormal property of the spherical harmonics, Eq. (1.27), then gives the multi-channel radial Schrödinger equation:

$$\left[\partial_r^2 + k_n^2 - \frac{\ell_n(\ell_n+1)}{r^2}\right] u_n(E,r) = \sum_{n'=1}^{N} V_{nn'}(r)u_{n'}(E,r), \tag{1.37}$$

which is a system of N coupled second-order differential equations, with the coupling due to the off-diagonal elements of the reduced potential matrix $V_{nn'}$, given by:

$$V_{nn'}(r) = \frac{2\mu_n}{\hbar^2}\int Y^*_{\ell_n m_n}(\theta,\varphi)U_{nn'}(r)Y_{\ell_{n'}m_{n'}}(\theta,\varphi)\,\mathrm{d}\Omega. \tag{1.38}$$

For single-channel scattering, $n = 1$ and the reduced potential simply becomes:

$$V(r) = \frac{2\mu}{\hbar^2}U(r), \tag{1.39}$$

due to the spherical harmonics being orthonormal (Eq. (1.27)).

The radial equation (1.37) is applicable to a system where the particle interaction is radially dependent only, in other words, a central potential. A similar expression can be obtained for non-central potentials, but only central potentials will be considered in this thesis. Also, the potential is still very general, as it can be short-ranged or long-ranged.

Furthermore, the channel wave-functions of Eq. (1.34) that can be obtained by solving the system of radial equations, (1.37), are the same for bound, resonance and scattering states. For systems with non-zero spin, the channel wave-function for discrete states (bound states and resonances) must be distinguished from the wave-function for scattering states.

1.5 Jost matrices and properties

1.5.1 Jost matrices

The boundary conditions for the radial equations are derived from the requirement that any physical wave-function must be finite at $r = 0$. From the separation (1.34), this implies that the channel radial wave-functions must have regular behaviour near the origin [3]:

$$u_n(E,r) \xrightarrow[r\to\infty]{} 0, \qquad n = 1,2,3,...,N \tag{1.40}$$

At $r \to \infty$ the system can be in a bound, resonance or scattering state with boundary conditions determined by the specific state. The system of N linear second-order differential equations given in (1.37) has $2N$ linearly-independent column solutions, only half of which are regular at the origin [13]. These regular solutions will be denoted by $\phi_{nn'}(E,r)$, with

$$\phi_{nn'}(E,r) \xrightarrow[r\to\infty]{} 0 \qquad \forall\, n,n'. \tag{1.41}$$

The *fundamental matrix of the regular solutions* is constructed from these regular solutions:

$$\Phi(E,r) = \begin{pmatrix} \phi_{11}(E,r) & \phi_{12}(E,r) & \cdots & \phi_{1N}(E,r) \\ \phi_{21}(E,r) & \phi_{22}(E,r) & \cdots & \phi_{2N}(E,r) \\ \vdots & \vdots & \ddots & \vdots \\ \phi_{N1}(E,r) & \phi_{N2}(E,r) & \cdots & \phi_{NN}(E,r) \end{pmatrix}. \tag{1.42}$$

Any physical solution for each channel of the system of radial equations, (1.37) must be a linear combination of the columns of Eq. (1.42), since the matrix elements are also solutions of Eq. (1.37) [13]:

$$\begin{pmatrix} u_1 \\ u_2 \\ \vdots \\ u_N \end{pmatrix} = C_1 \begin{pmatrix} \phi_{11} \\ \phi_{21} \\ \vdots \\ \phi_{N1} \end{pmatrix} + C_2 \begin{pmatrix} \phi_{12} \\ \phi_{22} \\ \vdots \\ \phi_{N2} \end{pmatrix} + \cdots + C_N \begin{pmatrix} \phi_{1N} \\ \phi_{2N} \\ \vdots \\ \phi_{NN} \end{pmatrix}.$$

Or, as a matrix equation,

$$U(E,r) = \Phi(E,r)\,\mathcal{C} \tag{1.43}$$

with

$$\mathcal{C} = \begin{pmatrix} C_1 \\ C_2 \\ \vdots \\ C_N \end{pmatrix}, \tag{1.44}$$

and

$$U(E,r) = \begin{pmatrix} u_1(E,r) \\ u_2(E,r) \\ \vdots \\ u_N(E,r) \end{pmatrix}. \tag{1.45}$$

Equivalently, as a summation over the channels,

$$u_n = \sum_{n'=1}^{N} \phi_{nn'} C_n. \tag{1.46}$$

This representation is sometimes preferred in derivations, as will be seen in the sections that follow. Correct behaviour of the physical solution when $r \to 0$ is then guaranteed and proper choice of the combination coefficients C_n results in correct asymptotic behaviour when $r \to \infty$.

It is now assumed that the central interaction potential, $U_{nn'}(r)$ and hence the reduced potential $V_{nn'}(r)$ in equation (1.37) is short-ranged. To be more precise, it obeys the three conditions given in Section 1.2.

When the interacting particles are far apart, $V_{nn'}(r \to \infty) \to 0$ and Eq. (1.37) reduces to N uncoupled second-order differential equations:

$$\left[\partial_r^2 + k_n^2 - \frac{\ell_n(\ell_n+1)}{r^2}\right] u_n(E,r) = 0, \qquad r \to \infty. \tag{1.47}$$

Two linearly-independent solutions for each of the N equation are the Riccati-Hankel functions, $h_\ell^{(\pm)}(kr)$, which physically corresponds with the incoming, $h_\ell^{(-)}$, and outgoing, $h_\ell^{(+)}$, spherical wave. This is clear when one considers the asymptotic behaviour of the Riccati-Hankel functions [14]:

$$h_\ell^{(\pm)}(kr) \xrightarrow[|kr|\to\infty]{} (\mp i)^{\ell+1} e^{\pm ikr} = e^{\pm i[kr - \pi/2(\ell+1)]} \tag{1.48}$$

Another possible pair of linearly-independent solutions are the Riccati-Bessel, $j_\ell(kr)$, and Riccati-Neumann, $n_\ell(kr)$, functions, which are related to the standard Bessel functions (see Ref. [14] for details) and can of course be written as a linear combination of the Riccati-Hankel functions:

$$h_\ell^{(\pm)}(kr) = j_\ell(kr) \pm i\, n_\ell(kr) \tag{1.49}$$

The Riccati-Bessel function, $j_\ell(kr)$ is of particular importance, as it is regular at the

origin and has the following behaviour there:

$$j_\ell(kr) \xrightarrow[r\to 0]{} \frac{(kr)^{\ell+1}}{(2\ell+1)!!}. \tag{1.50}$$

Returning to Eq. (1.47), there are $2N$ linearly-independent column solutions to the system of equations, which can be written as square, diagonal matrices where the matrix elements are the Riccati-Hankel functions:

$$W^{(\text{in})} = \begin{pmatrix} h^{(-)}_{\ell_1}(k_1 r) & 0 & \cdots & 0 \\ 0 & h^{(-)}_{\ell_2}(k_2 r) & \cdots & 0 \\ \vdots & \vdots & \ddots & \vdots \\ 0 & 0 & \cdots & h^{(-)}_{\ell_N}(k_N r) \end{pmatrix} \tag{1.51}$$

$$W^{(\text{out})} = \begin{pmatrix} h^{(+)}_{\ell_1}(k_1 r) & 0 & \cdots & 0 \\ 0 & h^{(+)}_{\ell_2}(k_2 r) & \cdots & 0 \\ \vdots & \vdots & \ddots & \vdots \\ 0 & 0 & \cdots & h^{(+)}_{\ell_N}(k_N r) \end{pmatrix} \tag{1.52}$$

Any particular column solution to Eq. (1.47) can be written as a linear combination of the $2N$ columns of Eq. (1.51) and (1.52), since they form a basis in the space of solutions of Eq. (1.47) [13].

At $r \to \infty$, the columns of the fundamental matrix of the regular solutions (1.42) have to be solutions of (1.47). Thus, at large r, (1.42) can be written as a linear combination of (1.51) and (1.52) [13]:

$$\Phi(E,r) \xrightarrow[r\to\infty]{} W^{(\text{in})}(E,r) f^{(\text{in})}(E) + W^{(\text{out})}(E,r) f^{(\text{out})}(E). \tag{1.53}$$

The energy dependent $N \times N$ matrices, $f^{(\text{in/out})}(E)$, are defined as the Jost matrices. By Eq. (1.43), the asymptotic behaviour of the physical radial wave-functions can

also be given in terms of the Jost matrices:

$$U(E,r) \xrightarrow[r\to\infty]{} W^{(\text{in})}(E,r)f^{(\text{in})}(E)\mathcal{C} + W^{(\text{out})}(E,r)f^{(\text{out})}(E)\mathcal{C}. \tag{1.54}$$

For $N = 1$, these matrices reduce to the Jost functions and Eq. (1.53) becomes the following:

$$\phi(E,r) \xrightarrow[r\to\infty]{} h_\ell^{(-)}(kr)f_\ell^{(\text{in})}(E) + h_\ell^{(+)}(kr)f_\ell^{(\text{out})}(E). \tag{1.55}$$

The single-channel Jost functions can then be defined as the energy-dependent amplitudes of the incoming and outgoing spherical waves of the regular solution to the radial wave-equation, with the Jost matrices being the multi-channel extension of this principle. The matrix elements of the Jost matrices can also be thought of as channel Jost functions.

In the single-channel case, the Jost functions have the following easily-proven symmetry relations [3]:

$$\left[f_\ell^{(\text{in})}(E)\right]^* = f_\ell^{(\text{out})}(E), \qquad E > 0 \tag{1.56}$$

This is why, in numerous texts (see, for example, Ref. [3]), only one Jost function is defined,

$$f_\ell^{(\text{in})}(E) = f_\ell(E), \tag{1.57}$$

since the other can be written in terms of this function:

$$f_\ell^{(\text{out})}(E) = \left[f_\ell(E)\right]^*. \tag{1.58}$$

The two Jost functions will continue to be distinguished, since the 'in' and 'out' notation links well with the definition and is easily extended to the multi-channel case.

The Jost function was first introduced by Swiss physicist Res Jost in 1947 in Ref. [15], and it has a number of useful and interesting properties. Most importantly, the

S-matrix will be defined as the "ratio" of the Jost matrices:

$$S(E) \equiv f^{(\text{out})}(E)\left[f^{(\text{in})}(E)\right]^{-1}, \tag{1.59}$$

which is equivalent to the definition given in Section 1.2 (see, for example, Ref. [3]).

The single-channel symmetry relation allows both the single-channel Jost functions to be written in terms of the same quantity, δ_ℓ, which is real and positive:

$$f_\ell^{(\text{in})}(E) = \left|f_\ell^{(\text{in})}(E)\right| e^{+i\delta_\ell(E)}, \qquad E>0 \tag{1.60}$$

$$f_\ell^{(\text{out})}(E) = \left|f_\ell^{(\text{in})}(E)\right| e^{-i\delta_\ell(E)}, \qquad E>0 \tag{1.61}$$

When these two expressions for the Jost functions are divided, the following is obtained:

$$\frac{f_\ell^{(\text{out})}(E)}{f_\ell^{(\text{in})}(E)} = e^{2i\delta_\ell(E)}, \tag{1.62}$$

which then implies that,

$$S_\ell(E) = e^{2i\delta_\ell}. \tag{1.63}$$

The quantity δ_ℓ is, of course, the scattering phase-shift. It is usually defined only for positive energies. While many texts on scattering theory introduce this quantity differently (see, for example, Ref. [3]), the definitions are equivalent. There is, however, a problem: the phase-shift is not uniquely defined, since the same S-matrix can be obtained by different phase-shifts, determined by j:

$$S_\ell(E) = e^{2i(\delta_\ell+\pi j)}, \qquad j=0,1,2,\ldots \tag{1.64}$$

This becomes particularly evident in calculating the phase-shifts for a singular, repulsive potential such as the Coulomb potential for like charges. A smooth set of data is rarely obtained, and in certain energy ranges, πj for some j must be added or subtracted to the phase-shifts to obtain a continuous curve.

This problem has been addressed in Ref. [16], where the phase-shift is uniquely

defined for any spherical potential. The definition can also be extended to multi-channel scattering.

Irrespective of the ambiguous term πj, the same S-matrix and hence the same scattering cross-section will always be obtained. It is thus more convenient to work with the scattering cross-section, which is typically the measured quantity in a scattering experiment. For multi-channel scattering, it is particularly convenient to work with the the scattering cross section rather than the phase shifts.

The Jost matrices allow the bound, resonance and scattering states of a system of colliding particles to be determined simultaneously. Further details are given in the sections that follow, but a method of determining the Jost matrices for a given potential will first be discussed.

Calculating the Jost matrices

Consider again the system of radial equations (1.37). The matrix elements of the fundamental matrix of regular solutions are solutions to the radial equation, as has been indicated. At large r, the matrix $\Phi(E,r)$ is then a linear combination of the matrices $W^{(\mathrm{out/in})}(E,r)$; see Eq. (1.53). This suggests that $\Phi(E,r)$ should be written in terms of these matrices for all r:

$$\Phi(E,r) \equiv W^{(\mathrm{in})}(E,r)F^{(\mathrm{in})}(E,r) + W^{(\mathrm{out})}(E,r)F^{(\mathrm{out})}(E,r). \tag{1.65}$$

where $F^{(\mathrm{in/out})}(E,r)$ are unknown matrix functions of both E and r. It is clear that these matrices become the Jost matrices at large r:

$$f^{(\mathrm{in/out})}(E) = \lim_{r\to\infty} F^{(\mathrm{in/out})}(E,r). \tag{1.66}$$

The matrix functions $F^{(\mathrm{in/out})}(E,r)$ cannot be independent of each other, and a suitable dependence, in this case the Lagrange condition, can be imposed:

$$W^{(\mathrm{in})}(E,r)\partial_r F^{(\mathrm{in})}(E,r) + W^{(\mathrm{out})}(E,r)\partial_r F^{(\mathrm{out})}(E,r) = 0 \tag{1.67}$$

Furthermore, using the Wronskian of the Riccati-Hankel functions $h_\ell^{(\pm)}(kr)$ (see Ref. [14], for example), it can be shown that:

$$W^{(\text{in})}\left[\partial_r W^{(\text{out})}\right] - \left[\partial_r W^{(\text{in})}\right] W^{(\text{out})} = 2iK, \tag{1.68}$$

with:

$$K = \begin{pmatrix} k_1 & 0 & \cdots & 0 \\ 0 & k_2 & \cdots & 0 \\ \vdots & \vdots & \ddots & \vdots \\ 0 & 0 & \cdots & k_N \end{pmatrix}. \tag{1.69}$$

Substituting Eq. (1.65) into the radial equation (1.37), implementing the condition (1.67) and using Eq. (1.68) results in the following system of first-order differential equations:

$$\partial_r F^{(\text{in})} = -\frac{1}{2i} K^{-1} W^{(\text{out})} V \left[W^{(\text{in})} F^{(\text{in})} + W^{(\text{out})} F^{(\text{out})}\right], \tag{1.70}$$

$$\partial_r F^{(\text{in})} = \frac{1}{2i} K^{-1} W^{(\text{in})} V \left[W^{(\text{in})} F^{(\text{in})} + W^{(\text{out})} F^{(\text{out})}\right]. \tag{1.71}$$

The functional dependence has been suppressed to simplify the expression. For the full derivation, see Refs. [13, 17] for example.

For a given spherically symmetric short-ranged potential, only the boundary conditions are then necessary to calculate the Jost matrices. Provided that the choice does not affect the behaviour of the fundamental matrix of regular solutions near the origin, these boundary conditions can be chosen arbitrarily [13, 17]. This is somewhat counter-intuitive, but can be understood when considering the properties of the Jost matrices. It will be shown that bound states and resonances correspond to discrete energies, $\mathcal{E}_i$ such that $\det\left[f^{(\text{in})}(\mathcal{E}_i)\right] = 0$. The scaling of $f^{(\text{in})}(E)$ is therefore irrelevant in locating the bound and resonance states. By Eq. (1.66), $f^{(\text{in})}(E)$ is determined as the limit of $F^{(\text{in})}(E,r)$, and the boundary condition at $r = 0$ can thus be chosen arbitrarily.

Furthermore, all other properties of the Jost matrices are obtained via their relation

to the S-matrix. If the boundary conditions of $F_\ell^{(\text{in/out})}(E,r)$ are the same, the scaling factors of the Jost matrices cancel out in the expression for the S-matrix. See Refs. [13, 17] for further details.

The following boundary condition will be chosen:

$$F^{(\text{in/out})}(E,r\to 0)=\frac{1}{2}I \tag{1.72}$$

where I is the $N\times N$ identity matrix.

If the matrix J, comprised of the Riccati-Bessel functions on the diagonal, is introduced:

$$J(E,r)=\begin{pmatrix} j_{\ell_1}(k_1r) & 0 & \cdots & 0 \\ 0 & j_{\ell_2}(k_2r) & \cdots & 0 \\ \vdots & \vdots & \ddots & \vdots \\ 0 & 0 & \cdots & j_{\ell_N}(k_Nr) \end{pmatrix}, \tag{1.73}$$

it is easy to show by Eq. (1.49) that:

$$J(E,r)=\frac{1}{2}W^{(\text{in})}+\frac{1}{2}W^{(\text{out})}. \tag{1.74}$$

Using this when implementing the boundary conditions (1.72) in Eq. (1.65) near the origin results in the following regular behaviour of the fundamental matrix of regular solutions:

$$\Phi(E,r\to 0)=J(E,r)\xrightarrow[r\to 0]{}\begin{pmatrix} \frac{(k_1r)^{\ell_1+1}}{(2\ell_1+1)!!} & 0 & \cdots & 0 \\ 0 & \frac{(k_2r)^{\ell_2+1}}{(2\ell_2+1)!!} & \cdots & 0 \\ \vdots & \vdots & \ddots & \vdots \\ 0 & 0 & \cdots & \frac{(k_Nr)^{\ell_N+1}}{(2\ell_N+1)!!} \end{pmatrix}. \tag{1.75}$$

The physical radial solutions are related to the regular solutions by Eq. (1.43), thus by Eq. (1.65) the following is also obtained:

$$U(E,r)=W^{(\text{in})}(E,r)F^{(\text{in})}(E,r)\,\mathcal{C}+W^{(\text{out})}(E,r)F^{(\text{out})}(E,r)\,\mathcal{C}. \tag{1.76}$$

Equivalently, the channel radial solutions are given by:

$$u_n(E,r) = \sum_{n'=1}^{N} \left[h_{\ell_n}^{(-)}(k_n r) F_{nn'}^{(\text{in})}(E,r) C_n + h_{\ell_n}^{(-)}(k_n r) F_{nn'}^{(\text{out})}(E,r) C_n \right], \tag{1.77}$$

and by Eq. (1.33) the time-independent wave-function for each channel is given by:

$$\psi_n(E,\mathbf{r}) = \frac{1}{r} \sum_{n'=1}^{N} \sum_{\ell_n m_n} \left[h_{\ell_n}^{(-)}(k_n r) F_{nn'}^{(\text{in})}(E,r) C_n + h_{\ell_n}^{(+)}(k_n r) F_{nn'}^{(\text{out})}(E,r) C_n \right] Y_{\ell_n m_n}(\theta,\varphi) \tag{1.78}$$

It is very important that the physical wave-function is normalised correctly and that is has the correct asymptotic behaviour. This will fix the constants, C_n. Determining $F^{(\text{in/out})}(E,r)$ with the coupled system of differential equations (1.70) and (1.71) also allows the wave-functions for each channel to be determined with Eq. (1.78), as well as determining the Jost matrices with Eq. (1.66).

This is of course only possible for a suitable short-ranged potential. The Jost matrices can also be constructed with appropriate fittings of experimental data, which is the focus of this thesis. The formalism will furthermore be expanded to include Coulomb interactions. The relationship between the Jost matrices and bound, resonance and scattering states will first be discussed in detail.

1.5.2 Bound states

Bound states are, per definition, stable states where scattered particles cannot leave the source of an attractive field [3]. In the case of two-body scattering, the two particles that are scattered become ‘stuck’ together.

Such states are energy eigenstates of the Hamiltonian and the eigenvalues correspond to the discrete bound state energies, as was mentioned in a previous section. Furthermore, these energy eigenvalues are real and, for a particular channel, must have energy smaller than the threshold energy of that channel [11]. The correspond-

ing channel momentum, k_n from Eq. (1.36) must then be purely imaginary and will be written as follows:

$$k_n = \pm\sqrt{\frac{2\mu_n}{\hbar^2}(E - E_n)} = \pm i|k_n|, \tag{1.79}$$

where the positive $k_n = +i|k_n|$ is chosen for all n, which corresponds to the so-called physical sheet of the energy Riemann surface. The negative choice of k_n, which corresponds with the unphysical sheet of the Riemann energy surface, results in a different relationship with the Jost matrices for bound states. Riemann surfaces will be discussed in detail in Chapter 3.

As previously mentioned, particles in a bound state are restricted so that they are close to the source of the attractive field. In a two-body system, the probability of finding one particle far away from the source of the attractive field, the other particle, is zero. Thus the two-body time-independent wave-functions for each channel, $\psi_n(E, r, \theta, \varphi)$, must also be zero for large r. In turn, this implies that $u_n(r \to \infty) \to 0$, from Eq. (1.34), and so the same is true for the matrix of solutions: $U(E, r \to \infty) \to 0$

.

By the asymptotic behaviour of the physical solutions, Eq. (1.54), the following requirement is then obtained for bound states:

$$W^{(\mathrm{in})}(\mathcal{E}_i, r \to \infty) f^{(\mathrm{in})}(\mathcal{E}_i)\, \mathcal{C} + W^{(\mathrm{out})}(\mathcal{E}_i, r \to \infty) f^{(\mathrm{out})}(\mathcal{E}_i)\, \mathcal{C} \to 0 \tag{1.80}$$

When considering the asymptotic behaviour of the Riccati-Hankel functions given in Eq. (1.48), and keeping in mind the channel momenta, k_n are positive and purely imaginary, it is clear that,

$$h^{(+)}_{\ell_n}(i|k_n|r) \xrightarrow[r\to\infty]{} 0,$$

$$h^{(-)}_{\ell_n}(i|k_n|r) \xrightarrow[r\to\infty]{} \infty.$$

This, in turn, implies that $W^{(\mathrm{out})}(\mathcal{E}_i, r \to \infty) = 0$ and $W^{(\mathrm{in})}(\mathcal{E}_i, r \to \infty)$ becomes an

infinite diagonal matrix. For Eq. (1.80) to hold, it is then required that

$$f^{(\mathrm{in})}(\mathcal{E}_i)\,\mathcal{C} = 0. \tag{1.81}$$

For a single-channel problem, this simply means the single-channel Jost function is zero at a bound state spectral energy, $\mathcal{E}_i$:

$$f_\ell^{(\mathrm{in})}(\mathcal{E}_i) = 0. \tag{1.82}$$

For a non-trivial solution, the column matrix $\mathcal{C}$ is non-zero. For the multi-channel case, Eq. (1.81) holds if and only if

$$\det\left[f^{(\mathrm{in})}(\mathcal{E}_i)\right] = 0, \tag{1.83}$$

on the physical sheet of the Riemann surface, by the positive choice of sign for k_n.

This corresponds exactly with the well-known fact that the energy poles of the S-matrix on the physical sheet correspond to the bound state spectral energies [3], which is clear when considering the relationship between the S-matrix and the Jost matrices, Eq. (1.59).

For a negative choice of k_n, it is easy to show by a similar discussion, that bound states also correspond to $\det\left[f^{(\mathrm{out})}(\mathcal{E}_i)\right] = 0$ on the unphysical sheet of the Riemann surface. This is also in line with the symmetry relations between $f^{(\mathrm{in})}(E)$ and $f^{(\mathrm{out})}(E)$ (see Refs. [3, 13], for example).

The more prickly problem of resonance states will be considered next.

1.5.3 Resonance states

The concept of resonance occurs in numerous divers branches of physics and, of course, the definition is similar in the various fields. In quantum scattering theory, resonances physically represent extremely short-lived ($\sim 10^{-20}$ s) excited states of particles, that decay by the strong interaction [2]. These particles can be in the

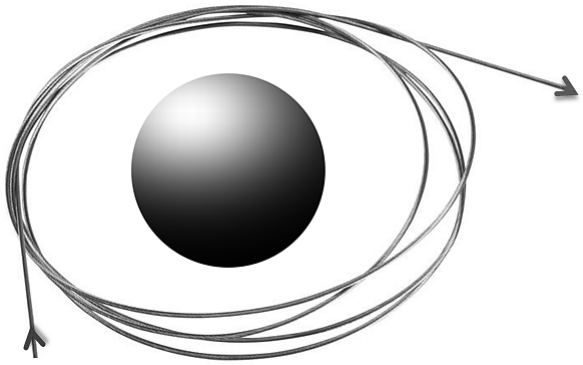

Figure 1.1: Intuitive representation of a resonance.

sub-nuclear, nuclear and atomic scale. In quantum few-body physics in particular, nuclear and atomic resonances are the focus of research.

The resonance phenomenon is one of the most fascinating aspects of quantum mechanics and has been the subject of numerous studies [2]. Much progress has been made to accurately describe quantum resonance states mathematically and numerous techniques exist in nuclear, atomic and particle physics to determine resonance parameters.

Resonance states are often called semi-bound or quasi-bound states, since they have similar physical and mathematical properties to bound states. This is because they behave exactly as bound states do, but for a limited time-interval until decay takes place.

Intuitively, quantum resonances can be understood by considering a single particle in a central potential. The kinetic energy of the particle may be such that its trajectory around the source of the potential is closed. It will thus orbit the source of the central potential indefinitely, which corresponds with a bound state. For a resonance state, the kinetic energy is such that the particle trajectory is *almost* closed - the particle will orbit the source of the central potential a number of times before dispersing, as illustrated in Figure 1.1.

The concept of a trajectory is, of course, meaningless for quantum particles. A resonance is then more accurately thought of as a slowly dissipating, partially localised

state. For discrete frequencies and corresponding discrete energies, accumulated energy exists in small regions of space. This energy dissipates through a frequency-window called the resonance width. A mathematical description of this principle follows. Firstly, resonances from simple, single-channel scattering will be considered.

Single-channel resonances

Unlike scattering states, resonance states are not governed by the initial state vector. A scattering state has a definite in-asymptote, and a resonance state does not [3]. Consequently, for resonances energies, only the outgoing spherical wave exists far from the interaction region, similar to bound states. From Eq. (1.54), this again implies that

$$f^{(\mathrm{in})}(\mathcal{E}_i) = 0, \tag{1.84}$$

but the spectral energies $\mathcal{E}_i$ are no longer necessarily real and negative, as for bound states. The resonance spectral energies will then be written as follows:

$$\mathcal{E}_i = E_r + iE_i, \tag{1.85}$$

where E_r and E_i are both real.

Since the rate of decay of an ensemble of resonance states is proportional to the number of such states in the system at a specific time, the decay can be modelled by the exponential decay law [3]:

$$N(t) = N_0 e^{-t\Gamma/\hbar}, \tag{1.86}$$

where $N(t)$ is the number of resonance or decaying states at time t, N_0 is the number of states at $t = 0$ and $\Gamma/\hbar$ is the decay constant, which is real and positive. Γ is known as the resonance width and has units of energy.

The decay law is the solution of the differential equation:

$$\frac{dN(t)}{dt} = -\frac{\Gamma}{\hbar}N(t), \tag{1.87}$$

which is derived from the premise that the rate of decay of a system of particles is proportional to the number of particles in the system [3].

The number of resonances at a specific time, $N(t)$, is proportional to the probability density of the outgoing wave-function, which describes the relative motion of the outgoing particles in a decaying system:

$$\rho(t,\mathbf{r}) \sim N_0 e^{-t\Gamma/\hbar}. \tag{1.88}$$

The probability density is given in terms of the wave-function (in the position representation) by [11, 22]:

$$\rho(t,\mathbf{r}) = |\mathbf{\Psi}_a(t,\mathbf{r})|^2. \tag{1.89}$$

Since Γ is real, the following proportionality is obtained:

$$\mathbf{\Psi}_a(t,\mathbf{r}) \sim N_0 e^{-t\Gamma/2\hbar}. \tag{1.90}$$

The time-dependent resonance wave-function can be written in terms of the time-independent wave-function and a time-dependent part at resonance energy $\mathcal{E}_i$ (see Eq. (1.3)). The following proportionality of the time-dependent part must hold [3]:

$$e^{-i\mathcal{E}_i t} = e^{(-iE_r+E_i)t} \sim e^{-t\Gamma/2}. \tag{1.91}$$

If the resonance energy is real, $E_i = 0$, and the time-dependent part would be oscillatory, instead of decaying exponentially. Furthermore, if $E_i > 0$, exponential growth instead of decay would occur. In conclusion, the imaginary part of the resonance energy must be negative.

Resonances then correspond to complex spectral energies, $\mathcal{E}_i$, which have a negative imaginary part, with $f^{\text{in}}(\mathcal{E}_i) = 0$. Furthermore, they occur on the unphysical sheet of the Riemann surface [3]. This will be covered in the next section for multi-channel resonances.

From the proportionality of Eq. (1.91),

$$E_i = -\Gamma/2, \tag{1.92}$$

and so the resonance spectral energy is given in terms of the resonance width:

$$\mathcal{E}_i = E_r - \frac{i}{2}\Gamma. \tag{1.93}$$

Furthermore, it is easy to show that the resonance width is related to the half-life of the decaying state as follows:

$$T_{1/2} = \hbar\frac{\ln 2}{\Gamma}. \tag{1.94}$$

Even though resonance energies are complex, they have a physical impact on the scattering cross-sections: typically, at the real part of the resonance energies, E_r, large variation, such as peaks and troughs, occur in the cross-section data.

This can be understood by considering the analytic properties of the Jost functions [17]. Only single-channel Jost functions are still considered, yet the principle is easily extended to multi-channel scattering. The Jost functions, $f_\ell^{(\text{in/out})}(E)$, are analytic functions of energy [3]. If the energy was to change from a resonance spectral energy, where $f_\ell^{(\text{in})}(E_r - i\Gamma/2) = 0$, to a real energy, where $f_\ell^{(\text{in})}(E_r) = C$ for some value C, the transition from 0 to C would have to be smooth. If the resonance width, Γ, is very small, the transition value C would also have to be small. By the conservation of the probability current (see Ref. [11], for example), the change in the function $f_\ell^{(\text{out})}(E)$ would also be small for an energy change from $E_r - i\Gamma/2$ to E_r.

By Eq. (1.59), the definition of the S-matrix, it will have a pole at the resonance spectral energy $E_r - i\Gamma/2$. Since, for small Γ, the difference in values of the Jost functions at energy $E_r - i\Gamma/2$ and at energy E_r is small, the S-matrix must have very large values at the energy E_r. It cannot, however, have a pole at this energy. The S-matrix is, in turn, related to the phase-shift and cross-section, which will also have comparatively large values at the real part of the resonance energy, E_r; hence the

peaks and troughs in the data at these energy values.

A wide resonance has a large resonance width, Γ. Corresponding peaks in cross-section data at resonance energies will thus be flatter and wider too, and will have very short lifetimes, by Eq. (1.94).

For multi-channel scattering, the total cross-section is the sum of all the partial wave cross-sections, where the effect of all the possible resonances add together. Thus, all the peaks in the data do not necessarily represent resonances, and can arise from channel overlap. Such overlap can even occur with resonances of the same partial wave. If, however, the Jost matrices can accurately be constructed from the scattering data, all spectral points can accurately be determined. This is the crux of this thesis. Multi-channel resonances must first be discussed in more detail.

Multi-channel resonances

Consider the following hypothetical multi-channel scattering process which occurs via the intermediate resonance state R:

$$A+B \to R \to \begin{cases} A+B \\ C+D \\ \text{etc.} \end{cases} .$$

After it is formed, the resonance state R may decay into any one of the open channels, irrespective of how it is formed. This again implies that only the outgoing spherical wave exists far from the interaction region. By Eq. (1.54), for resonance spectral energies $\mathcal{E}_i$,

$$\det\left[f^{(\text{in})}(\mathcal{E}_i)\right] = 0. \tag{1.95}$$

Using identical arguments to the single-channel case, it can again be shown that resonances correspond to spectral energies with:

$$\mathcal{E}_i = E_r - \frac{i}{2}\Gamma, \tag{1.96}$$

where Γ is now the total resonance width of the multi-channel resonance.

As with bound states, there are two possible choices of the sign for k_n from Eq. (1.36), since $k_n = \pm\sqrt{\frac{2\mu_n}{\hbar^2}(E - E_n)}$. The positive choice for all n corresponds with the physical sheet, and the negative choice with the unphysical sheet of the Riemann surface. It must still be shown that the resonance energy, $\mathcal{E}_i$, belongs to the unphysical sheet. It has been mentioned that only the outgoing spherical waves for each channel can exist for large r. The asymptotic behaviour of the radial wave-functions at a resonance energy is then given by:

$$\begin{aligned} U(\mathcal{E}_i, r) &\xrightarrow[r\to\infty]{} W^{(\text{out})}(\mathcal{E}_i, r) f^{(\text{out})}(\mathcal{E}_i) \\ &\xrightarrow[r\to\infty]{} \begin{pmatrix} -i^{\ell_1+1}e^{ik_1 r} & 0 & \cdots & 0 \\ 0 & -i^{\ell_2+1}e^{ik_2 r} & \cdots & 0 \\ \vdots & \vdots & \ddots & \vdots \\ 0 & 0 & \cdots & -i^{\ell_N+1}e^{ik_N r} \end{pmatrix} f^{(\text{out})}(\mathcal{E}_i), \end{aligned}$$

where $k_n = \pm\sqrt{\frac{2\mu_n}{\hbar^2}(\mathcal{E}_i - E_n)}$. If $\text{Im}(k_n) > 0$, the wave-function will vanish at large r, which is only possible for bound state solutions. Thus $\text{Im}(k_n) < 0$, which corresponds with a negative choice in the sign of k_n, and resonances must be located on the unphysical sheet of the Riemann surface. Similar to bound states, resonances correspond to poles of the S-matrix, but these energy poles are complex with negative imaginary part and they are specifically on the unphysical sheet of the Riemann surface.

There are further complications with multi-channel resonances. Consider the decay for a multi-channel system of particles, which can occur via numerous channels. This means that the multi-channel differential equation describing decay is given by [2]:

$$\frac{dN(t)}{dt} = -\frac{\Gamma_1}{\hbar}N(t) - \frac{\Gamma_2}{\hbar}N(t) - \ldots = -\frac{1}{\hbar}(\Gamma_1 + \Gamma_2 + \ldots)N(t) = -\frac{\Gamma}{\hbar}N(t). \quad (1.97)$$

Each open channel then has a decay constant, and therefore also a channel resonance

width, associated with it. The sum of the channel widths gives the total width:

$$\Gamma = \Gamma_1 + \Gamma_2 + ...\Gamma_N, \tag{1.98}$$

which can be seen from Eq. (1.97). The ratio of a particular channel partial width and the total width, Γ_n/Γ, gives the probability that a resonance will decay through, or can be excited from that particular channel [17].

There are different methods for determining the partial widths, but these methods unfortunately do not always agree. The most common method approximates the S-matrix elements near a resonance energy as follows [3]:

$$S_{nn'}(E \to \mathcal{E}_i) \approx \text{const}\left(1 - \frac{i\sqrt{\Gamma_n \Gamma'_n}}{E - \mathcal{E}_i + \frac{i}{2}\Gamma}\right), \tag{1.99}$$

which is obtained from the Breit-Wigner parameterisation, given in Ref. [1]. From this approximation it can be shown, for a two channel problem, that the ratio of the two channel widths is given by:

$$\frac{\Gamma_1}{\Gamma_2} = \lim_{E \to \mathcal{E}_i} \left| \frac{S_{11}(E)}{S_{22}(E)} \right|. \tag{1.100}$$

At the spectral energy $\mathcal{E}_i$, from Eq. (1.59), the matrix elements S_{11} and S_{22} have singularities which arise from the factor $1/\det\left[f^{(\text{in})}(\mathcal{E}_i)\right]$. This factor is the same in both S_{11} and S_{22} and comes from the fact that the inverse matrix, $f^{(\text{in})}$, can be written in terms of the inverse of its determinant. In dividing these matrix elements, the singular factors cancel out exactly, and it can be shown that,

$$\frac{\Gamma_1}{\Gamma_2} = \left| \frac{f_{11}^{(\text{out})} f_{22}^{(\text{in})} - f_{12}^{(\text{out})} f_{21}^{(\text{in})}}{f_{22}^{(\text{out})} f_{11}^{(\text{in})} - f_{21}^{(\text{out})} f_{12}^{(\text{in})}} \right|_{E=\mathcal{E}_i}. \tag{1.101}$$

The elements of the Jost matrices therefore allow the partial widths for a two-channel problem to be calculated. This particular method belongs to a group of methods which relies on principles similar to the "Fermi Golden Rule" (see Ref. [18] for example). In general, for the methods of this group, Eq. (1.98) holds very well for

sharp, long-lived resonances, but not necessarily for wider, short-lived resonances.

In a second group of methods, partial widths are determined by considering the asymptotic behaviour of the multi-channel resonance state vector:

$$|R\rangle \xrightarrow[r\to-\infty]{} \begin{pmatrix} \mathcal{A}_1|\psi_1\rangle \\ \mathcal{A}_2|\psi_2\rangle \\ \vdots \end{pmatrix}, \tag{1.102}$$

where ψ_n is the wave-vector associated with the channel, n. The amplitude, $\mathcal{A}_n$, gives the probability of finding the system in the channel n and is therefore related to Γ_n. Such a method is discussed in great detail in Ref. [18], where the ratio of two channel widths is shown to depend on the probability amplitudes as follows:

$$\frac{\Gamma_n}{\Gamma_{n'}} = \frac{\mu_{n'}\mathrm{Re}(k_n)|\mathcal{A}_n|^2}{\mu_n\mathrm{Re}(k_{n'})|\mathcal{A}_{n'}|^2}. \tag{1.103}$$

These probability amplitudes are, in fact, the resonance state Asymptotic Normalisation Coefficients (ANC), which will be discussed in detail in Chapter 4. It will also be shown that the ANC is related to the S-matrix residue by:

$$\mathrm{Res}[S_{nn'},\mathcal{E}_i] = i(-1)^{\ell_n+1}\frac{\hbar^2 k_n}{\mu_n}\mathcal{A}_n^2, \tag{1.104}$$

where $\mathrm{Res}[S_{nn'},\mathcal{E}_i]$ is the S-matrix residue at resonance energy $\mathcal{E}_i$, μ_n is the reduced mass for the channel n and k_n is the channel momentum given by Eq. (1.36).

Using this, the ratio of widths are then determined with:

$$\frac{\Gamma_n}{\Gamma_{n'}} = \left|\frac{\mathrm{Res}[S_{nn}]}{\mathrm{Res}[S_{n'n'}]}\cdot\frac{k_{n'}\mathrm{Re}(k_n)}{k_n\mathrm{Re}(k_{n'})}\right|_{E=\mathcal{E}_i}. \tag{1.105}$$

For a two-channel problem, the S-matrix residue, which is also a matrix, can be calculated with the Jost matrices as follows (which will be derived in the next section):

$$\mathrm{Res}[S,E] = f^{(\mathrm{out})}(E) \begin{pmatrix} f_{22}^{(\mathrm{in})}(E) & -f_{12}^{(\mathrm{in})}(E) \\ -f_{21}^{(\mathrm{in})}(E) & f_{11}^{(\mathrm{in})}(E) \end{pmatrix} \frac{1}{\frac{d}{dE}\det\left[f^{(\mathrm{in})}(E)\right]}. \tag{1.106}$$

Implementing this, the ratio of partial widths for two channel scattering is given by:

$$\frac{\Gamma_1}{\Gamma_2} = \left| \frac{f_{11}^{(\mathrm{out})} f_{22}^{(\mathrm{in})} - f_{12}^{(\mathrm{out})} f_{21}^{(\mathrm{in})}}{f_{22}^{(\mathrm{out})} f_{11}^{(\mathrm{in})} - f_{21}^{(\mathrm{out})} f_{12}^{(\mathrm{in})}} \cdot \frac{k_2 \mathrm{Re}(k_1)}{k_1 \mathrm{Re}(k_2)} \right|_{E=\mathcal{E}_i}. \tag{1.107}$$

For very sharp resonances, the total width Γ is very small. From Eq. (1.36), the channel momentum at a resonance energy $\mathcal{E}_i = E_r - (i/2)\Gamma$ has a small imaginary part, thus $k_n \approx \mathrm{Re}(k_n)$, and Eq. (1.107) reduces to (1.101), as expected. This principle is applicable to multi-channel scattering with any number of channels, not just two.

This kinematic factor, $[k_{n'}\mathrm{Re}(k_n)]/[k_n\mathrm{Re}(k_{n'})]$, arises from the differences in the time of flight of the decay in the different channels, as discussed in Ref. [18]. The approximation, Eq. (1.99), requires a similar kinematic factor for greater accuracy.

The partial widths calculated for the two-channel scattering problems in Chapter 3 of this thesis are for sufficiently narrow resonances so that Eq. (1.101) may safely be used.

Much more can be said about resonances in general, but the discussion so far is almost sufficient for the purposes of this thesis. A few words on other possible spectral points as well as the distribution of bound and resonance state spectral points follows.

1.5.4 Other spectral points and distribution

Apart from the spectral points, $\mathcal{E}_i$, such that $\det[f_\ell^{(\mathrm{in})}(\mathcal{E}_i)] = 0$, which represent true bound and resonances states that have a clear physical interpretation, there are other spectral points that do not necessarily correspond to a physical realisable state. Con-

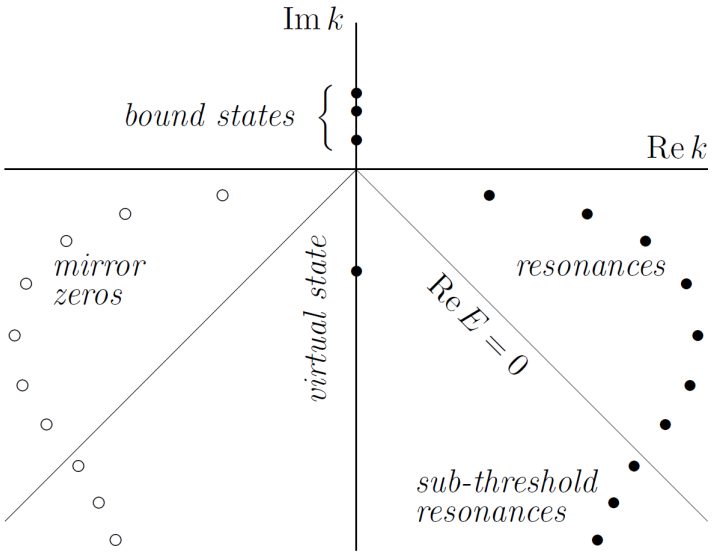

Figure 1.2: Typical distribution of the spectral points on the complex momentum plane, as published in Ref. [19].

sider the spectral points located at real, negative energies on the unphysical sheet of the energy Riemann surface. These are usually referred to as *virtual* states, but some texts also use the term *anti-bound* states. They correspond to pure complex, negative channel momenta:

$$k_n = -i\sqrt{2\mu_n|E_n|/\hbar^2}. \tag{1.108}$$

As shown in Figure 1.2, they are on the negative imaginary axis of the complex plane. Mathematically they are identical to resonances, but with zero width. They cannot exist for physical energies, though. Bound states of course exist due to attractive potentials between particles, but if the attraction is too weak, virtual states can be obtained. These virtual states are bound states *in potentia*, as it were. If the attraction is stronger, they can "move" up the imaginary k-axis to become proper bound states. Apart from virtual states, bound states can also "transform" into resonances if the attractive part of a potential is weakened.

Figure 1.2 also shows the typical distribution of the resonances. The resonances, given by $\mathcal{E}_i = E_r - \frac{i}{2}\Gamma$, will usually appear in a type of trajectory or curve formed by discrete points in the complex k-plane. Furthermore, there are technically infinitely many possible resonances [19], with the trajectory curving in such a way that

corresponds with $E_r \to -\infty$ and $\Gamma \to \infty$. Generally, resonances that occur at physical (positive) energies are the most important. Furthermore, wide resonances with large Γ are so short-lived, they are often difficult to locate and of less importance in a physical process.

Those resonances with $E_r < 0$ are known as sub-threshold resonances, and are obviously physically unattainable. However, such resonance can have a marked impact on the physical cross-sections at low, positive energies and can influence low-energy scattering significantly. Virtual states are then specifically sub-threshold resonances with zero width.

A third resonance spectral point with negative $\mathrm{Re}(k)$ arises due to the symmetries of the Jost matrices. As shown in Figure 1.2, each of the true resonances (including sub-threshold resonances) has a mirror resonance with negative $\mathrm{Re}(k)$ [19]. These mirror resonances have no influence on the physical scattering process.

The Jost matrices provide a unified method to calculate all of these spectral points, as well as the corresponding S-matrix residues. The relationship between the Jost matrices and the S-matrix residue will be discussed in the next section, before moving on to scattering states.

1.5.5 The S-matrix residue

The S-matrix residue is a useful quantity in numerous respects. Most importantly, it can be calculated with the Jost matrices, as will be shown in this section. For the purpose of this thesis, its relationship with the ANC is used to determine these values for the two physical systems of Chapters 5 and 6.

Firstly, the S-matrix residue must be defined. The S-matrix elements are complex functions of energy and can be expanded in the Laurent series as follows:

$$S_{nm}(E) = \frac{R_{nm}}{E-\mathcal{E}_i} + D^{(0)}_{nm} + D^{(1)}_{nm}(E-\mathcal{E}_i) + D^{(2)}_{nm}(E-\mathcal{E}_i)^2 + \cdots, \tag{1.109}$$

where $\mathcal{E}_i$ represents a spectral point energy (either a bound state or a resonance). At

the limit $E \to \mathcal{E}_i$, the first term dominates the expansion, so:

$$S_{nm}(E) \xrightarrow[E\to\mathcal{E}_i]{} \frac{R_{nm}}{E-\mathcal{E}_i}. \tag{1.110}$$

The residue of each S-matrix element at a spectral point, $\mathcal{E}_i$, is then defined as $\text{Res}\left[S_{nm},\mathcal{E}_i\right] = R_{nm}$, which can then be determined with:

$$\text{Res}\left[S_{nm},\mathcal{E}_i\right] = \lim_{E\to\mathcal{E}_i}(E-\mathcal{E}_i)S_{nm}(E). \tag{1.111}$$

Since the S-matrix is related to the Jost matrices, a direct relationship between the S-matrix residue and the Jost matrices can be derived. First consider $\det\left[f^{(\text{in})}(E)\right]$, which is an energy dependent function. The analytic structure of the Jost matrices will be discussed in a Chapter 3, but they are analytic in energy except, possibly, at the threshold energies E_n. Thus the determinant of the Jost matrices must also be entire in energy, and so $\det\left[f^{(\text{in})}(E)\right]$ can be expanded in the Taylor series around a spectral energy $\mathcal{E}_i$:

$$\det\left[f^{(\text{in})}(E)\right] = \det\left[f^{(\text{in})}(\mathcal{E}_i)\right] + (E-\mathcal{E}_i)\frac{d}{dE}\det\left[f^{(\text{in})}(E)\right]\Big|_{\mathcal{E}_i} + \cdots. \tag{1.112}$$

At a spectral point, $\det\left[f^{(\text{in})}(\mathcal{E}_i)\right] = 0$. Also, if $E \to \mathcal{E}_i$, all higher-order terms may be omitted. Thus:

$$\lim_{E\to\mathcal{E}_i}\det\left[f^{(\text{in})}(E)\right] \approx (E-\mathcal{E}_i)\frac{d}{dE}\det\left[f^{(\text{in})}(E)\right]\Big|_{\mathcal{E}_i} \tag{1.113}$$

Now the inverse of a matrix can be written in terms of the determinant of said matrix and its adjugate [20], thus the S-matrix can be written as follows:

$$S(E) = f^{(\text{out})}(E)\left[f^{(\text{in})}(E)\right]^{-1} = f^{(\text{out})}(E)\,\text{adj}\left[f^{(\text{in})}(E)\right]\frac{1}{\det\left[f^{(\text{in})}(E)\right]}. \tag{1.114}$$

For an arbitrary 2×2 matrix, M, given by:

$$M = \begin{pmatrix} m_{11} & m_{12} \\ m_{21} & m_{22} \end{pmatrix}, \tag{1.115}$$

the adjugate, also called the classical adjoint or adjunct, is given by:

$$\text{adj}(M) = \begin{pmatrix} m_{22} & -m_{12} \\ -m_{21} & m_{11} \end{pmatrix}. \tag{1.116}$$

The adjugate for a $N \times N$ matrix is more complex, but it can easily be determined with an appropriate algorithm. For further details, see Ref. [20].

Multiplying Eq. (1.114) by $(E - \mathcal{E}_i)$, taking the limit as $E \to \mathcal{E}_i$ and substituting Eq. (1.113) then gives:

$$\lim_{E \to \mathcal{E}_i} (E - \mathcal{E}_i) S(E) = \lim_{E \to \mathcal{E}_i} f^{(\text{out})}(E) \, \text{adj} \left[f^{(\text{in})}(E) \right] \frac{1}{\frac{d}{dE} \det \left[f^{(\text{in})}(E) \right]_{\mathcal{E}_i}}. \tag{1.117}$$

And so, using Eq. (1.111), the S-matrix residue is given by:

$$\text{Res}\left[S, \mathcal{E}_i\right] = f^{(\text{out})}(\mathcal{E}_i) \, \text{adj} \left[f^{(\text{in})}(\mathcal{E}_i) \right] \frac{1}{\frac{d}{dE} \det \left[f^{(\text{in})}(E) \right]_{\mathcal{E}_i}}, \tag{1.118}$$

which is exactly Eq. (1.106) used to determine partial resonance widths. For single-channel scattering, this reduces to the following simple relation:

$$\text{Res}\left[S, \mathcal{E}_i\right] = \frac{f^{(\text{out})}(\mathcal{E}_i)}{\dot{f}_{\ell}^{(\text{in})}(\mathcal{E}_i)}, \tag{1.119}$$

where the dot indicates the energy derivative of the Jost function.

The derivative of the determinant (or for any function) can be determined numerically with:

$$\frac{d}{dE} \det \left[f^{(\text{in})}(E) \right] = \frac{\det \left[f^{(\text{in})}(E + \varepsilon) \right] - \det \left[f^{(\text{in})}(E - \varepsilon) \right]}{2\varepsilon}. \tag{1.120}$$

A value of $\varepsilon = 10^{-6}$ MeV is generally used in the calculations, resulting in an accuracy of at least five digits.

So much on the S-matrix residue. In the next section on scattering states, the scattering cross-section will be discussed in particular.

1.5.6 Scattering states

An important distinguishing feature of scattering states in a specific channel is that the initial incoming state of the channel, which will be defined by its channel momentum vector $\mathbf{k}_n$, with $|\mathbf{k}_n| = k_n$, together with the outgoing state, determines the scattering. Bound and resonances states, on the other hand, are not defined by the incoming state vector. Furthermore, physical scattering occurs at positive energies above the threshold energies. Also recall that the two-body scattering of particles is effectively equivalent to the scattering of a single particle in a central potential.

Differential scattering cross-section

In the quantum ensemble picture, the scattering states do not describe the effective interaction of a single particle, but of a flux of particles. The particle flux, or probability current of each channel, is given in terms of the time-independent wave function by [11]:

$$\mathbf{j}_n = \frac{\hbar}{2i\mu_n}\left[\psi_n^*(\mathbf{r})\nabla\psi_n(\mathbf{r}) - \psi_n(\mathbf{r})\nabla\psi_n^*(\mathbf{r})\right]. \tag{1.121}$$

The scattering cross-section, σ, is a measure of the probability that scattering will take place for an incoming beam of particles that interact with a target. It is determined from the differential cross-section with:

$$\sigma = \int \frac{d\sigma}{d\Omega} d\Omega. \tag{1.122}$$

The differential cross-section, in turn, is the number of particles scattered into the element of solid angle, $d\Omega$, in the direction of $\mathbf{r}$, given by $\hat{r} = (\theta, \varphi)$, per unit time

and incident flux, $\mathbf{j}^{\text{in}}$:

$$\frac{d\sigma}{d\Omega} = \frac{1}{|\mathbf{j}^{\text{in}}|}\frac{dN}{d\Omega}, \tag{1.123}$$

where N is the number of particles scattered in the direction $\hat{r}$. The infinitesimal number of particles, dN, scattered into an element of solid angle, $d\Omega$, in the direction, $\hat{r}$, and passing through the surface element, $dA = r^2 d\Omega$ per unit time, is given by [11]:

$$dN = j^{\text{sc}} r^2 d\Omega \tag{1.124}$$

where j^{sc} is the scattered flux in the direction $\hat{r}$. The differential cross-section for a specific channel n, is then related to the ratio of the outgoing radial flux and the incoming flux for the relevant channel:

$$d\sigma = \frac{j_n^{\text{sc}} r^2}{|\mathbf{j}_n^{\text{in}}|} d\Omega. \tag{1.125}$$

All that remains is to determine the nature of the incoming and outgoing waves to calculate the corresponding flux.

The incident beam consists of plane waves at $r \to -\infty$, well before interaction with the target, the source of the central potential, takes place. After scattering, far from the target and the interaction region, the physical wave consists of unscattered plane waves as well as outgoing scattered spherical waves [11]. Refer to Figure 1.3, which represents this process for a single channel. The channel wave-functions as $r \to \infty$ are then given by:

$$\psi_n(E,r) \xrightarrow[r\to\infty]{} (2\pi)^{-3/2} e^{i\mathbf{k}_n\cdot\mathbf{r}} + (2\pi)^{-3/2} \mathbf{f}_n(\hat{r} \leftarrow \hat{k}_n)\frac{e^{ik_n r}}{r}, \tag{1.126}$$

where the first term is the incoming plane-wave part and will be denoted by,

$$\psi_n^{(\text{in})} = (2\pi)^{-3/2} e^{i\mathbf{k}_n\cdot\mathbf{r}}. \tag{1.127}$$

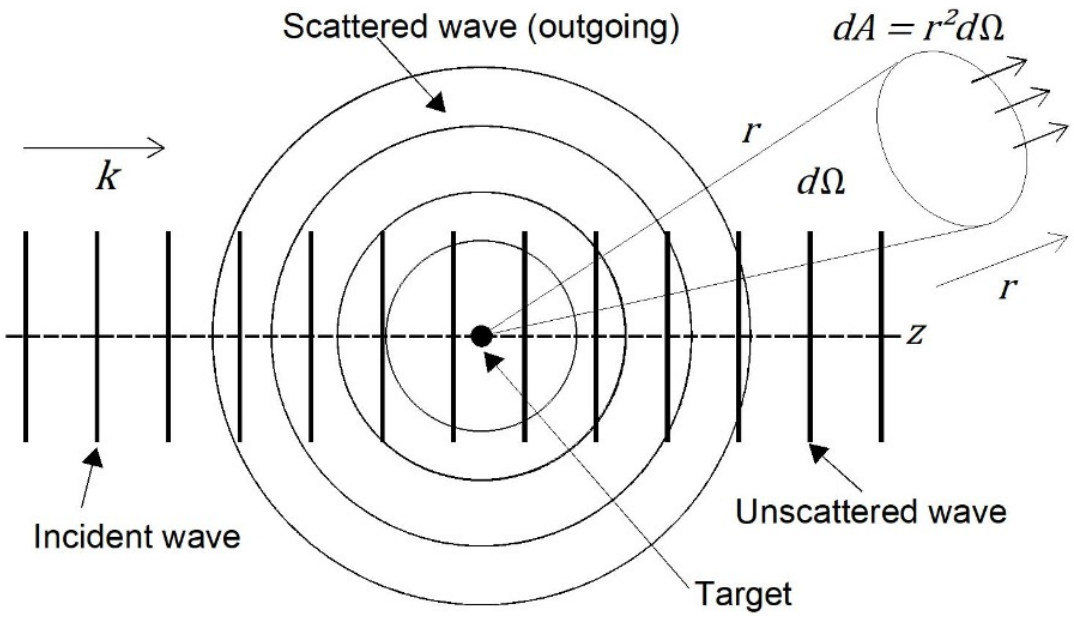

Figure 1.3: Incident and scattered waves.

The second term is the outgoing scattered radial wave, denoted by,

$$\psi_n^{(\mathrm{sc})} = (2\pi)^{-3/2}\mathbf{f}_n(\hat{r} \leftarrow \hat{k}_n)\frac{e^{ik_n r}}{r}. \tag{1.128}$$

This can be seen by considering the asymptotic behaviour of the outgoing Riccati-Hankel function, Eq. (1.48). The constant, $(2\pi)^{-3/2}$, arises from the correct normalisation of the wave-function [3]. The factor $\mathbf{f}_n(\hat{r} \leftarrow \hat{k}_n)$ is called the scattering amplitude for the channel n, and is a very important quantity in quantum scattering. It will also be defined in terms of the Jost matrices in this work.

The corresponding flux magnitude for the incoming wave is then:

$$|\mathbf{j}_n^{\mathrm{in}}| = (2\pi)^{-3}\frac{\hbar k_n}{\mu_n}, \tag{1.129}$$

and the flux in the direction $\hat{r}$ of the outgoing wave is:

$$j_n^{\mathrm{sc}} = (2\pi)^{-3}\frac{\hbar k_n}{\mu_n r^2}\left|\mathbf{f}_{\mathrm{n}}(\hat{r} \leftarrow \hat{k}_n)\right|^2. \tag{1.130}$$

Substituting these expressions into Eq. (1.125) gives the very important result for

the channel differential cross-section:

$$\frac{d\sigma}{d\Omega} = \left|\mathbf{f}_n(\hat{r} \leftarrow \hat{k}_n)\right|^2. \tag{1.131}$$

This result holds for all scattering processes, since it can be shown that the asymptotic behaviour of the time-independent wave-function for any scattering process can be written in the form of Eq. (1.126). In the remainder of this introductory chapter, it will be shown how this structure can be obtained for multi-channel scattering with zero spin. The structure can also be obtained for the scattering of charged particles and particles with with non-zero spin, which is the focus of Chapter 2.

The simplest possible scattering state, where there is no interaction potential, will first be considered.

Free-particle scattering

The time-independent equation (1.20) for a free-particle (there is no interaction potential; $U_{nn'}(\mathbf{r}) = 0$) reduces to the following:

$$\left[\frac{\hbar^2}{2\mu_n}\Delta_{\mathbf{r}} + (E - E_n)\right] \psi_n(E, r) = 0,$$

with the solution of each channel given by [11]:

$$\psi_{\mathbf{k}_n}(\mathbf{r}) = (2\pi)^{-3/2} e^{i\mathbf{k}_n \cdot \mathbf{r}}, \qquad U_{nn'} = 0, \tag{1.132}$$

where the channel states are defined by the incoming channel momentum vectors, $\mathbf{k}_n$, with $|\mathbf{k}_n| = k_n$.

These solutions are correctly normalised by:

$$\int \psi^*_{\mathbf{k}'}(\mathbf{r})\psi_{\mathbf{k}}(\mathbf{r})d\mathbf{r} = \delta(\mathbf{k}' - \mathbf{k}), \tag{1.133}$$

which is obtained from Eq. (1.1), the normalisation requirement of the state vector.

Notice that the plane wave-solution, Eq. (1.132), is not a physically realisable state in itself, and the normalisation is not discrete [22].

The full wave-solution for an N-channel scattering problem is the column matrix comprised of these channel plane waves:

$$\Psi(E,r) = \begin{pmatrix} \psi_{\mathbf{k}_1}(E,\mathbf{r}) \\ \psi_{\mathbf{k}_2}(E,\mathbf{r}) \\ \vdots \\ \psi_{\mathbf{k}_N}(E,\mathbf{r}) \end{pmatrix}. \tag{1.134}$$

If the interaction potential is zero, the reduced potential $V_{nn'}(r) = 0$ and the radial equation (1.37) has a solution similar to Eq. (1.54), with

$$f^{(\text{in/out})}(E) = F^{(\text{in/out})}(E) = \frac{1}{2}I,$$

by Eq. (1.70) and (1.71) as well as boundary conditions (1.72) on page 24. By Eq. (1.76), the physical radial solutions are then given by:

$$U(E,r) = \frac{1}{2}W^{(\text{in})}(E,r)\,\mathcal{C} + \frac{1}{2}W^{(\text{out})}(E,r)\,\mathcal{C} = J(E,r)\,\mathcal{C}, \qquad V = 0, \tag{1.135}$$

where Eq. (1.73) has also been used. The elements of the column-matrix of radial solutions are then given by,

$$u_n(E,r) = j_{\ell_n}(k_n r)\,C_n, \qquad V_{nn'} = 0. \tag{1.136}$$

Using Eq. (1.34), the time-independent partial wave-solutions for each channel is given by:

$$\psi_n(E,\mathbf{r}) = \frac{1}{r}j_{\ell_n}(k_n r)C_n Y_{\ell_n m_n}(\theta,\varphi), \qquad V_{nn'} = 0. \tag{1.137}$$

Recall that the summation over all partial waves is omitted, since a partial wave defined by a specific ℓ_n and m_n can be considered as another channel.

In general, however (see Ref. [21] for example), the channel plane wave in the partial

wave expansion is given by:

$$\psi_{\mathbf{k}_n}(\mathbf{r}) = \sqrt{\frac{2}{\pi}}\frac{1}{k_n r}\sum_{\ell_n m_n} i^{\ell_n} j_{\ell_n}(k_n r_n) Y^*_{\ell_n m_n}(\hat{k}_n) Y_{\ell_n m_n}(\hat{r}) \tag{1.138}$$

where $\hat{k}_n = (\theta_{k_n}, \varphi_{k_n})$ is the unit vector in the direction of $\mathbf{k}_n$. Similarly, $\hat{r} = (\theta, \varphi)$ is the unit vector in the direction of $\mathbf{r}$.

The axes can be chosen so that the direction of the incoming channel vectors $\mathbf{k}_n$ correspond to the z-axis, then $Y^*_{\ell_n, m_n}(\hat{k}_n)$ reduces to a constant [11]. Furthermore, a single partial wave defined by a specific ℓ_n and m_n can be considered, thus the summation can be omitted. The expression (1.138) then becomes identical to Eq. (1.137), with specific values for the channel constants, C_n.

The expression (1.138) is then consistent with the preceding discussion, but it is more general. Comparison with Eq. (1.132) then gives the following useful relation:

$$e^{i\mathbf{k}_n\cdot\mathbf{r}} = \frac{4\pi}{k_n r}\sum_{\ell_n m_n} i^{\ell_n} j_{\ell_n}(k_n r) Y^*_{\ell_n m_n}(\hat{k}_n) Y_{\ell_n m_n}(\hat{r}) \tag{1.139}$$

Further notice that Eq. (1.138) is a solution of the time-independent equation, (1.20), and that it must be normalised by Eq. (1.133) on page 44. This can easily be shown, since the Riccati-Bessel function has the following normalisation [14]:

$$\int_0^\infty j_\ell(k'r) j_\ell(kr) dr = \frac{\pi}{2}\delta(k'-k), \tag{1.140}$$

and the Spherical harmonics are orthonormal (see Eq. (1.27)). Now consider general scattering where the interaction potential is non-zero.

Scattering amplitude

From the structure of the plane wave-solution, Eq. (1.138), the following is proposed for the general time-independent solution for a non-zero, short-ranged potential:

$$\psi_n(E,\mathbf{r}) = \sqrt{\frac{2}{\pi}}\frac{1}{k_n r}\sum_{n'}^{N}\sum_{\ell_n m_n} i^{\ell_n}\left[h_{\ell_n}^{(-)}(k_n r)F_{nn'}^{(\text{in})}(E,r)+\right.$$

$$\left.h_{\ell_n}^{(+)}(k_n r)F_{nn'}^{(\text{out})}(E,r)\right]\frac{1}{2}[f^{(\text{in})}(E,r)]^{-1}_{nn'}Y^*_{\ell_n m_n}(\hat{k}_n)Y_{\ell_n m_n}(\hat{r}). \tag{1.141}$$

As required, this expression has the same normalisation as the plane wave expression, Eq. (1.138). Furthermore, if a single partial wave is considered (instead of summing over all possible partial waves), the proposed expression becomes exactly Eq. (1.78) on page 25 for certain C_n. It can also be shown that Eq. (1.138) is a solution of the time-independent Schrödinger equation (1.20). The inclusion of the inverse Jost matrix factor, $[f^{(\text{in})}(E,r)]^{-1}$, ensures that, at the limit where $r\to\infty$, the expression can be written in the form of Eq. (1.126), as will be shown. The proposed solution is, therefore, entirely valid. Using Eq. (1.66) and the definition of the S-matrix, Eq. (1.59), the following asymptotic behaviour of Eq. (1.141) is obtained:

$$\psi_n(E,\mathbf{r}) \xrightarrow[r\to\infty]{} \frac{1}{2}\sqrt{\frac{2}{\pi}}\frac{1}{k_n r}\sum_{n'}^{N}\sum_{\ell_n m_n} i^{\ell_n}\left[h_{\ell_n}^{(-)}(k_n r)+\right.$$

$$\left.h_{\ell_n}^{(+)}(k_n r)S_{nn'}(E)\right]Y^*_{\ell_n m_n}(\hat{k}_n)Y_{\ell_n m_n}(\hat{r}). \tag{1.142}$$

When adding and subtracting a term $h_{\ell_n}^{(+)}(k_n r)$ inside the bracket and using the fact that $2j_\ell(kr) = h_\ell^{(-)}(kr) + h_\ell^{(+)}(kr)$ from Eq. (1.49), the expression becomes:

$$\psi_n(E,\mathbf{r}) \xrightarrow[r\to\infty]{} \frac{1}{2}\sqrt{\frac{2}{\pi}}\frac{1}{k_n r}\sum_{n'}^{N}\sum_{\ell_n m_n} i^{\ell_n}[2j_{\ell_n}(k_n r)+$$

$$\left.h_{\ell_n}^{(+)}(k_n r)(S_{nn'}(E)-\delta_{nn'})\right]Y^*_{\ell_n m_n}(\hat{k}_n)Y_{\ell_n m_n}(\hat{r}),$$

thus

$$\psi_n(E,\mathbf{r}) \xrightarrow[r\to\infty]{} \sqrt{\frac{2}{\pi}}\frac{1}{k_n r}\sum_{\ell_n m_n} i^{\ell_n} j_{\ell_n}(k_n r) Y^*_{\ell_n m_n}(\hat{k}_n) Y_{\ell_n m_n}(\hat{r})$$

$$+\sqrt{\frac{2}{\pi}}\frac{1}{k_n r}\sum_{n'}^{N}\sum_{\ell_n m_n}\frac{i^{\ell_n}}{2} h^{(+)}_{\ell_n}(k_n r)\left[(S_{nn'}(E)-\delta_{nn'})\right] Y^*_{\ell_n m_n}(\hat{k}_n) Y_{\ell_n m_n}(\hat{r}).$$

Recognising Eq. (1.139) in the first term and substituting the asymptotic behaviour of the Riccati-Hankel function, Eq (1.48) in the second term, gives:

$$\psi_n(E,\mathbf{r}) \xrightarrow[r\to\infty]{} (2\pi)^{-3/2} e^{i\mathbf{k}_n\cdot\mathbf{r}} +$$

$$(2\pi)^{-3/2}\frac{e^{ikr}}{r}\sum_{n'}^{N}\sum_{\ell_n m_n} 4\pi\frac{1}{2ik_n}\left[(S_{nn'}(E)-\delta_{nn'})\right] Y^*_{\ell_n m_n}(\hat{k}_n) Y_{\ell_n m_n}(\hat{r}) \quad .$$

Now the matrix elements of the partial wave amplitude are defined as follows:

$$\mathrm{f}_{nm}(E) \equiv \frac{1}{2ik_n}\left[(S_{nm}(E,r)-\delta_{nm})\right], \tag{1.143}$$

with the full scattering amplitude for a specific channel defined by:

$$\mathbf{f}_n(\hat{r}\leftarrow\hat{k}_n) \equiv 4\pi\sum_{n'=1}^{N}\sum_{\ell_n m_n}\mathrm{f}_{nn'}(E) Y^*_{\ell_n m_n}(\hat{k}_n) Y_{\ell_n m_n}(\hat{r}), \tag{1.144}$$

which results in the required structure for the time-independent state wave-function of each channel, identical to Eq. (1.126):

$$\psi_n(E,r) \xrightarrow[r\to\infty]{} (2\pi)^{-3/2} e^{i\mathbf{k}_n\cdot\mathbf{r}} + (2\pi)^{-3/2}\mathbf{f}_n(\hat{r}\leftarrow\hat{k}_n)\frac{e^{ik_n r}}{r}.$$

Scattering cross-section

The goal is now to find an expression for the scattering cross section from the expression for the partial wave scattering amplitude. Begin by considering the addition

theorem of spherical harmonics, given by [21]:

$$P_\ell(\cos\theta) = \frac{4\pi}{2\ell+1}\sum_{\ell m} Y^*_{\ell m}(\hat{k})Y_{\ell m}(\hat{r}), \tag{1.145}$$

where P_ℓ represent the ordinary Legendre polynomials. The channel scattering amplitude then becomes the following:

$$\mathbf{f}_n(\hat{r} \leftarrow \hat{k}_n) = \sum_{n'=1}^{N}\sum_{\ell_n} \mathrm{f}_{nn'}(E)(2\ell_n+1)P_{\ell_n}(\cos\theta). \tag{1.146}$$

Using Eq. (1.131) and taking the sum over all channels, the total differential cross-section is then:

$$\frac{d\sigma}{d\Omega} = \sum_{n=1}^{N}\sum_{n'=1}^{N}\sum_{\ell_n}\sum_{\ell_n^*}(2\ell_n+1)(2\ell_n^*+1)\left|\mathrm{f}_{nn'}(E)\right|^2 P_{\ell_n}(\cos\theta)P_{\ell_n^*}(\cos\theta)$$

Integrating over the Legendre polynomials give the following [11],

$$\int_0^\pi P_\ell(\cos\theta)P_{\ell^*}(\cos\theta)\sin\theta d\theta = \int_{-1}^{1} P_\ell(x)P_{\ell^*}(x)dx = \frac{2}{2\ell+1}\delta_{\ell\ell^*}, \tag{1.147}$$

and

$$\int_0^{2\pi} d\varphi = 2\pi.$$

Using these expressions in Eq. (1.122) then results in the following total cross-section:

$$\sigma = \sum_{n=1}^{N}\sum_{n'=1}^{N}\sum_{\ell_n} 4(2\ell_n+1)\left|\mathrm{f}_{nn'}(E)\right|^2. \tag{1.148}$$

If only a single partial wave defined by ℓ_n for a specific channel n is considered, it is no longer necessary to sum over all partial waves and the total cross-section can be written in terms of the channel partial wave cross-sections, σ_{nm}:

$$\sigma = \sum_{n=1}^{N}\sum_{n'=1}^{N}\sigma_{nn'}, \tag{1.149}$$

with the channel partial wave cross-sections given by:

$$\sigma_{nm} = 4(2\ell_n + 1)\left|\mathrm{f}_{nm}(E)\right|^2 = \frac{\pi}{k_n^2}(2\ell_n + 1)\left|S_{nm}(E) - \delta_{nm}\right|^2, \tag{1.150}$$

where Eq. (1.143) has also been used.

In general, the partial wave channel cross-sections will be calculated rather than the total cross-section. For the total cross-section, there is much overlap of the various channels and resonance structures often disappear, while these usually appear clearly in the partial wave channel cross-sections.

Eq. (1.150) is then the main result for this section. If the Jost matrices can be determined, the corresponding S-matrix can be found and the partial wave channel cross-sections at scattering energies can also be calculated.

While the derivations have been done for general multi-channel scattering, the single-channel expressions can be obtained by letting the number of channels equal one, $N = 1$. The single-channel partial wave cross-section, for example, is given by:

$$\sigma_\ell = 4(2\ell + 1)\left|\mathrm{f}_\ell(E)\right|^2 = \frac{\pi}{k^2}(2\ell + 1)\left|S_\ell(E) - 1\right|^2. \tag{1.151}$$

The Jost matrices therefore allows bound, resonance and scattering states to be treated in a unified way. There are, however, complications that arise when considering the scattering of particles with non-zero spin, which will be covered in the next chapter. These ideas will also be extend to the scattering of charged particles.

Chapter 2

Scattering with charge and spin

The Jost matrices were introduced in the previous chapter and their relation to scattering quantities such as the cross-section were shown. This was only done for short-range interactions, or the scattering of particles with no charge (neutral particles). The scattered particles also had zero spin. In this chapter, the formalism in terms of the Jost matrices will be extended to include the scattering of charged particles. The scattering of particles with spin will also be considered. The inclusion if spin influences the expression for the scattering cross-section in terms of the Jost matrices.

2.1 Scattering including Coulomb interactions

The derivations that follow are in the context of multi-channel scattering with zero spin. The discussion is, however, very similar for the scattering of particles with non-zero spin involving Coulomb interactions, which will not explicitly be considered in this chapter.

The Coulomb potential describes the interaction between charged particles. The simple charge dependent structure of the potential is obtained from Coulomb's inverse-square law, which was first published in 1785 by the French physicist, Charles-Augustin de Coulomb. The attractive Coulomb interaction between protons in the nucleus of an atom and its orbiting electrons are responsible for atomic

interactions that form molecular compounds, therefore governing all chemical reactions. When considering the scattering of charged nuclei, the Coulomb interactions as well as the short-ranged strong-force nuclear interactions must be taken into consideration.

The Coulomb potential for the interaction between two particles of charge eZ_1 and eZ_2 is given by:

$$U^c(r) = \frac{e^2 Z_1 Z_2}{r}. \tag{2.1}$$

The Sommerfeld parameter, η, is defined by:

$$\eta \equiv \frac{\mu e^2 Z_1 Z_2}{k\hbar^2}, \tag{2.2}$$

which allows the reduced Coulomb potential for a single channel to be written as follows, by Eq. (1.39) on page 15:

$$V^c(r) = \frac{2k\eta}{r}. \tag{2.3}$$

It is clear that the Coulomb potential is less singular than $1/r^2$ at the origin, but it tends to zero slowly as $r \to \infty$. Therefore it is long-ranged. The mathematical implication is that, in the radial Schrödinger equation (1.37), the term $\ell(\ell+1)/r^2$ would tend to zero faster than the Coulomb potential. This is problematic, as the Jost matrices are defined at $r \to \infty$ where it is assumed the potential is zero, but the term $\ell(\ell+1)/r^2$ is still present. Some modification of the formalism is necessary. The modification of the radial equation will first be considered.

2.1.1 Radial wave-equation for Coulomb scattering

For scattering involving short- and long-ranged interactions, the two-body Hamiltonian of Eq. (1.5) will be modified by including a Coulomb operator, U^c:

$$\hat{H} = \hat{H}_1^0 + \hat{H}_2^0 + \hat{U}(\mathbf{r}_1 - \mathbf{r}_2) + \hat{U}^c(\mathbf{r}_1 - \mathbf{r}_2) + \hat{h}, \tag{2.4}$$

with:

$$\langle n|\hat{U}^c|n'\rangle = U^c_{nn'} = \frac{e^2 Z_1 Z_2}{r}\delta_{nn'}. \tag{2.5}$$

Proceeding in exactly the same way as Section 1.4, it can be shown that the N coupled Schrödinger equations (1.20) for scattering involving Coulomb interaction is given by:

$$\left[\frac{\hbar^2}{2\mu_n}\Delta_{\mathbf{r}} + (E - E_n) - \frac{e^2 Z_1 Z_2}{r}\right]\psi_n(E,r) = \sum_{n'=1}^{N} U_{nn'}(\mathbf{r})\psi_{n'}(E,r). \tag{2.6}$$

Following the same procedure of Section 1.3, but taking this extra potential term into account, it can be shown that the N coupled radial Schrödinger equations (1.37) on page 15 then becomes:

$$\left[\partial_r^2 + k_n^2 - \frac{\ell_n(\ell_n+1)}{r^2} - \frac{2k_n\eta_n}{r}\right]u_n(E,r) = \sum_{n'=1}^{N} V_{nn'}(r)u_{n'}(E,r). \tag{2.7}$$

where $V_{nn'}$ represents the short-ranged reduced potential matrix responsible for the coupling. It is determined by Eq. (1.38) and its elements tend to zero faster than $1/r^2$. The extra term $2k_n\eta_n/r$ is the reduced Coulomb potential for the channel n, with the channel Sommerfeld parameters given by:

$$\eta_n \equiv \frac{\mu e^2 Z_1 Z_2}{k_n \hbar^2}. \tag{2.8}$$

It is always the requirement that any physical wave-function must be finite at $r = 0$. For this reason, the channel radial wave-functions must still have regular behaviour near the origin [3], identical to Eq. (1.40):

$$u_n(E,r) \xrightarrow[r\to\infty]{} 0, \qquad n = 1,2,3,...,N.$$

As before, there are $2N$ linearly-independent column solutions to Eq. (2.7), and only half are regular at the origin. The regular columns are again combined to form the square *fundamental matrix of the regular solutions* identical to Eq. (1.42). For non-

Coulomb scattering and specific choices of the boundary conditions of the matrices $F^{(\text{in/out})}$, it was shown that, at the origin, this matrix specifically behaves like a diagonal matrix with the Riccati-Bessel functions on the diagonal; Eq. (1.75). This will now be used as condition for $\Phi(E,r)$, which, by Eq. (1.50) can then be written in terms of the diagonal matrix L near the origin:

$$\Phi(E,r) \underset{r\to 0}{\longrightarrow} L^{-1} \begin{pmatrix} (k_1 r)^{\ell_1+1} & 0 & \cdots & 0 \\ 0 & (k_2 r)^{\ell_2+1} & \cdots & 0 \\ \vdots & \vdots & \ddots & \vdots \\ 0 & 0 & \cdots & (k_N r)^{\ell_1+1} \end{pmatrix},$$

with L defined as follows:

$$L \equiv \begin{pmatrix} (2\ell_1+1)!! & 0 & \cdots & 0 \\ 0 & (2\ell_2+1)!! & \cdots & 0 \\ \vdots & \vdots & \ddots & \vdots \\ 0 & 0 & \cdots & (2\ell_N+1)!! \end{pmatrix}. \tag{2.9}$$

Since the only prerequisite is that the matrix elements are regular at the origin, this condition for $\Phi(E,r)$ is perfectly acceptable. Also as before, any physical solution is a linear combination of the columns of $\Phi(E,r)$, thus $U(E,r) = \Phi(E,r)\mathcal{C}$ from Eq. (1.43) and regular behaviour of the physical solution as $r \to 0$ is guaranteed. The Jost matrices will be defined with the asymptotic behaviour of $\Phi(E,r)$, as before. This behaviour for Coulomb scattering will be determined.

2.1.2 Pure Coulomb scattering

If there is no short-ranged interaction potential, $U_{nn'} = 0$ and Eq. (2.6) becomes an uncoupled system of pure Coulomb Schrödinger equations:

$$\left[\frac{\hbar^2}{2\mu_n}\Delta_{\mathbf{r}} + (E - E_n) - \frac{e^2 Z_1 Z_2}{r}\right] \psi_n(E,r) = 0. \tag{2.10}$$

The solutions are complicated Coulomb-modified plane-waves, with the requirement that they become like plane waves for large r [22]. The boundary condition for the solutions are then given by [3]:

$$\psi^{(\pm)}_{\mathbf{k}_n}(\mathbf{r}) \xrightarrow[r\to\infty]{} e^{\pm i\mathbf{k}_n\cdot\mathbf{r}\pm i\eta\ln(k_n r-\mathbf{k}_n\cdot\mathbf{r})}. \tag{2.11}$$

The N pure Coulomb radial equations are given by:

$$\left[\partial_r^2 + k_n^2 - \frac{\ell_n(\ell_n+1)}{r^2} - \frac{2k_n\eta_n}{r}\right] u_n(E,r) = 0, \tag{2.12}$$

which is obtained by setting $V_{nn'} = 0$ in Eq. (2.7).

Two possible linearly-independent solutions of the differential equation for each channel are the so-called Regular and Irregular Coulomb functions, denoted by $F_\ell(kr,\eta)$ and $G_\ell(kr,\eta)$ respectively. These functions are given in terms of the Confluent Hypergeometric Function, which can in turn be written as a product of Gamma functions [14]. This is typically how the Coulomb functions are determined numerically.

The Coulomb functions have the following limiting forms:

$$F_\ell(\eta,kr) \xrightarrow[r\to 0]{} C_\ell(\eta)(kr)^{\ell+1}, \tag{2.13}$$

$$G_\ell(\eta,kr) \xrightarrow[r\to 0]{} \frac{1}{(2\ell+1)C_\ell(\eta)(kr)^\ell}, \tag{2.14}$$

where $C_\ell(\eta)$ is the Coulomb barrier factor, defined by:

$$C_\ell(\eta) \equiv \frac{2^\ell e^{-\pi\eta/2}}{\Gamma(2\ell+1)}\left|\Gamma(\ell+1\pm i\eta)\right|. \tag{2.15}$$

This shows that $F_\ell(\eta,kr)$ is regular at the origin and $G_\ell(\eta,kr)$ is irregular, as the

names of the functions suggest. For large r:

$$F_\ell(\eta,kr) \xrightarrow[r\to\infty]{} \sin(kr-\eta\ln(2kr)-\frac{1}{2}\ell\pi+\delta_\ell^c), \tag{2.16}$$

$$G_\ell(\eta,kr) \xrightarrow[r\to\infty]{} \cos(kr-\eta\ln(2kr)-\frac{1}{2}\ell\pi+\delta_\ell^c), \tag{2.17}$$

where δ_ℓ^c is the Coulomb phase-shift, which is related to the Sommerfeld parameter by [3]:

$$e^{2i\delta_\ell^c}=\frac{\Gamma(\ell+1+i\eta)}{\Gamma(\ell+1-i\eta)}. \tag{2.18}$$

Furthermore, if there is no Coulomb interaction, $\eta=0$ and the Regular and Irregular functions become the Riccati-Bessel and Riccati-Neumann functions (with a sign difference for the Irregular function):

$$F_\ell(0,kr)=j_\ell(kr), \tag{2.19}$$

$$G_\ell(0,kr)=-n_\ell(kr). \tag{2.20}$$

The full solution for each channel can be expanded over these partial wave-solutions, and it can be shown that [22]:

$$\psi_{\mathbf{k}_n}(\mathbf{r})=\frac{4\pi}{k_nr}\sum_{\ell_nm_n} i^{\ell_n}e^{i\delta_{\ell_n}^c}F_{\ell_n}(\eta_n,k_nr)Y^*_{\ell_nm_n}(\hat{k_n})Y^*_{\ell_nm_n}(\hat{r}), \tag{2.21}$$

and so by the boundary condition, Eq. (2.11),

$$\frac{4\pi}{k_nr}\sum_{\ell_nm_n} i^{\ell_n}e^{i\delta_{\ell_n}^c}F_{\ell_n}(\eta_n,k_nr)Y^*_{\ell_nm_n}(\hat{k}_n)Y^*_{\ell_nm_n}(\hat{r}) \xrightarrow[r\to\infty]{} e^{i\mathbf{k}_n\cdot\mathbf{r}+i\eta\ln(k_nr-\mathbf{k}_n\cdot\mathbf{r})}. \tag{2.22}$$

This useful relation will be used when discussing the scattering cross-section for nuclear (short-ranged) and Coulomb scattering.

Returning to the Regular and Irregular Coulomb functions, the following two linear

combinations are introduced:

$$H_\ell^{(\pm)}(\eta,kr) = F_\ell(\eta,kr) \mp iG_\ell(\eta,kr), \tag{2.23}$$

both of which are also then solutions to the differential equations of each channel in Eq. (2.34). Their asymptotic behaviour is determined by Eq. (2.16) and (2.17):

$$H_\ell^{(\pm)}(\eta,kr) \xrightarrow[r\to\infty]{} \mp ie^{\pm i\left[kr-\eta\ln(2kr)-\ell\pi/2+\delta_\ell^c\right]}. \tag{2.24}$$

Using the asymptotic behaviour of the Riccati-Hankel functions (Eq. (1.48) on page 18), the asymptotic behaviour of $H_\ell^{(\pm)}(\eta,kr)$ can also be written as follows:

$$H_\ell^{(\pm)}(\eta,kr) \xrightarrow[r\to\infty]{} h_\ell^{(\pm)}(\eta,kr)e^{\mp i\eta\ln(kr)}e^{\pm i\delta^c}. \tag{2.25}$$

Furthermore, $H_\ell^{(\pm)}(\eta,kr)$ simply become the Riccati-Hankel functions for $\eta = 0$:

$$H_\ell^{(\pm)}(0,kr) = h_\ell^{(\pm)}(kr). \tag{2.26}$$

The two pairs of solutions for each channel are combined in the following diagonal matrices:

$$F(E,r) = \begin{pmatrix} F_{\ell_1}(\eta_1,k_1r) & 0 & \cdots & 0 \\ 0 & F_{\ell_2}(\eta_2,k_2r) & \cdots & 0 \\ \vdots & \vdots & \ddots & \vdots \\ 0 & 0 & \cdots & F_{\ell_N}(\eta_N,k_Nr) \end{pmatrix}, \tag{2.27}$$

$$G(E,r) = \begin{pmatrix} G_{\ell_1}(\eta_1,k_1r) & 0 & \cdots & 0 \\ 0 & G_{\ell_2}(\eta_2,k_2r) & \cdots & 0 \\ \vdots & \vdots & \ddots & \vdots \\ 0 & 0 & \cdots & G_{\ell_N}(\eta_N,k_Nr) \end{pmatrix}, \tag{2.28}$$

$$H^{(\pm)}(E,r) = \begin{pmatrix} H^{(\pm)}_{\ell_1}(\eta_1,k_1r) & 0 & \cdots & 0 \\ 0 & H^{(\pm)}_{\ell_1}(\eta_1,k_1r) & \cdots & 0 \\ \vdots & \vdots & \ddots & \vdots \\ 0 & 0 & \cdots & H^{(\pm)}_{\ell_1}(\eta_1,k_1r) \end{pmatrix}, \tag{2.29}$$

with

$$H^{(\pm)}(E,r) = F(E,r) \mp iG(E,r). \tag{2.30}$$

If $\eta = 0$, $H^{(\mp)} = W^{(\text{in/out})}$ by Eq. (1.51) and (1.52).

Furthermore, by Eq. (2.25), the asymptotic behaviour of the matrix $H^{(\pm)}$ can be given in terms of the three diagonal matrices $W^{(\text{in/out})}$, $\sigma^{(\pm)}$ and $\Upsilon^{(\pm)}(E,r)$:

$$H^{(\pm)} \xrightarrow[r\to\infty]{} W^{(\text{out/in})}(E,r)\Upsilon^{(\pm)}(E,r)\,\sigma^{(\pm)}, \tag{2.31}$$

with

$$\sigma^{(\pm)} = \begin{pmatrix} e^{\pm i\delta^c_{\ell_1}} & 0 & \cdots & 0 \\ 0 & e^{\pm i\delta^c_{\ell_2}} & \cdots & 0 \\ \vdots & \vdots & \ddots & \vdots \\ 0 & 0 & \cdots & e^{\pm i\delta^c_{\ell_N}} \end{pmatrix}, \tag{2.32}$$

and

$$\Upsilon^{(\pm)}(E,r) = \begin{pmatrix} e^{\mp i\eta_1 \ln(2k_1r)} & 0 & \cdots & 0 \\ 0 & e^{\mp i\eta_2 \ln(2k_2r)} & \cdots & 0 \\ \vdots & \vdots & \ddots & \vdots \\ 0 & 0 & \cdots & e^{\mp i\eta_N \ln(2k_Nr)} \end{pmatrix}. \tag{2.33}$$

These relations will soon come in useful.

2.1.3 Regular solutions for Coulomb and nuclear scattering

Consider again the radial equations (2.7), where there are short-ranged nuclear interactions as well as Coulomb interactions. As $r \to \infty$, the short-ranged potential disappears and the resulting system of differential equations is similar to the system for pure Coulomb scattering:

$$\left[\partial_r^2 + k_n^2 - \frac{\ell_n(\ell_n+1)}{r^2} - \frac{2k_n\eta_n}{r}\right] u_n(E,r) = 0, \qquad r \to \infty. \tag{2.34}$$

Two possible solutions for each channel are, again, the Regular and Irregular Coulomb functions. Since the matrices $F(E,r)$ and $G(E,r)$ are then solutions of the system of differential equations (2.34) at $r \to \infty$, solutions of Eq. (2.7) for all r can be written as follows:

$$U_M(E,r) = F(E,r)A(E,r) + G(E,r)B(E,r), \tag{2.35}$$

where $A(E,r)$ and $B(E,r)$ are unknown matrix functions. The subscript M is used to indicate the difference between the *column matrix* of correctly normalised physical solutions, $U(E,r)$, and the $N \times N$ matrix of solutions, $U_M(E,r)$, which is not necessarily normalised.

The Lagrange condition is also imposed:

$$F(E,r)\partial_r A(E,r) + G(E,r)\partial_r B(E,r) = 0. \tag{2.36}$$

When the proposed matrix of radial solutions, Eq. (2.35), is then substituted into the system of coupled radial Coulomb Schrödinger equation, (2.7), with the Lagrange condition (2.36) used, the following differential equations for $A(E,r)$ and $B(E,r)$ are obtained [6]:

$$\partial_r A = K^{-1}GV\left(FA + GB\right), \tag{2.37}$$

$$\partial_r B = -K^{-1}FV\left(FA + GB\right), \tag{2.38}$$

where the functional dependence is suppressed to facilitate ease of reading. The diagonal matrix K comprised of each channel momentum, k_n, on the diagonals is given by Eq. (1.69) on page 23.

To reflect physical behaviour, the matrix $U_M(E,r)$ is required to be regular at the origin. To ensure that this is the case, the boundary conditions of (2.37) and (2.38) are chosen as follows:

$$A(E,0) = I, \qquad B(E,0) = 0. \tag{2.39}$$

The term containing the irregular matrix, $G(E,r)$, in Eq. (2.35) is then killed off as $r \to 0$.

$A(E,0)$ can of course be any constant matrix, but the identity matrix is chosen for simplicity. The physical wave-function can be normalised correctly at a later stage. At the origin, $U_M(E,r)$ thus becomes:

$$U_M(E,r) \xrightarrow[r\to 0]{} F(E,r) = \begin{pmatrix} F_{\ell_1}(\eta_1,k_1r) & 0 & \cdots & 0 \\ 0 & F_{\ell_2}(\eta_2,k_2r) & \cdots & 0 \\ \vdots & \vdots & \ddots & \vdots \\ 0 & 0 & \cdots & F_{\ell_N}(\eta_N,k_Nr) \end{pmatrix}$$

$$\xrightarrow[r\to 0]{} \begin{pmatrix} C_{\ell_1}(\eta_1)(k_1r)^{\ell_1+1} & 0 & \cdots & 0 \\ 0 & C_{\ell_2}(\eta_2)(k_2r)^{\ell_2+1} & \cdots & 0 \\ \vdots & \vdots & \ddots & \vdots \\ 0 & 0 & \cdots & C_{\ell_N}(\eta_N)(k_Nr)^{\ell_N+1} \end{pmatrix}$$

$$\therefore U_M(E,r) \xrightarrow[r\to 0]{} C \begin{pmatrix} (k_1r)^{\ell_1+1} & 0 & \cdots & 0 \\ 0 & (k_2r)^{\ell_2+1} & \cdots & 0 \\ \vdots & \vdots & \ddots & \vdots \\ 0 & 0 & \cdots & (k_Nr)^{\ell_N+1} \end{pmatrix}, \tag{2.40}$$

with the matrix, C, defined in terms of the Coulomb barrier function by:

$$C \equiv \begin{pmatrix} C_{\ell_1} & 0 & \cdots & 0 \\ 0 & C_{\ell_2} & \cdots & 0 \\ \vdots & \vdots & \ddots & \vdots \\ 0 & 0 & \cdots & C_{\ell_N}(\eta_N) \end{pmatrix}. \tag{2.41}$$

Comparing Eq. (2.40) with Eq. (2.9) gives the following relationship, which must hold for all r:

$$\Phi(E,r) = C^{-1}L^{-1}U_M(E,r). \tag{2.42}$$

2.1.4 Jost matrices for Coulomb and nuclear scattering

Now the following linear combination of the unknown matrices $A(E,r)$ and $B(E,r)$ are introduced:

$$\mathcal{F}^{(\text{in/out})}(E,r) = \frac{1}{2}\left[A(E,r) \mp iB(E,r)\right]. \tag{2.43}$$

Using Eq. (2.39), the behaviour at the origin is given by,

$$\mathcal{F}^{(\text{in/out})}(E,0) = \frac{1}{2}I. \tag{2.44}$$

By also implementing Eq. (2.30), it can easily be shown that the matrix U_M of Eq. (2.35) can also be written as follows:

$$U_M(E,r) = H^{(-)}(E,r)\mathcal{F}^{(\text{in})}(E,r) + H^{(+)}(E,r)\mathcal{F}^{(\text{out})}(E,r). \tag{2.45}$$

By Eq. (2.42), the fundamental matrix of regular solutions is then given by:

$$\Phi(E,r) = H^{(-)}(E,r)C^{-1}L^{-1}\mathcal{F}^{(\text{in})}(E,r) + H^{(+)}(E,r)C^{-1}L^{-1}\mathcal{F}^{(\text{out})}(E,r). \tag{2.46}$$

Since $H^{(\pm)}$, C and L are diagonal, the order of the products of these three matrices

can be changed. Using Eq. (2.31), the asymptotic behaviour is then given by:

$$\Phi(E,r) \xrightarrow[r\to\infty]{} W^{(\mathrm{in})}(E,r)\Upsilon^{(-)}(E,r)\,\sigma^{(-)} \lim_{r\to\infty} C^{-1}L^{-1}\mathcal{F}^{(\mathrm{in})}(E,r) + W^{(\mathrm{out})}(E,r)\Upsilon^{(+)}(E,r)\,\sigma^{(+)} \lim_{r\to\infty} C^{-1}L^{-1}\mathcal{F}^{(\mathrm{out})}(E,r). \tag{2.47}$$

For a single channel, this reduces to:

$$\phi(E,r) \xrightarrow[r\to\infty]{} h_\ell^{(-)}(kr)e^{+i\eta\ln(2kr)} \lim_{r\to\infty} \frac{e^{-i\delta_\ell^c}}{C_\ell(2\ell+1)!!}\mathcal{F}_\ell^{(\mathrm{in})}(E,r) + h_\ell^{(+)}(kr)e^{-i\eta\ln(2kr)} \lim_{r\to\infty} \frac{e^{i\delta_\ell^c}}{C_\ell(2\ell+1)!!}\mathcal{F}_\ell^{(\mathrm{out})}(E,r). \tag{2.48}$$

For short-ranged single-channel scattering, the Jost functions are defined as the amplitudes of the outgoing and incoming spherical waves, given by the Riccati-Hankel functions, $h_\ell^{(\pm)}(kr)$, of the regular solution as $r\to\infty$: see Eq. (1.53) on page 19. For scattering including Coulomb interactions, the spherical waves are now modified by a radially dependent Coulomb factor, and are given by $h_\ell^{(\pm)}(kr)e^{\mp i\eta\ln(2kr)}$, as can be seen from Eq. (2.48). If the Jost functions, $f_\ell^{(\mathrm{in/out})}$, are then defined as the amplitudes of these Coulomb modified spherical waves, the asymptotic behaviour of the regular solution is given by:

$$\phi(E,r) \xrightarrow[r\to\infty]{} h_\ell^{(-)}(kr)e^{+i\eta\ln(2kr)} f_\ell^{(\mathrm{in})}(E) + h_\ell^{(+)}(kr)e^{-i\eta\ln(2kr)} f_\ell^{(\mathrm{out})}(E), \tag{2.49}$$

which can also be written in following form, using Eq. (2.25). This corresponds with the expression in Ref. [6]:

$$\phi(E,r) \xrightarrow[r\to\infty]{} H_\ell^{(-)}(\eta,kr)e^{+i\delta^c} f_\ell^{(\mathrm{in})}(E) + H_\ell^{(-)}(\eta,kr)e^{-i\delta^c} f_\ell^{(\mathrm{out})}(E). \tag{2.50}$$

Comparing this with Eq. (2.48), the Jost functions are then given by:

$$f_\ell^{(\text{in/out})}(E) = \lim_{r\to\infty} \frac{e^{\mp i\delta_\ell^c}}{C_\ell(2\ell+1)!!}\mathcal{F}_\ell^{(\text{in/out})}(E,r). \tag{2.51}$$

Extending this principle to the multi-channel equation (2.47), the Jost matrices are defined by:

$$\begin{aligned}\Phi(E,r) \xrightarrow[r\to\infty]{} & W^{(\text{in})}(E,r)\Upsilon^{(-)}(E,r)f^{(\text{in})}(E) \\ & + W^{(\text{out})}(E,r)\Upsilon^{(+)}(E,r)f^{(\text{out})}(E),\end{aligned} \tag{2.52}$$

which, by Eq. (2.31), can also be written in the form given in Ref. [6]:

$$\Phi(E,r) \xrightarrow[r\to\infty]{} H^{(-)}(E,r)\sigma^{(+)}f^{(\text{in})}(E) + H^{(+)}(E,r)\sigma^{(-)}f^{(\text{out})}(E). \tag{2.53}$$

The Jost matrices are then given by,

$$f^{(\text{in/out})}(E) = \lim_{r\to\infty} C^{-1}L^{-1}\sigma^{(\mp)}\mathcal{F}^{(\text{in/out})}(E,r). \tag{2.54}$$

For the pure Coulomb case where there is no short-ranged interaction potential, the differential equations (2.37) and (2.38) imply that $A(E,r)$ and $B(E,r)$ are constant values determined by the chosen boundary conditions (2.39). This, in turn, implies that $f^{(\text{in/out})}(E,r)$ are also constant for all r. Using Eq. (2.54) with Eq. (2.44), the Jost matrices for pure Coulomb scattering are given by:

$$f^{(\text{in/out})}(E) = \frac{1}{2}C^{-1}L^{-1}\sigma^{(\mp)}. \tag{2.55}$$

The S-matrix is still defined in terms of the Jost matrices by Eq. (1.59). For pure Coulomb scattering, it is then given by:

$$S^c(E) = f^{(\text{out})}(E)\left[f^{(\text{in})}(E)\right]^{-1} = [\sigma^{(+)}]^2, \tag{2.56}$$

which is a diagonal matrix with the matrix elements given by:

$$S^c_{nm}(E) = e^{2i\delta^c_{\ell_n}}\delta_{nm}. \tag{2.57}$$

For the single-channel case, $S^c = e^{2i\delta^c_\ell}$. Comparison with (1.63) on page 21 implies that, as expected, the phase-shift for pure Coulomb scattering is $\delta^c_{\ell_n}$, the Coulomb phase-shift.

Since, by Eq. (1.43), the matrix of physical radial solutions is given by $U(E,r) = \Phi(E,r)\mathcal{C}$, with $\mathcal{C}$ the column matrix comprised of entries $C_1, C_2, ..., C_n$, the full physical wave-solution for each channel can be given by,

$$\psi_n(E,\mathbf{r}) = \frac{1}{r}\sum_{n'=1}^{N}\sum_{\ell_n m_n}\left[H^{(-)}_{\ell_n}(k_n r)\frac{1}{C_{\ell_n}(2\ell_n+1)!!}\mathcal{F}^{(\text{in})}_{nn'}(E,r) + H^{(+)}_{\ell_n}(k_n r)\frac{1}{C_{\ell_n}(2\ell_n+1)!!}\mathcal{F}^{(\text{out})}_{nn'}(E,r)\right]\frac{1}{2}C_n Y_{\ell_n m_n}(\hat{r}), \tag{2.58}$$

where Eq. (1.33) on page 14 as well as Eq. (2.46) were used.

The Jost matrices have been defined for Coulomb and nuclear scattering, with a few further results that will be useful in the sections that follow. It must, however, first be confirmed that the properties of the Jost matrices hold when Coulomb interactions are included. This will be covered in the next section.

2.1.5 Bound and resonance states for Coulomb and nuclear scattering

Bound states with discrete energies $\mathcal{E}_i$ are defined in exactly the same way as before, therefore bound state channel momenta are purely imaginary and chosen on the physical Riemann surface of energy. The momenta can be given by:

$$k_n = i|k_n|.$$

By Eq. (2.2), the product $i\eta_n$ must then be a real, positive quantity. Also as before, at large r, the physical radial solutions must disappear: $u_n(r\to\infty)\to 0$. The asymptotic behaviour of the fundamental matrix of regular solutions for Coulomb interactions, Φ, is given by Eq. (2.53), and the column matrix of physical solutions can of course be written in terms of Φ. An expression similar to Eq. (1.80) on page 26 is then obtained:

$$H^{(-)}(\mathcal{E}_i, r\to\infty)\sigma^{(+)}f^{(\mathrm{in})}(\mathcal{E}_i)\,\mathcal{C} + H^{(+)}(\mathcal{E}_i, r\to\infty)\sigma^{(-)}f^{(\mathrm{out})}(\mathcal{E}_i)\,\mathcal{C}\to 0. \qquad (2.59)$$

If k_n is positive and purely imaginary and $i\eta_n$ is thus real and positive, for large r, the exponent, $e^{-ikr+i\eta\ln(2kr)}\to\infty$ and $e^{ikr-i\eta\ln(2kr)}\to 0$. The asymptotic behaviour of the functions $H_\ell^{(\pm)}$ given in Eq. (2.24) is then:

$$H_{\ell_n}^{(+)}(i|k_n|r) \xrightarrow[r\to\infty]{} 0,$$

$$H_{\ell_n}^{(-)}(i|k_n|r) \xrightarrow[r\to\infty]{} \infty.$$

This, in turn, implies that the matrix, $H^{(+)}(\mathcal{E}_i, r\to\infty) = 0$ and $H^{(-)}(\mathcal{E}_i, r\to\infty)$ becomes an infinite diagonal matrix. For Eq. (2.59) to hold, it is then required that

$$f^{(\mathrm{in})}(\mathcal{E}_i)\,\mathcal{C} = 0. \qquad (2.60)$$

Therefore, for a single-channel problem,

$$f^{(\mathrm{in})}(\mathcal{E}_i) = 0, \qquad (2.61)$$

and for a multi-channel problem:

$$\det\left[f^{(\mathrm{in})}(\mathcal{E}_i)\right] = 0. \qquad (2.62)$$

which, as expected, corresponds exactly to the result for scattering where there are no Coulomb interactions.

Concerning resonances, the discussion in Sections 1.5.3 and 1.5.3 are exactly the same for scattering involving Coulomb interactions. The only important difference is in Eq. (1.104) on page 35, which has an extra factor a for Coulomb scattering. This will be discussed in detail in Chapter 4. This factor simply cancels in the ratio of two-channel partial widths, Eq. (1.105).

In the next section, scattering states for Coulomb and nuclear interactions will be discussed.

2.1.6 Cross-section for Coulomb and nuclear scattering

By considering the structure of the time-independent wave-solution for pure Coulomb scattering, Eq (2.21), the following time-independent wave-solution for each channel is proposed for scattering involving Coulomb and nuclear interactions:

$$\psi_n(E,\mathbf{r}) = \sqrt{\frac{2}{\pi}}\frac{1}{k_n r}\sum_{n'=1}^{N}\sum_{\ell_n m_n} i^{\ell_n}\left[H_{\ell_n}^{(-)}(k_n r)\frac{1}{C_{\ell_n}(2\ell_n+1)!!}\mathcal{F}_{nn'}^{(\mathrm{in})}(E,r)+\right.$$

$$\left. H_{\ell_n}^{(+)}(k_n r)\frac{1}{C_{\ell_n}(2\ell_n+1)!!}\mathcal{F}_{nn'}^{(\mathrm{out})}(E,r)\right]\frac{1}{2}[f^{(\mathrm{in})}(E,r)]^{-1}_{nn'}Y^{*}_{\ell_n m_n}(\hat{k}_n)Y_{\ell_n m_n}(\hat{r}). \tag{2.63}$$

It can be shown that it is a solution to the system of equations, (2.6), as required. Furthermore, the factor, $\left[f^{(\mathrm{in})}(E)\right]^{-1}_{nn'}$ is introduced so that the wave-function has the correct behaviour of Eq. (1.126) at large r, which will be shown. Finally, this proposed solution corresponds exactly to Eq. (2.58) for specific values of the combination coefficients, C_n. Using Eq. (2.54) and implementing the definition of the S-matrix, Eq. (1.59) when considering the asymptotic behaviour gives:

$$\psi_n(E,\mathbf{r}) \xrightarrow[r\to\infty]{} \sqrt{\frac{2}{\pi}}\frac{1}{k_n r}\sum_{n'=1}^{N}\sum_{\ell_n m_n} i^{\ell_n}\left[H_{\ell_n}^{(-)}(k_n r)e^{+i\delta^{c}_{\ell_n}}+\right.$$

$$\left. H_{\ell_n}^{(+)}(k_n r)e^{-i\delta^{c}_{\ell_n}}S_{nn'}(E,r)\right]\frac{1}{2}Y^{*}_{\ell_n m_n}(\hat{k}_n)Y_{\ell_n m_n}(\hat{r}). \tag{2.64}$$

When applying the same trick as Section 1.5.6 by adding and subtracting a function, in this case $H_{\ell_n}^{(+)} e^{+i\delta_{\ell_n}^c}$, and using Eq. (2.23) the following is obtained:

$$\psi_n(E,\mathbf{r}) \xrightarrow[r\to\infty]{} (2\pi)^{-3/2}\frac{4\pi}{k_n r}\sum_{\ell_n m_n} i^{\ell_n} e^{i\delta_{\ell_n}^c} F_{\ell_n}(k_n r) Y^*_{\ell_n m_n}(\hat{k}_n) Y_{\ell_n m_n}(\hat{r}) + \\ \frac{1}{2} H_{\ell_n}^{(+)}(k_n r)\left[e^{-i\delta_{\ell_n}^c} S_{nn'}(E,r) - e^{i\delta_{\ell_n}^c}\right] Y^*_{\ell_n m_n}(\hat{k}_n) Y_{\ell_n m_n}(\hat{r}). \tag{2.65}$$

When using Eq. (2.24) and substituting the expression (2.22),

$$\psi_n(E,\mathbf{r}) \xrightarrow[r\to\infty]{} (2\pi)^{-3/2} e^{i\mathbf{k}_n\cdot\mathbf{r} + i\eta\ln(k_n r - \mathbf{k}_n\cdot\mathbf{r})} + \\ (2\pi)^{-3/2}\frac{4\pi}{2ik_n r}\frac{e^{ikr - i\eta\ln(2kr)}}{r}\sum_{n'}^{N}\sum_{\ell_n m_n}\left[S_{nn'}(E,r) - e^{2i\delta_{\ell_n}^c}\right] Y^*_{\ell_n m_n}(\hat{k}_n) Y_{\ell_n m_n}(\hat{r}). \tag{2.66}$$

The Coulomb-nuclear partial amplitude for each channel is then defined by:

$$\mathrm{f}^{\mathrm{cn}}_{nm}(E) \equiv \frac{1}{2ik_n}\left[S_{nn'}(E,r) - e^{2i\delta_{\ell_n}^c}\delta_{nn'}\right], \tag{2.67}$$

and the full Coulomb-nuclear amplitude for each channel by:

$$\mathbf{f}^{\mathrm{cn}}_n(\hat{r}\leftarrow\hat{k}_n) \equiv 4\pi\sum_{n'=1}^{N}\sum_{\ell_n m_n}\mathrm{f}^{\mathrm{cn}}_{nn'}(E) Y^*_{\ell_n m_n}(\hat{k}_n) Y_{\ell_n m_n}(\hat{r}).$$

The asymptotic behaviour of each partial wave for scattering involving Coulomb interactions can then be written as follows:

$$\psi_n(E,r) \xrightarrow[r\to\infty]{} (2\pi)^{-3/2} e^{i\mathbf{k}_n\cdot\mathbf{r} + i\eta\ln(k_n r - \mathbf{k}_n\cdot\mathbf{r})} + (2\pi)^{-3/2}\mathbf{f}^{\mathrm{cn}}_n(\hat{r}\leftarrow\hat{k}_n)\frac{e^{ikr - i\eta\ln(2kr)}}{r}, \tag{2.68}$$

which is very similar to Eq. (1.126) on page 42. As with the scattering of neutral particles, the outgoing wave is again comprised of an unscattered plane wave part and

an outgoing spherical part - see Figure 1.3. However, the spherical part is modified by a Coulomb factor, and the outgoing scattered radial wave is given by:

$$\psi_n^{(\mathrm{sc})} = (2\pi)^{-3/2}\mathbf{f}_n^{\mathrm{cn}}(\hat{r} \leftarrow \hat{k}_n)\frac{e^{ik_n r - i\eta \ln 2kr}}{r}. \tag{2.69}$$

The outgoing channel flux then becomes:

$$j_n^{\mathrm{sc}} = (2\pi)^{-3}\frac{\hbar}{\mu_n r^2}\left(k_n - \frac{\eta_n}{r}\right)\left|\mathbf{f}_{\mathrm{n}}^{\mathrm{cn}}(\hat{r} \leftarrow \hat{k}_n)\right|^2. \tag{2.70}$$

For very large r, $\left(k_n - \frac{\eta_n}{r}\right) \approx k_n$, since k_n is real and positive for scattering states. Then:

$$j_n^{\mathrm{sc}} \approx (2\pi)^{-3}\frac{\hbar k_n}{\mu_n r^2}\left|\mathbf{f}_{\mathrm{n}}^{\mathrm{cn}}(\hat{r} \leftarrow \hat{k}_n)\right|^2. \tag{2.71}$$

The incoming channel plane wave and incoming channel flux remain the same, given by Eq. (1.127) and (1.129):

$$\begin{aligned}\psi_n^{(\mathrm{in})} &= (2\pi)^{-3/2}e^{i\mathbf{k}_n\cdot\mathbf{r}},\\ |\mathbf{j}_n^{\mathrm{in}}| &= (2\pi)^{-3}\frac{\hbar k_n}{\mu_n}.\end{aligned}$$

The channel Coulomb-nuclear differential cross-section is then given by:

$$\frac{d\sigma^{\mathrm{cn}}}{d\Omega} = \frac{j_n^{\mathrm{sc}} r^2}{|\mathbf{j}_n^{\mathrm{in}}|} = \left|\mathbf{f}_n^{\mathrm{cn}}(\hat{r} \leftarrow \hat{k}_n)\right|^2. \tag{2.72}$$

This allows the calculation of the Coulomb-nuclear scattering cross-section in a similar way to the method discussed in Section 1.5.6. The result for the channel Coulomb-nuclear cross-section in a specific partial wave is:

$$\sigma_{nm}^{\mathrm{cn}} = \frac{\pi}{k_n^2}(2\ell_n + 1)e^{2i\delta_{\ell_n}^c}\left|S_{nm}(E)e^{-2i\delta_{\ell_n}^c} - \delta_{nm}\right|^2. \tag{2.73}$$

This reduces to the following partial Coulomb-nuclear cross-section for single-

channel scattering:

$$\sigma_\ell^{\text{cn}} = \frac{\pi}{k^2}(2\ell+1)e^{2i\delta_\ell^c}\left|S(E)e^{-2i\delta_\ell^c}-1\right|^2. \tag{2.74}$$

The corresponding total phase-shift, in terms of the S-matrix, is given by Eq. (1.63):

$$S_\ell(E) = e^{2i\delta_\ell}. \tag{2.75}$$

If the total phase-shift is written as the sum of the Coulomb-nuclear and pure Coulomb phase-shift:

$$\delta_\ell = \delta_\ell^{\text{cn}} + \delta_\ell^c, \tag{2.76}$$

the single-channel Coulomb-nuclear cross-section can then be written in terms of the Coulomb-nuclear phase-shift:

$$\sigma_\ell^{\text{cn}} = \frac{\pi}{k^2}(2\ell+1)e^{2i\delta_\ell^c}\left|e^{2i\delta_\ell^{\text{cn}}}-1\right|^2. \tag{2.77}$$

In initial fittings of experimental results of the scattering of charged particles, like R-matrix fittings, the Coulomb-nuclear phase-shift at corresponding energies are often obtained. However, it is clear that the Coulomb-nuclear partial amplitude of Eq. (2.67) differs somewhat from the partial amplitude for neutral scattering, Eq. (1.143), which results in a difference in the expression for the Coulomb-nuclear cross-section as compared to Eq. (1.150) on page 50.

In order to correspond to the formalism for the scattering of neutral particles, the quantity known as the full partial wave amplitude will rather be used, which will allow the calculation of the full scattering cross-section. This includes the effect of the Coulomb-nuclear interactions as well as the pure Coulomb interaction. For a full discussion, see Ref. [3], where the concept of the cut-off radius is introduced.

Ref. [3] also gives the pure Coulomb partial wave amplitude for a specific channel,

which can be defined as follows:

$$\mathrm{f}^{c}_{nm}(E) \equiv \frac{1}{2ik_n}\left[S^{c}_{nm}(E,r) - \delta_{nm}\right] = \frac{1}{2ik_n}\left[e^{2i\delta^{c}_{n}}\delta_{nm} - \delta_{nm}\right], \tag{2.78}$$

where $S^{c}_{nm}(E,r)$ are the matrix elements of the pure Coulomb S-matrix, given in terms of the channel Coulomb phase-shifts by Eq. (2.57).

The full partial wave scattering amplitude is defined as the sum of the Coulomb-nuclear partial amplitude and the pure Coulomb partial amplitude:

$$\mathrm{f}_{nm}(E) \equiv \mathrm{f}^{\mathrm{cn}}_{nm}(E) + \mathrm{f}^{c}_{nm}(E) = \frac{1}{2ik_n}\left[S_{nm}(E,r) - \delta_{nm}\right], \tag{2.79}$$

which corresponds exactly to the partial amplitude, Eq. (1.143) on page 48, for the scattering of neutral particles. The full scattering amplitude for a specific channel is then given by Eq. (1.144):

$$\mathbf{f}_n(\hat{r} \leftarrow \hat{k}_n) \equiv 4\pi \sum_{n'=1}^{N} \sum_{\ell_n m_n} \mathrm{f}_{nn'}(E) Y^{*}_{\ell_n m_n}(\hat{k}_n) Y_{\ell_n m_n}(\hat{r}),$$

and the full differential cross-section, as usual, by:

$$\frac{d\sigma}{d\Omega} = \left|\mathbf{f}_n(\hat{r} \leftarrow \hat{k})\right|^2.$$

It can then be shown that the full channel cross-section in a specific partial wave, including the Coulomb-nuclear and Coulomb effects, is given by:

$$\sigma_{nm} = \frac{\pi}{k_n^2}(2\ell_n + 1)\left|S_{nm}(E) - \delta_{nm}\right|^2,$$

which corresponds exactly to Eq. (1.150). The full channel cross-section is the preferred quantity for the calculations in this thesis, instead of the Coulomb-nuclear cross-section or Coulomb-nuclear phase-shift. It is, however, easy to calculate the full channel cross-section from the other quantities.

The scattering of particles with non-zero spin will now be considered.

2.2 Scattering of particles with non-zero spin

The scattering of particles with zero spin as well as non-zero spin will be considered in this thesis. In the previous chapter, the radial Schrödinger equation was derived for the multi-channel scattering of two particles with zero spin and a central interaction potential. The Jost matrices could then be defined and their properties explored. This was done for the scattering of neutral particles in Chapter 1 and for the scattering of charged particles in the previous sections of this chapter.

For the scattering of particles with non-zero spin, a similar radial equation is obtained for discrete states (bound states and resonances), which implies that the Jost matrices can be defined in the same way. Furthermore, the properties of the Jost matrices for bound states and resonances are identical to the properties of the Jost matrices for the scattering of particles with zero spin. However, for scattering states of particles with non-zero spin, there are certain complications, and the expression for the cross-section in terms of the S-matrix differs to incorporate the spin quantum number.

In the derivation that follows, only one energy channel will be considered, but with different possible orbital angular momentum and spin states. This is elastic scattering but, as has been mentioned, due to different possible orbital angular momentum and spin, such scattering is also multi-channelled (but degenerate in energy).

The general result for multi-channel scattering with non-zero spin, where there are different channels due to multiple energy thresholds as well as different angular momentum and spin states, is more complicated but very similar. It is not required for the systems under consideration in this thesis, and will therefore not be discussed.

The derivations that follow are very similar to those in Chapter 1, but Hilbert space vectors will mostly be used, instead of functions in the configuration space projection. The results apply to the scattering of charged particles too, but this will not be shown explicitly.

2.2.1 Angular momentum quantum numbers

Since two-body scattering is considered, the total orbital angular momentum operator, $\hat{\boldsymbol{\ell}}$, as well as the total spin angular momentum operator, $\hat{\boldsymbol{s}}$, are given as the sum of the individual particle angular momenta:

$$\hat{\boldsymbol{\ell}} = \hat{\boldsymbol{\ell}}_1 + \hat{\boldsymbol{\ell}}_2, \tag{2.80}$$

$$\hat{\boldsymbol{s}} = \hat{\boldsymbol{s}}_1 + \hat{\boldsymbol{s}}_2.$$

Spin is an intrinsic property of a particle, but the properties of the spin operator are identical to that of the orbital angular momentum operator [11]. The total angular momentum operator for the scattering system, $\hat{\boldsymbol{J}}$, is given by;

$$\hat{\boldsymbol{J}} = \hat{\boldsymbol{\ell}} + \hat{\boldsymbol{s}}, \tag{2.81}$$

and is equivalent to

$$\hat{\boldsymbol{J}} = \hat{\boldsymbol{J}}_1 + \hat{\boldsymbol{J}}_2. \tag{2.82}$$

where $\hat{\boldsymbol{J}}_1$ and $\hat{\boldsymbol{J}}_2$ are the total angular momentum operators for particle 1 and 2 respectively.

The angular momentum operators for the two particle system, $\hat{\boldsymbol{\ell}}$, $\hat{\boldsymbol{s}}$ and $\hat{\boldsymbol{J}}$, as well as the operators for the individual particles (indicated with a subscript 1 or 2), all obey the same commutator relations [11]. This leads to specific eigenvalues for the square of the operators, $\hat{\boldsymbol{\ell}}^2$, $\hat{\boldsymbol{s}}^2$ and $\hat{\boldsymbol{J}}^2$, which act on the vector spaces $|\ell m\rangle$, $|s\mu\rangle$ and $|JM\rangle$ respectively:

$$\begin{aligned} \hat{\boldsymbol{\ell}}^2|\ell m\rangle &= \ell(\ell+1)\hbar^2|\ell m\rangle, \\ \hat{\boldsymbol{s}}^2|s\mu\rangle &= s(s+1)\hbar^2|s\mu\rangle, \\ \hat{\boldsymbol{J}}^2|JM\rangle &= J(J+1)\hbar^2|JM\rangle, \end{aligned} \tag{2.83}$$

with ℓ still representing the orbital angular momentum quantum number with corresponding magnetic quantum number, m, and the spin quantum number is indicated by s with corresponding spin-magnetic quantum number, μ, (not to be confused with the reduced mass - the distinction should be clear by the context in which it is used). For a system with non-zero spin, ℓ and m are no longer conserving. For such a system, the total angular momentum quantum number, J, with corresponding total magnetic quantum number, M, are the conserving quantities.

The quantum numbers m, μ and M are the eigenvalues of the projection operators along an arbitrary Cartesian coordinate, usually chosen as z: $\hat{\ell}_z$, $\hat{s}_z$ and $\hat{J}_z$, which act on the same vector spaces $|\ell m\rangle$, $|s\mu\rangle$ and $|JM\rangle$ respectively (since $[\hat{\boldsymbol{\ell}}^2, \hat{\ell}_z] = [\hat{\boldsymbol{s}}^2, \hat{s}_z] = [\hat{\boldsymbol{J}}^2, \hat{J}_z] = 0$):

$$\begin{aligned} \hat{\ell}_z|\ell m\rangle &= m\hbar|\ell m\rangle, \\ \hat{s}_z|s\mu\rangle &= \mu\hbar|s\mu\rangle, \\ \hat{J}_z|JM\rangle &= M\hbar|JM\rangle. \end{aligned} \tag{2.84}$$

The quantum numbers can only take the following discrete values:

$$\begin{aligned} m &\in \{-\ell, -(\ell-1), ..., (\ell-1), \ell\}, \qquad \ell \in \{0, 1, 2, ...\} \\ \mu &\in \{-s, -(s-1), ..., (s-1), s\}, \\ M &\in \{-J, -(J-1), ..., (J-1), J\}, \\ M &= m + \mu, \qquad J = |\ell + s|. \end{aligned} \tag{2.85}$$

All of the above is also applicable to the individual particles labelled 1 and 2. Furthermore, the operators for the individual particles act on different vector subspaces and must therefore commute. Since the spin of the two particles in the incoming channel are usually known, but the total spin is not, the basis of eigenvectors of total spin for the two interacting particles is given in terms of the individual spin vector

spaces:

$$|s\mu\rangle = \sum_{\mu_1\mu_2} C^{s\mu}_{s_1\mu_1,s_2\mu_2}|s_1\mu_1, s_2\mu_2\rangle. \tag{2.86}$$

with the Clebsch-Gordan coefficients defined as follows [11]:

$$C^{ij}_{i_1 j_1, i_2 j_2} \equiv \langle i_1 j_1 i_2 j_2|(i_1 i_2) i j\rangle, \qquad i, i_1, i_2, j \in \mathbb{Z}. \tag{2.87}$$

The quantum numbers that describe a two-body scattering system with non-zero spin have now been established. The adjusted spherical harmonics for such systems will now be considered.

2.2.2 Spin spherical harmonics

When the total orbital angular momentum eigenvectors, $|\ell m\rangle$, are combined with total spin eigenvectors, $|s\mu\rangle$, a set of eigenvectors common to the operators $\hat{\boldsymbol{\ell}}^2$, $\hat{\boldsymbol{s}}^2$, $\hat{\boldsymbol{J}}^2$ and $\hat{J}_z$ are obtained:

$$|\mathcal{Y}^{JM}_{[\ell]}\rangle \equiv |(\ell s)JM\rangle = \sum_{m\mu} |\ell m, s\mu\rangle C^{JM}_{\ell m s\mu}, \tag{2.88}$$

with

$$[\ell] \equiv \{\ell, s\}. \tag{2.89}$$

Since the spherical harmonics are orthonormal (Eq. (1.27) on page 13), it can be shown that the vector $|\mathcal{Y}^{JM}_{[\ell]}\rangle$ is also orthonormal:

$$\begin{aligned}
\langle \mathcal{Y}^{JM}_{[\ell]}|\mathcal{Y}^{J'M'}_{[\ell']}\rangle &= \int \langle \mathcal{Y}^{JM}_{[\ell]}|\theta,\varphi\rangle\langle\theta,\varphi|\mathcal{Y}^{J'M'}_{[\ell']}\rangle d\Omega \\
&= \sum_{m\mu m'\mu'} C^{JM}_{\ell m s\mu} C^{J'M'}_{\ell' m' s'\mu'} \langle s\mu|s'\mu'\rangle\langle \ell m|\ell' m'\rangle \\
&= \sum_{m\mu m'\mu'} C^{JM}_{\ell m s\mu} C^{J'M'}_{\ell' m' s'\mu'} \delta_{ss'}\delta_{\mu\mu'}\delta_{\ell\ell'}\delta_{mm'} \\
&= \delta_{[\ell][\ell']} \sum_{m\mu} C^{JM}_{\ell m s\mu} C^{J'M'}_{\ell' m' s'\mu'} = \delta_{[\ell][\ell']}\delta_{JJ'}\delta_{MM'}.
\end{aligned} \tag{2.90}$$

Projecting the spherical-angle part of configuration space vector, $|\mathbf{r}\rangle$, on the combined orbital angular momentum-spin vector, $|\mathcal{Y}^{JM}_{[\ell]}\rangle$, of Eq. (2.88) then gives the following useful vector in spin-space:

$$\begin{aligned} |\mathcal{Y}^{JM}_{[\ell]}(\theta,\varphi)\rangle &= \langle\theta,\varphi|\mathcal{Y}^{JM}_{[\ell]}\rangle && (2.91)\\ &= \sum_{m\mu} C^{JM}_{\ell m s\mu} Y_{\ell m}(\theta,\varphi)|s\mu\rangle && (2.92)\\ &= \sum_{\mu} C^{JM}_{\ell,(M-\mu),s\mu} Y_{\ell,(M-\mu)}(\theta,\varphi)|s\mu\rangle. && (2.93)\end{aligned}$$

Furthermore, projecting the spherical-angle part of $|\mathbf{r}\rangle$ as well as the total spin eigenvector, $|s\mu\rangle$, on the eigenvector $|\mathcal{Y}^{JM}_{[\ell]}\rangle$ gives a function that will be called the spin spherical harmonics, which can conveniently be written in terms of the standard spherical harmonics:

$$\begin{aligned} \mathcal{Y}^{JM}_{\ell s\mu}(\theta,\varphi) &= \langle\theta,\varphi,s\mu|\mathcal{Y}^{JM}_{[\ell]}\rangle\\ &= \sum_{m} C^{JM}_{\ell m s\mu} Y_{\ell m}(\theta,\varphi)\\ &= C^{JM}_{\ell,(M-\mu),s\mu} Y_{\ell,(M-\mu)}(\theta,\varphi). && (2.94)\end{aligned}$$

The spin spherical harmonics allow the radial wave-equation to be determined.

2.2.3 Radial wave-equation for discrete states

Consider the discrete states, $|\psi_{EJM}\rangle$, which have definite values of energy, $E=\mathcal{E}_i$, and are further defined by quantum numbers J and M. These states are Hilbert vectors in the tensor product of the configuration space vectors and spin-space vectors. The basis can be constructed as the tensor product of the states with definite values of the coordinate, $|\mathbf{r}\rangle$, and the basis vectors of spin-space, $|s\mu\rangle$. The wave-function of a two-body scattering system is then the set of projections of the state $|\psi_{EJM}\rangle$ on

these basis vectors:

$$\langle \mathbf{r}, s\mu | \psi_{EJM} \rangle = \psi_{EJM}(\mathbf{r}, s, \mu). \tag{2.95}$$

Consider only the configuration space projection (in spherical coordinates) on $|\psi_{EJM}\rangle$, which is a vector in spin-space:

$$\langle \mathbf{r} | \psi_{EJM} \rangle = |\psi_{EJM}(r, \theta, \varphi)\rangle. \tag{2.96}$$

This vector is expanded over the orthonormal basis of eigenvectors in Eq. (2.88):

$$\begin{aligned} |\psi_{EJM}(r,\theta,\varphi)\rangle &= \sum_{[\ell]} \langle \mathbf{r} | \mathcal{Y}^{JM}_{[\ell]} \rangle \langle \mathcal{Y}^{JM}_{[\ell]} | \psi_{EJM} \rangle \\ &= \sum_{[\ell]} \langle r, \theta, \varphi | \mathcal{Y}^{JM}_{[\ell]} \rangle \langle (\ell s) JM | \psi_{EJM} \rangle \\ &= \sum_{[\ell]} \langle \theta, \varphi | \mathcal{Y}^{JM}_{[\ell]} \rangle \langle r, (\ell s) JM | \psi_{EJM} \rangle. \end{aligned}$$

Implementing the definition of the projection (2.91) and defining the radial wave-function by the following:

$$u^{J}_{[\ell]}(E, r) \equiv r \langle r, (\ell s) JM | \psi_{EJM} \rangle, \tag{2.97}$$

then gives,

$$|\psi_{EJM}(\mathbf{r})\rangle = \sum_{[\ell]} |\mathcal{Y}^{JM}_{[\ell]}(\theta, \varphi)\rangle \frac{u^{J}_{[\ell]}(E, r)}{r}. \tag{2.98}$$

Projecting the spin-space vector, $|s\mu\rangle$, on the above and using Eq. (2.94) then results in the following expression for the wave-function:

$$\psi_{EJM}(\mathbf{r}, s, \mu) = \sum_{\ell} \mathcal{Y}^{JM}_{\ell s \mu}(\theta, \varphi) \frac{u^{J}_{[\ell]}(E, r)}{r}. \tag{2.99}$$

Now return to the time-independent Schrödinger equation (1.4) on page 6, which

can be written as follows:

$$(\hat{H}-E)|\psi_{EJM}\rangle = 0,$$

which is projected on the configuration space basis $\langle \mathbf{r}|$:

$$\langle \mathbf{r}|(\hat{H}-E)|\psi_{EJM}\rangle = 0. \tag{2.100}$$

For scattering in a single energy-channel, the two-body Hamiltonian is given by:

$$\hat{H} = \frac{\hat{\mathbf{p}}^2}{2\mu} + U(r).$$

The potential $U(r)$ is once again assumed to be radially dependent. Using Eq. (2.98), the following is obtained for the time-independent Schrödinger equation:

$$\left[-\frac{\hbar^2}{2\mu}\Delta_{\mathbf{r}} + U(r) - E\right] \sum_{[\ell]} |\mathcal{Y}^{JM}_{[\ell]}(\theta,\varphi)\rangle \frac{u^J_{[\ell]}(E,r)}{r} = 0. \tag{2.101}$$

It is assumed that the radial wave-solution, $u^J_{[\ell]}(E,r)$, is in a specific ℓ state. Since $|\mathcal{Y}^{JM}_{[\ell]}(\theta,\varphi)\rangle$ is an eigenstate of $\hat{\boldsymbol{\ell}}^2$,

$$\hat{\boldsymbol{\ell}}^2|\mathcal{Y}^{JM}_{[\ell]}(\theta,\varphi)\rangle = \hbar^2\ell(\ell+1)|\mathcal{Y}^{JM}_{[\ell]}(\theta,\varphi)\rangle. \tag{2.102}$$

The following is then obtained:

$$\sum_{[\ell]} \left[\partial_r^2 + k^2 - \frac{\ell(\ell+1)}{r^2} - \frac{2\mu}{\hbar^2}U(\mathbf{r})\right] |\mathcal{Y}^{JM}_{[\ell]}(\theta,\varphi)\rangle u^J_{[\ell]}(E,r) = 0, \tag{2.103}$$

with the wave-momentum as usual given by:

$$k^2 = 2\mu E/\hbar^2. \tag{2.104}$$

Applying $\langle \mathcal{Y}^{JM}_{[\ell]}(\theta,\varphi)|$ and integrating over the spherical angles, θ and φ, yields the following result, which is *the radial Schrödinger equation for discrete states of*

elastic two-body scattering of particles with non-zero spin:

$$\left[\partial_r^2 + k^2 - \frac{\ell(\ell+1)}{r^2}\right] u^J_{[\ell]}(E,r) = \sum_{[\ell']} V^J_{[\ell][\ell']}(r) u^J_{[\ell']}(E,r), \tag{2.105}$$

with the matrix elements of the reduced potential given by the following, in terms of the interaction potential:

$$\begin{aligned} V^J_{[\ell][\ell']}(r) &= \frac{2\mu}{\hbar^2}\int \langle \mathcal{Y}^{JM}_{[\ell]}(\theta,\varphi)|U(r)|\mathcal{Y}^{JM}_{[\ell']}(\theta,\varphi)\rangle d\Omega \\ &= \frac{2\mu}{\hbar^2} C^{JM}_{\ell m s\mu} C^{JM}_{\ell' m' s'\mu'} \iint Y^*_{\ell m}(\theta,\varphi)\langle s\mu|U(r)|s'\mu'\rangle Y_{\ell' m'}(\theta,\varphi)\sin\theta d\theta d\varphi, \end{aligned} \tag{2.106}$$

and with $[\ell'] = \{\ell', s'\}$.

This radial equation is only applicable to discrete states. In the next section, a similar result is also obtained for scattering states.

2.2.4 Radial wave-equation for scattering states

Consider an incoming plane-wave vector, $|\mathbf{k}, s\mu\rangle$, defined by its momentum vector, $\mathbf{k}$, and spin quantum numbers, s and μ. These incoming states are Hilbert vectors in the tensor product of the momentum space vectors $|\mathbf{k}\rangle = |k,\theta_k,\varphi_k\rangle$ (in spherical coordinates) and spin-space vectors, $|s\mu\rangle$. They can be expanded over all possible states defined by different ℓ and m:

$$\begin{aligned} |\mathbf{k}, s\mu\rangle = |k,\theta_k,\varphi_k,s\mu\rangle &= \sum_{\ell m} |k,\theta_k,\varphi_k,s\mu\rangle|\ell m\rangle\langle \ell m| \\ &= \sum_{\ell m} |k,\ell m,s\mu\rangle Y^*_{\ell m}(\theta_k,\varphi_k), \end{aligned} \tag{2.107}$$

where the definition of the spherical harmonics, Eq. (1.25) is also implemented. The result can further be written in terms of vectors defined by the total angular momentum quantum numbers, M and J, by implementing an appropriate Clebsch-

Gordan coefficient:

$$|\mathbf{k},s\mu\rangle = \sum_{\ell mJM} |k,(\ell s),JM\rangle C^{JM}_{\ell ms\mu} Y^*_{\ell m}(\theta_k,\varphi_k). \tag{2.108}$$

When the Møller operator, $\hat{\Omega}^{(+)}$, of Eq. (1.15) on page 9 acts on this incoming state, the state vector, $|\psi_{\mathbf{k}s\mu}\rangle$ at $t = 0$ (the time of the interaction) is obtained. If the scattering partial wave state with definite values of J and M is then defined as follows,

$$|\psi^{JM}_{k[\ell]}\rangle \equiv \hat{\Omega}^{(+)}|k,(\ell s),JM\rangle, \tag{2.109}$$

the state vector $|\psi_{\mathbf{k}s\mu}\rangle$ can be written as follows:

$$|\psi_{\mathbf{k}s\mu}\rangle = \hat{\Omega}^{(+)}|\mathbf{k},s\mu\rangle = \sum_{\ell mJM} |\psi^{JM}_{k[\ell]}\rangle C^{JM}_{\ell ms\mu} Y^*_{\ell m}(\theta_k,\varphi_k). \tag{2.110}$$

If Eq. (2.94) is implemented, the following is obtained:

$$|\psi_{\mathbf{k}s\mu}\rangle = \sum_{JM\ell} |\psi^{JM}_{k[\ell]}\rangle \mathcal{Y}^{JM*}_{\ell s\mu}(\theta_k,\varphi_k) = \sum_{JM[\ell]} |\psi^{JM}_{k[\ell]}\rangle \langle \mathcal{Y}^{JM}_{[\ell]}(\theta_k,\varphi_k)|s\mu\rangle. \tag{2.111}$$

The wave-function is then the amplitude of the probability that the system is at a coordinate, $\mathbf{r}$ in the spin state, $|s'\mu'\rangle$:

$$\psi_{\mathbf{k}s\mu}(\mathbf{r},s',\mu') = \langle \mathbf{r},s',\mu'|\psi_{\mathbf{k}s\mu}\rangle. \tag{2.112}$$

Expanding over the vectors, $|r,(\ell's')JM\rangle$, and using the definition of the spin spherical harmonics, Eq. (2.88) then gives:

$$\psi_{\mathbf{k}s\mu}(\mathbf{r},s',\mu') = \sum_{JM[\ell'][\ell]} \langle s'\mu'|\mathcal{Y}^{JM}_{[\ell']}(\theta,\varphi)\rangle \langle r,(\ell's')JM|\psi^{JM}_{k[\ell]}\rangle \langle \mathcal{Y}^{JM}_{[\ell]}(\theta_k,\varphi_k)|s\mu\rangle. \tag{2.113}$$

The radial wave-function is then defined similar to Eq. (2.99), but in this case it is a matrix:

$$u^J_{[\ell'][\ell]}(E,r) \equiv \frac{r}{N_{[\ell]}(k)} \langle r,(\ell's')JM|\psi^{JM}_{k[\ell]}\rangle. \tag{2.114}$$

The energy dependent constant,

$$N_{[\ell]}(k) = i^{\ell}/\sqrt{2\pi}k, \tag{2.115}$$

is introduced to ensure the proper normalisation of the wave-function, as well as to ensure the proper asymptotic behaviour at $r \to \infty$, so that it can be written in the form of Eq. (1.126) on page 42. The state wave-function is then given by:

$$\psi_{\mathbf{k}s\mu}(\mathbf{r}, s', \mu') = \sum_{JM} \sum_{[\ell'][\ell]} \langle s'\mu' | \mathcal{Y}^{JM}_{[\ell']}(\theta, \varphi) \rangle \frac{u^{J}_{[\ell'][\ell]}(E, r) N_{[\ell]}(k)}{r} \langle \mathcal{Y}^{JM}_{[\ell]}(\theta_k, \varphi_k) | s\mu \rangle. \tag{2.116}$$

Proceeding in exactly the same way as for discrete states, it can then be shown that the radial equation for scattering states is given by:

$$\left[\partial_r^2 + k^2 - \frac{\ell(\ell+1)}{r^2}\right] u^{J}_{[\ell][\ell']}(E, r) = \sum_{[\ell'']} V^{J}_{[\ell][\ell'']}(r) u^{J}_{[\ell''][\ell']}(E, r). \tag{2.117}$$

This radial equation is very similar to the one obtained for discrete states, Eq. (2.105), as well as the radial equation obtained for the scattering of particles with zero spin, Eq. (1.37).

2.2.5 Jost matrices for systems with non-zero spin

The discussion that follows is almost identical to Section 1.5 for the scattering of particles with zero spin. The physical wave-function must still be finite at $r = 0$. By Eq. (2.99) for discrete states and Eq. (2.116) for scattering states, this implies that the radial wave-functions distinguished by different spin and angular momentum states must tend to zero. Recall that only one energy channel will be considered for the scattering of particles with non-zero spin. The following is then applicable for discrete states:

$$u^{J}_{[\ell]}(r \to 0) = 0, \qquad \forall J, [\ell], \tag{2.118}$$

and for scattering states, the matrix:

$$u^J_{[\ell],[\ell']}(r \to 0) = 0, \qquad \forall J, [\ell]. \tag{2.119}$$

The superscript J indicates that the total angular momentum is the conserving quantity in the scattering, and that different states will be distinguished by J in particular.

The fundamental matrix of regular solutions, Eq. (1.42), can be constructed in exactly the same way as for a system with zero spin. In particular, the asymptotic behaviour is given by:

$$\Phi^J(E,r) \xrightarrow[r\to\infty]{} W^{(\text{in})}(E,r) f^{(\text{in})J}(E) + W^{(\text{out})}(E,r) f^{(\text{out})J}(E), \tag{2.120}$$

with the Jost matrices given by $f^{(\text{in/out})J}(E)$. The S-matrix is again defined in terms of the Jost matrices:

$$S^J(E) \equiv f^{(\text{out})J}(E) \left[f^{(\text{in})J}(E) \right]^{-1}. \tag{2.121}$$

Similar to Eq. (1.46), the physical radial-wave for discrete states can then be written as follows:

$$u^J_{[\ell]} = \sum_{\ell'} \phi^J_{[\ell][\ell']} C^J_{[\ell']}, \tag{2.122}$$

and the physical radial-wave for scattering states given by:

$$u^J_{[\ell][\ell']} = \sum_{\ell''} \phi^J_{[\ell][\ell'']} C^J_{[\ell''][\ell']}, \tag{2.123}$$

where $C^J_{[\ell']}$ and $C^J_{[\ell''][\ell']}$ once again represent combination coefficients, which are the elements of a matrix $\mathcal{C}^J$. For discrete states, $\mathcal{C}^J$ is a column-matrix. The matrix U^J is then defined in a similar way, with the elements for discrete states given by $u^J_{[\ell]}$ (hence it is a column matrix) and the entries for scattering states given by $u^J_{[\ell][\ell']}$.

The asymptotic behaviour of the radial physical wave-functions for discrete and scat-

tering states can then be written as follows:

$$U^J(E,r) \xrightarrow[r\to\infty]{} W^{(\mathrm{in})}(E,r) f^{(\mathrm{in})J}(E)\, C^J + W^{(\mathrm{out})}(E,r) f^{(\mathrm{out})J}(E)\, C^J. \tag{2.124}$$

This expression is identical to Eq. (1.54) on page 20, which was used to determine the Jost matrix relation to bound and resonance states. Consequently, the discussions in Sections 1.5.2 and 1.5.3 are also applicable here, and the properties of the Jost matrices with respect to discrete states are the same. The scattering cross-section for the scattering of particles with zero spin and nonzero spin is, however, not the same. This will be addressed in the next section.

2.2.6 Cross-section for systems with non-zero spin

For the two-body scattering of particles with non-zero spin where there is only one available energy channel, the channels are determined by the different angular momentum states, distinguished by the quantum number ℓ.

Consider again the wave-function for scattering states with spin, Eq. (2.116) derived in Section 2.2.4:

$$\psi_{\mathbf{k}s\mu}(\mathbf{r},s',\mu') = \sum_{JM}\sum_{[\ell'][\ell]} \langle s'\mu'|\mathcal{Y}^{JM}_{[\ell']}(\theta,\varphi)\rangle \frac{u^J_{[\ell'][\ell]}(E,r) N_{[\ell]}(k)}{r} \langle \mathcal{Y}^{JM}_{[\ell]}(\theta_k,\varphi_k)|s\mu\rangle.$$

To obtain the correct asymptotic form of this equation which corresponds with Eq. (1.126) on page 42, choose $C^J_{[\ell'']][\ell']} = [f^{(\mathrm{in})J}(E)]^{-1}$ in Eq. (2.123) and substitute this into Eq. (2.116). By taking the limit at large r and applying similar tricks as in Sections 1.5.6 and 2.1.6 gives the following:

$$\psi_{\mathbf{k}s\mu}(\mathbf{r},s',\mu') \xrightarrow[r\to\infty]{} \frac{1}{(2\pi)^{3/2}} \left[e^{i\mathbf{kr}} + \frac{e^{ikr}}{r} \langle s'\mu'|\mathrm{f}(\hat{r}\leftarrow\hat{k})|s\mu\rangle \right], \tag{2.125}$$

where the total spin scattering amplitude is defined by:

$$\mathrm{f}(\hat{r}\leftarrow\hat{k}) \equiv 4\pi \sum_{JM} \mathcal{Y}^{JM}(\theta,\varphi)\mathrm{f}^J(E)\mathcal{Y}^{JM\dagger}(\theta_k,\varphi_k), \tag{2.126}$$

which is an operator in spin-space. The partial wave scattering amplitude with spin is, in turn, defined as follows:

$$\mathrm{f}^J(E) \equiv \frac{1}{2ik}\mathcal{I}^\dagger[S^J(E)-1]\mathcal{I}, \tag{2.127}$$

with the matrix $\mathcal{I}$ given by:

$$\mathcal{I} \equiv \begin{pmatrix} i^{\ell_1} & 0 & \cdots & 0 \\ 0 & i^{\ell_2} & \cdots & 0 \\ \vdots & \vdots & \ddots & \vdots \\ 0 & 0 & \cdots & i^{\ell_N} \end{pmatrix}. \tag{2.128}$$

The probability-amplitude of colliding particles with incoming momentum $\mathbf{k}$ and the initial spin state $|s\mu\rangle$, and outgoing motion along $\mathbf{r}$ in the spin state $|s'\mu'\rangle$, is then given by:

$$\langle s'\mu'|\mathrm{f}(\hat{r}\leftarrow\hat{k})|s\mu\rangle = 4\pi\sum_{JM\ell'\ell}\mathcal{Y}^{JM}_{\ell's'\mu'}(\theta,\varphi)\,\mathrm{f}^J_{[\ell'][\ell]}(E)\left[\mathcal{Y}^{JM}_{\ell s\mu}(\theta_k,\varphi_k)\right]^*. \tag{2.129}$$

Since the final and initial spin states are fixed, the summation is over ℓ and not $[\ell]$. As for the scattering of particles with zero spin, the differential scattering cross-section is the square of this amplitude:

$$\left(\frac{d\sigma}{d\Omega}\right)_{s'\mu'\leftarrow s\mu} = \left|\langle s'\mu'|\mathrm{f}(\hat{r}\leftarrow\hat{k})|s\mu\rangle\right|^2. \tag{2.130}$$

If the z-axis is then chosen along the collision line, the spherical angles of the incoming momentum, θ_k and φ_k, will be zero. Furthermore, for a free incoming wave, $m=0$, which implies $M=\mu$ from Eq. (2.85). Thus, from Eq. (2.94) and (1.26),

$$\mathcal{Y}^{JM}_{\ell s\mu}(\theta_k,\varphi_k) = C^{JM}_{\ell 0 s\mu}Y_{\ell,0}(0,0) = C^{JM}_{\ell 0 s\mu}\sqrt{\frac{2\ell+1}{4\pi}}, \qquad \mathbf{k}\parallel z \tag{2.131}$$

and

$$C^{JM}_{\ell 0 s\mu} = \delta_{\mu M}C^{J\mu}_{\ell 0 s\mu}. \tag{2.132}$$

Implementing these expressions in the differential cross-section of Eq. (2.130) with the amplitude of Eq. (2.129) results in the following:

$$\begin{aligned}\left(\frac{d\sigma}{d\Omega}\right)_{s'\mu'\leftarrow s\mu} &= (4\pi)^2 \sum_{J_1\ell_1'\ell_1} \mathcal{Y}^{J_1\mu}_{\ell_1' s_1' \mu'}(\theta,\varphi)\, \mathrm{f}^{J_1}_{[\ell_1'][\ell_1]}(E) \left[\mathcal{Y}^{J_1\mu}_{\ell_1 s_1 \mu}(\theta_k,\varphi_k)\right]^* \\ &\quad \times \sum_{J_2\ell_2'\ell_2} \left[\mathcal{Y}^{J_2\mu}_{\ell_2' s_2' \mu'}(\theta,\varphi)\right]^* \mathrm{f}^{J_2*}_{[\ell_2'][\ell_2]}(E)\, \mathcal{Y}^{J_2\mu}_{\ell_2 s_2 \mu}(\theta_k,\varphi_k) \\ &= 4\pi \sum_{J_1\ell_1'\ell_1} \sum_{J_2\ell_2'\ell_2} \sqrt{(2\ell_1+1)(2\ell_2+1)}\mathrm{f}^{J_1*}_{[\ell_1'][\ell_1]}(E)\mathrm{f}^{J_2}_{[\ell_2'][\ell_2]}(E) \\ &\quad \times C^{J_1\mu}_{\ell_1 0 s\mu} C^{J_2\mu}_{\ell_2 0 s\mu} \left[\mathcal{Y}^{J_1 M}_{\ell_1' s' \mu'}(\theta,\varphi)\right]^* \mathcal{Y}^{J_2 M}_{\ell_2' s' \mu'}(\theta,\varphi), \quad (2.133)\end{aligned}$$

where the subscripts 1 and 2 distinguish between the different summations, and no longer the different values for the two-body system. Also, $[\ell_1] = \{\ell_1, s\}$ and $[\ell_2] = \{\ell_2, s\}$.

The differential cross-section is integrated over the spherical angles to obtain the total cross-section:

$$\sigma_{s'\mu'\leftarrow s\mu} = \int \left(\frac{d\sigma}{d\Omega}\right)_{s'\mu'\leftarrow s\mu} d\Omega. \quad (2.134)$$

If the expression for the differential cross-section, (2.133), is substituted into this integral, the only quantities that depend on the spherical angles are the functions, $\mathcal{Y}^{JM}_{\ell s\mu}(\theta,\varphi)$. Using Eq. (2.94) and the fact that the spherical harmonics are orthonormal (Eq. (1.27)) the following integral is obtained:

$$\int \left[\mathcal{Y}^{J_1 M}_{\ell_1' s' \mu'}(\theta,\varphi)\right]^* \mathcal{Y}^{J_2 M}_{\ell_2' s' \mu'}(\theta,\varphi) d\Omega = \delta_{\ell_1'\ell_2'} C^{J_1\mu}_{\ell'(\mu-\mu')s'\mu'} C^{J_2\mu}_{\ell'(\mu-\mu')s'\mu'}, \quad (2.135)$$

which results in the following expression for the total scattering cross-section:

$$\begin{aligned}\sigma_{s'\mu'\leftarrow s\mu} &= 4\pi \sum_{J_1\ell_1 J_2\ell_2\ell'} \sqrt{(2\ell_1+1)(2\ell_2+1)}\mathrm{f}^{J_1*}_{[\ell][\ell_1]}\mathrm{f}^{J_2}_{[\ell'][\ell_2]} \\ &\quad \times C^{J_1\mu}_{\ell'(\mu-\mu')s'\mu'} C^{J_2\mu}_{\ell'(\mu-\mu')s'\mu'} C^{J_1\mu}_{\ell_1 0 s\mu} C^{J_2\mu}_{\ell_2 0 s\mu}. \quad (2.136)\end{aligned}$$

The incident beam of particles is not, in general, polarised. All possible orientations of spin then have equal probabilities. It is therefore necessary to average over the states with different spin-magnetic quantum number, μ. Since this depends on s by the relations in Eq. (2.85), the number of possible differing states in μ for a specific spin, s is $2s+1$. This is why, when averaging the cross-section over all μ, the total cross-section is the sum of the cross-sections in different μ states, divided by this factor:

$$\sigma_{s'\mu'\leftarrow s} = \frac{1}{2s+1}\sum_{\mu}\sigma_{s'\mu'\leftarrow s\mu}. \tag{2.137}$$

If the final spin orientation, μ' is not measured, the summation must be done over these states as well:

$$\sigma_{s'\leftarrow s} = \frac{1}{2s+1}\sum_{\mu'\mu}\sigma_{s'\mu'\leftarrow s\mu}, \tag{2.138}$$

which results in the following:

$$\begin{aligned}\sigma_{s'\mu'\leftarrow s\mu} = \frac{4\pi}{2s+1}\sum_{J_1\ell_1 J_2\ell_2\ell'}&\sqrt{(2\ell_1+1)(2\ell_2+1)}\mathrm{f}^{J_1*}_{[\ell][\ell_1]}\mathrm{f}^{J_2}_{[\ell'][\ell_2]}\\ &\times\sum_{\mu'\mu}C^{J_1\mu}_{\ell'(\mu-\mu')s'\mu'}C^{J_2\mu}_{\ell'(\mu-\mu')s'\mu'}C^{J_1\mu}_{\ell_1 0s\mu}C^{J_2\mu}_{\ell_2 0s\mu}.\end{aligned} \tag{2.139}$$

Using the definition of the Clebsch-Gordan coefficient, Eq (2.87), and expanding over an appropriate vector basis, the following relation can be proven [22]:

$$\sum_{\mu'\mu}C^{J_1\mu}_{\ell'(\mu-\mu')s'\mu'}C^{J_2\mu}_{\ell'(\mu-\mu')s'\mu'}C^{J_1\mu}_{\ell_1 0s\mu}C^{J_2\mu}_{\ell_2 0s\mu} = \sum_{Mm\mu'\mu}C^{J_1M}_{\ell' ms'\mu'}C^{J_2M}_{\ell' ms'\mu'}C^{J_1M}_{\ell_1 0s\mu}C^{J_2M}_{\ell_2 0s\mu}.$$

Furthermore,

$$\sum_{m\mu'}C^{J_1M}_{\ell' ms'\mu'}C^{J_2M}_{\ell' ms'\mu'} = \delta_{J_1J_2},$$

and

$$\sum_{M\mu}C^{JM}_{\ell_1 0s\mu}C^{JM}_{\ell_2 0s\mu} = \frac{2J+1}{2\ell_1+1}\delta_{\ell_1\ell_2}.$$

Implementing these relations in Eq. (2.139) gives the final result for the total scat-

tering cross-section for the elastic scattering of particles with spin:

$$\sigma_{s\leftarrow s'} = \frac{4\pi}{2s+1}\sum_{J\ell\ell'}(2J+1)\left|\mathrm{f}^{J}_{[\ell'][\ell]}\right|^2, \tag{2.140}$$

and for a specific partial wave, the channel cross-sections are then given by:

$$\sigma^{J}_{s\leftarrow s'} = 4\pi\frac{2J+1}{2s+1}\left|\mathrm{f}^{J}_{[\ell'][\ell]}\right|^2. \tag{2.141}$$

Using Eq. (2.127) for the partial scattering amplitude with spin, the main result for this section is obtained:

$$\sigma^{J}_{s\leftarrow s'}(E) = \frac{\pi}{k^2}\frac{2J+1}{2s+1}\left|S^{J}(E)-I\right|^2. \tag{2.142}$$

If the spin of the system is zero, $s=0$ and $J=\ell$, thus Eq. (1.150) is retrieved. Furthermore, although it will not explicitly be shown, this result is also applicable to the scattering of particles with non-zero spin involving charged particle (where Coulomb interactions are present).

This concludes the introductory chapters. Most of the required building blocks to analyse specific scattering problems have been discussed. However, the most important aspect of this thesis still needs to be covered: the analytic structure of the Jost matrices. This will be discussed in the next chapter.

Chapter 3

The method of analysis

In this chapter, the new parameterisation of the multi-channel S-matrix, introduced in Ref. [6], will be discussed. It is this parameterisation that will allow the accurate fitting of experimental cross-sections for scattering involving Coulomb interactions to obtain relevant scattering parameters.

The S-matrix is constructed in terms of the Jost matrices, which cannot directly be fitted to experimental data, since they are energy dependent via the channel momenta, k_n, and the Sommerfeld parameter, η_n. This causes both square-root and logarithmic branching of the Riemann surface at each threshold energy. The Jost matrix must furthermore be analytically continued onto the complex plane to locate resonances. It is well known in complex analysis that the procedure of analytic continuation is "unforgiving". Problems often arise if the properties of the starting information or the method of continuation is somehow flawed (see, for example, Ref. [23]).

To overcome these challenges, it will be shown how the Jost matrices can be given in a semi-analytic form where the quantities responsible for the branching, k_n and η_n, are factorised explicitly. The remaining factors in the semi-analytic form of the Jost matrices are shown to be analytic and single-valued functions of energy and are then expanded in Taylor series around an appropriate energy. The expansion coefficients serve as the fitting parameters.

In Ref. [4], this parameterisation is tested on a two-channel model, using a set of

artificially generated data points with typical error bars and a typical random noise in the positions of the points. This chapter is mostly based on the results of this article, which is the first of the three articles this thesis is based on.

3.1 Riemann surface

Even though complex energies have no direct physical meaning, an analysis of the analytic properties of the Jost matrices at complex energies can reveal certain properties of the physical system and provide valuable information concerning the behaviour at physical energies, which are real. In particular, resonances correspond to complex energy poles of the S-matrix and have a definite effect on the scattering cross-section, as mentioned in Section 1.5.3.

Before discussing the analytic structure of the Jost matrices and the fitting of experimental data, the Riemann surface concept, which appeared in the previous chapters, must be understood. Consider the channel momenta, given by Eq. (1.36):

$$k_n = \pm\sqrt{\frac{2\mu_n}{\hbar^2}(E - E_n)}.$$

Each energy corresponds with two possible momentum values per channel. The Jost matrices, $f^{(\text{in/out})}(E)$, are energy dependent via k_n, which implies that each of the Jost matrix elements will have two possible values for a specific energy, except at the threshold energies where $E = E_n$ and $k_n = 0$.

In complex analysis, multi-valued functions are treated as if they are single-valued, but defined on a multi-layered surface consisting of several parallel planes. This complex manifold is called the Riemann surface.

For a simple single-channel problem with no Coulomb interactions, square-root branching occurs at the threshold $E = 0$ and thus there are two parallel momentum sheets in the complex plane. Refer to Figure 3.1, which represents the Riemann surface for this square-root branching. If a vertical line is drawn through the Riemann surface for this scenario, the points where this line intersects each of the k-sheets

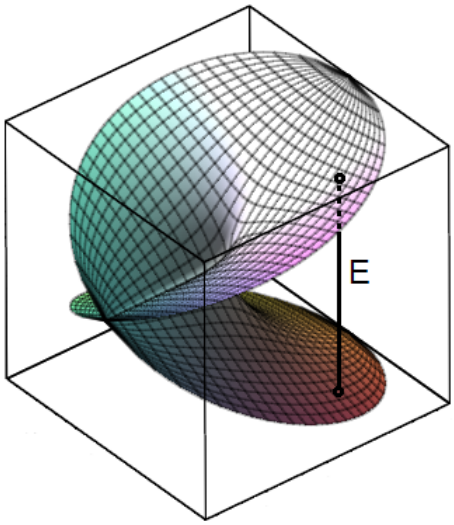

Figure 3.1: Riemann surface for square-root branching at the thresholds $E = 0$.

correspond to the same value of the independent variable, E. For N channels, there are 2^N square-root branching points of the Riemann surface. As has been mentioned, the sheet which corresponds with a positive choice for k_n for all n is known as the physical sheet, and a negative choice of k_n for all n corresponds with the unphysical sheet.

If Coulomb interactions are included, the situation becomes even more complicated. As will be shown when the Jost matrices are written in the semi-analytic form, a factor $\ln(k_n)$ appears in the expressions for the Jost matrices, which implies logarithmic branching at $E = 0$. The Riemann surface for single-channel logarithmic branching is shown in Figure 3.2, and forms a distinct spiral. If a line is drawn at momentum k, not only two but infinitely many $\ln(k)$ sheets are intersected. If the logarithm is written as follows:

$$\ln(k) = \ln\left[|k|e^{i[\arg(k)+2\pi m]}\right] = \ln|k| + i\arg(k) + i2\pi m, \tag{3.1}$$

it is clear the different sheets correspond to different m. The branch which corresponds with $m = 0$ is the principal branch and is the only relevant branch for practical calculations [6].

For multi-channel scattering, logarithmic and square-root branching will occur at

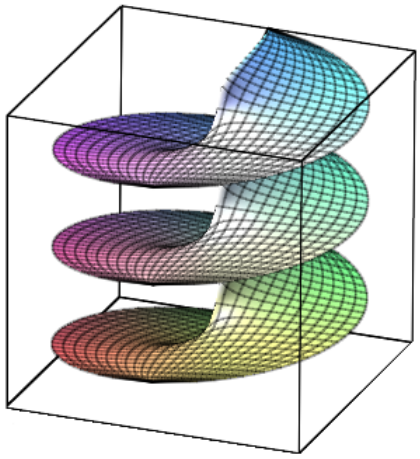

Figure 3.2: Riemann surface for logarithmic branching at $E = 0$.

each channel threshold and the complicated Riemann surface becomes impossible to draw.

Fittings of experimental data are done at real, positive energies to construct the appropriate function for extracting relevant scattering parameters. In this study, these functions are the Jost matrices. However, bound states occur on the physical sheet of the Riemann surface and resonances on the unphysical sheet. When analytically continuing the Jost matrices onto the complex plane to determine the spectral points, which may correspond to bound and resonance states, it is imperative that the continuation is done on the correct sheet of the Riemann surface.

Unless the factors responsible for the branching in the Jost matrices can be isolated, there can never be certainty in the analytic continuation of the Jost matrices. This is the reason for writing the Jost matrices in the semi-analytic form where the parameters responsible for the branching are factorised.

3.2 Analytic structure of the Jost matrices

3.2.1 Analytic structure of the Jost matrices for short-range interactions

For a simple, single-channel problem with short-range interactions only, the momentum dependence of the Jost functions, which makes them double-valued, can easily be isolated. See, for example, Ref. [24], where it is shown that the single-channel Jost functions in a particular partial wave can be written as follows:

$$f_\ell^{(\text{out/in})} = \frac{1}{2}\hat{A}_\ell(E) \pm \frac{i}{2}k^{2\ell+1}\hat{B}_\ell(E), \tag{3.2}$$

where $\hat{A}_\ell(E)$ and $\hat{B}_\ell(E)$ are single-valued, entire functions of energy, defined on a single complex energy plane. They can therefore be approximated by finite Taylor series. Using these expressions for the Jost functions, the single-channel S-matrix can be written as follows:

$$S_\ell(E) = \frac{\hat{A}_\ell(E) + ik^{2\ell+1}\hat{B}_\ell(E)}{\hat{A}_\ell(E) - ik^{2\ell+1}\hat{B}_\ell(E)}. \tag{3.3}$$

If the functions $\hat{A}_\ell(E)$ and $\hat{B}_\ell(E)$ are expanded around the energy $E = 0$, their ratio gives the well-known effective range expansion:

$$\frac{\hat{A}_\ell(E)}{\hat{B}_\ell(E)} = k^{2\ell+1}\cot\delta_\ell, \tag{3.4}$$

which is frequently used in fitting experimental data, with the expansion coefficients of $\hat{A}_\ell(E)$ and $\hat{B}_\ell(E)$ serving as fitting parameters. Although expanding around $E = 0$ is the traditional choice, the functions $\hat{A}_\ell(E)$ and $\hat{B}_\ell(E)$ can be expanded around any arbitrary E. The choice will not affect the analytic structure given by Eq. (3.3). For this reason, proper branching is always preserved.

Historically, much work was done to generalise the effective-range expansion (3.4) for multi-channel scattering as well as to derive an expression for the multi-channel

S-matrix similar to Eq. (3.3). Most authors (see, for example, Refs. [25, 26]) involve the term $\cot(\delta)$ to maintain similarity with the single-channel effective-range expansion. The approaches are consequently very complicated. Furthermore, they are technically only applicable to real energies, since the scattering phase-shift, δ, is only defined for real energies. However, by exploiting the analytic structure of the Regular and Irregular Coulomb functions (as is done in this study), useful single-channel effective range methods for the scattering of charged particles are developed in Ref. [27]. These are particularly useful in determining bound state energies from the fitting of scattering data (see Ref. [28], for example).

A two-channel equivalent to Eq. (3.3) has been developed in Ref. [29], known as the Dalitz-Tuan representation. However, it becomes problematic to obtain the S-matrix with correct branching at all the thresholds for more than two channels, with more traditional approaches [6].

As can be seen from Eq. (3.3), which is applicable to the single-channel scattering of neutral particles, the Jost functions do not have poles. The situation is similar for the multi-channel scattering of neutral particles, but poles may occur at the energy thresholds, as will be shown. The analytic structure of the Jost matrices is somewhat simpler than the corresponding S-matrix, consequently the Jost matrices are preferred over the S-matrix. Also, other than expressions involving the channel phase-shifts, the Jost matrices can be analytically continued to complex and negative energies, where they are equally well-defined as for real energies. The S-matrix can, of course, also be determined from the Jost matrices and the obtained expansion is of the Padé type.

As shown in Ref. [24], for multi-channel scattering with short-range interactions only, the Jost matrix elements are given by:

$$f_{nm}^{(\text{out/in})} = \frac{k_m^{\ell_m+1}}{2k_n^{\ell_n+1}}\hat{A}_{nm}(E) \pm i\frac{k_n^{\ell_n}k_m^{\ell_m+1}}{2}\hat{B}_{nm}(E), \tag{3.5}$$

where $\hat{A}(E)$ and $\hat{B}(E)$ now become $N \times N$ matrices. Here there are possible poles at threshold energies, but the structure is relatively simple. This representation was

successfully used in Ref. [24] to fit two-channel scattering data at energies far away from the thresholds and to determine the resonance parameters from the fitting.

For multi-channel scattering involving Coulomb interactions, the analytic structure of the Jost matrices is somewhat more complicated. In the fitting of experimental data and the analytic continuation to obtain resonances parameters, it is still mathematically more rigorous and computationally simpler to exploit the analytic structure of the Jost matrices rather than attempting fittings directly with the S-matrix or with effective-range-like expressions.

The analytic structure of the Jost matrices for scattering including Coulomb interactions will be derived next.

3.2.2 Analytic structure of the Jost matrices for Coulomb interactions

The derivation of the analytic structure rests on the fact that the Regular and Irregular Coulomb functions can be written as the product of k- and η-dependent functions, and functions that are entire (analytic and single-valued) in energy, E. Such a factorisation is done in Ref. [30] and is equivalent to the factorisation of Ref. [31] for repulsive interaction. The single-channel Regular and Irregular Coulomb functions are given by:

$$F_\ell(\eta,kr) = D_\ell(\eta,k)\tilde{F}_\ell(E,r), \tag{3.6}$$

$$G_\ell(\eta,kr)) = M(\eta)D_\ell(\eta,k)\tilde{F}_\ell(E,r) + \frac{k}{D_\ell(\eta,k)}\tilde{G}_\ell(E,r), \tag{3.7}$$

where $\tilde{F}_\ell(E,r)$ and $\tilde{G}_\ell(E,r)$ are unknown, entire functions in E. The k- and η-dependence is then explicitly isolated via the following:

$$D_\ell(\eta,k) = C_\ell(\eta)k^{\ell+1}, \qquad M(\eta) = \frac{2\eta h(\eta)}{C_0^2(\eta)}, \tag{3.8}$$

with:

$$h(\eta) = \frac{1}{2}\left[\psi(i\eta) + \psi(-i\eta)\right] - \ln\hat{\eta}, \qquad \psi(z) = \frac{\Gamma'(z)}{\Gamma(z)}, \qquad \hat{\eta} = \frac{\mu e^2 |Z_1 Z_2|}{k\hbar^2}. \quad (3.9)$$

For multi-channel scattering, the following diagonal matrices are now constructed, as done in Ref. [6]:

$$D = \begin{pmatrix} C_{\ell_1}(\eta_1)k_1^{\ell_1+1} & 0 & \cdots & 0 \\ 0 & C_{\ell_2}(\eta_2)k_2^{\ell_2+1} & \cdots & 0 \\ \vdots & \vdots & \ddots & \vdots \\ 0 & 0 & \cdots & C_{\ell_N}(\eta_N)k_N^{\ell_N+1} \end{pmatrix}, \quad (3.10)$$

$$M = \begin{pmatrix} \frac{2\eta_1 h(\eta_1)}{C_0^2(\eta_1)} & 0 & \cdots & 0 \\ 0 & \frac{2\eta_2 h(\eta_2)}{C_0^2(\eta_2)} & \cdots & 0 \\ \vdots & \vdots & \ddots & \vdots \\ 0 & 0 & \cdots & \frac{2\eta_N h(\eta_N)}{C_0^2(\eta_N)} \end{pmatrix}. \quad (3.11)$$

By the factorisation (3.6) and (3.7), the diagonal matrices comprised of the Regular and Irregular function, given in Eq. (2.27) and (2.28) on page 57, can then be written in terms of the matrices D and M as follows:

$$F(E,r) = D\tilde{F}(E,r), \quad (3.12)$$

$$G(E,r) = MD\tilde{F}(E,r) + KD^{-1}\tilde{G}(E,r), \quad (3.13)$$

where $\tilde{F}(E,r)$ and $\tilde{G}(E,r)$ are unknown diagonal matrices comprised of functions entire in E:

$$\tilde{F}(E,r) = \begin{pmatrix} \tilde{F}_{\ell_1}(E,r) & 0 & \cdots & 0 \\ 0 & \tilde{F}_{\ell_2}(E,r) & \cdots & 0 \\ \vdots & \vdots & \ddots & \vdots \\ 0 & 0 & \cdots & \tilde{F}_{\ell_N}(E,r) \end{pmatrix}, \quad (3.14)$$

$$\tilde{G}(E,r) = \begin{pmatrix} \tilde{G}_{\ell_1}(E,r) & 0 & \cdots & 0 \\ 0 & \tilde{G}_{\ell_2}(E,r) & \cdots & 0 \\ \vdots & \vdots & \ddots & \vdots \\ 0 & 0 & \cdots & \tilde{G}_{\ell_N}(E,r) \end{pmatrix}. \tag{3.15}$$

If Eq. (3.12) and Eq. (3.13) are then substituted into Eq. (2.35), the matrix of radial wave solutions, $U_M(E,r)$ given in terms of the matrices $A(E,r)$ and $B(E,r)$, the following is obtained:

$$\begin{aligned} U_M(E,r) &= \left[\tilde{F}(E,r)\left(DA(E,r)D^{-1} + MDB(E,r)D^{-1}\right)\right. \\ &\quad \left. + \tilde{G}(E,r)KD^{-1}B(E,r)D^{-1}\right] D. \end{aligned} \tag{3.16}$$

Recall that the matrices $A(E,r)$ and $B(E,r)$ can be determined by solving the system of differential equations (2.37) and (2.38) on page 59 for a known potential. The following matrices are now defined:

$$\tilde{A}(E,r) = DA(E,r)D^{-1} + MDB(E,r)D^{-1}, \tag{3.17}$$

$$\tilde{B}(E,r) = KD^{-1}B(E,r)D^{-1}. \tag{3.18}$$

Re-arranging in terms of $A(E,r)$ and $B(E,r)$ gives:

$$A(E,r) = D^{-1}\tilde{A}(E,r)D - MK^{-1}D\tilde{B}(E,r)D, \tag{3.19}$$

$$B(E,r) = K^{-1}D\tilde{B}(E,r)D. \tag{3.20}$$

It should be mentioned again that diagonal matrices commute, thus they can be re-ordered as desired. However, $A(E,r)$ and $B(E,r)$ are not diagonal. In terms of the newly defined matrices, $U_M(E,r)$ can then be written as follows:

$$U_M(E,r) = \left[\tilde{F}(E,r)\tilde{A}(E,r) + \tilde{G}(E,r)\tilde{B}(E,r)\right] D, \tag{3.21}$$

and the Lagrange condition (2.36) becomes:

$$\left[\tilde{F}(E,r)\partial_r\tilde{A}(E,r)+\tilde{G}(E,r)\partial_r\tilde{B}(E,r)\right]D=0. \tag{3.22}$$

By substituting these into the coupled radial Coulomb Schrödinger equation (2.7), the following system of differential equations is then obtained:

$$\partial_r\tilde{A}(E,r) = \tilde{G}(E,r)V(r)\left[\tilde{F}(E,r)\tilde{A}(E,r)+\tilde{G}(E,r)\tilde{B}(E,r)\right] \tag{3.23}$$

$$\partial_r\tilde{B}(E,r) = -\tilde{F}(E,r)V(r)\left[\tilde{F}(E,r)\tilde{A}(E,r)+\tilde{G}(E,r)\tilde{B}(E,r)\right], \tag{3.24}$$

where the factors responsible for the branching conveniently disappear. This system of differential equations can also be obtained by substituting Eq. (3.14), (3.15), (3.17) and (3.18) into the system of differential equations (2.37) and (2.38). From (2.39) it can also be shown that:

$$\tilde{A}(E,0)=I\,, \qquad \tilde{B}(E,0)=0. \tag{3.25}$$

Therefore, since $\tilde{F}_\ell(E,r)$ and $\tilde{G}_\ell(E,r)$ are entire functions, it follows from the Poincaré theorem (see Ref. [32]) that the elements of the matrices $\tilde{A}(E,r)$ and $\tilde{B}(E,r)$ are also entire functions of E for any finite r [6].

Recall that the matrices $\mathcal{F}^{(\mathrm{in/out})}(E,r)$, which are related to the Jost matrices for large r, are defined in terms of $A(E,r)$ and $B(E,r)$ with Eq. (2.43) on page 61. Substituting Eq. (3.19) and (3.20) into this definition gives:

$$\mathcal{F}^{(\mathrm{in/out})}(E,r)=\frac{1}{2}\left[D^{-1}\tilde{A}(E,r)D-(M\pm i)K^{-1}D\tilde{B}(E,r)D\right]. \tag{3.26}$$

Taking the limit as $r\to\infty$ and using Eq. (2.54) gives:

$$f^{(\mathrm{in/out})}(E)=C^{-1}L^{-1}\sigma^{(\mp)}\frac{1}{2}\lim_{r\to\infty}\left[D^{-1}\tilde{A}(E,r)D-(M\pm i)K^{-1}D\tilde{B}(E,r)D\right]. \tag{3.27}$$

The Jost matrix elements are then given explicitly by:

$$f_{mn}^{(\text{in/out})}(E) = \frac{e^{\pi\eta_m/2}\ell_m!}{2\Gamma(\ell_m+1\pm i\eta_m)}\left\{\frac{C_{\ell_n}(\eta_n)k_n^{\ell_n+1}}{C_{\ell_m}(\eta_m)k_m^{\ell_m+1}}\mathcal{A}_{mn}(E)\right. \tag{3.28}$$

$$\left.-\left[\frac{2\eta_m h(\eta_m))}{C_0^2(\eta_m)}\pm i\right]C_{\ell_m}(\eta_m)C_{\ell_n}(\eta_n)k_m^{\ell_m}k_n^{\ell_n+1}\mathcal{B}_{mn}(E)\right\},$$

with

$$\mathcal{A}(E) = \lim_{r\to\infty}\tilde{A}(E,r), \tag{3.29}$$

$$\mathcal{B}(E) = \lim_{r\to\infty}\tilde{B}(E,r). \tag{3.30}$$

If $m = n = 1$, the single-channel results is obtained:

$$f_\ell^{(\text{in/out})}(E) = \frac{e^{\pi\eta/2}\ell!}{\Gamma(\ell+1\pm i\eta)}\left\{\mathcal{A}(E)-\left[\frac{2\eta h(\eta)}{C_0^2(\eta)}\pm i\right]C_\ell^2(\eta)k^{2\ell+1}\mathcal{B}(E)\right\}, \tag{3.31}$$

which can also be proven from first principles, as done in Ref [6].

These equations are the Coulomb equivalent of the equations (3.5) and (3.2) respectively, which are retrieved when $\eta_n = 0$ with $\mathcal{A}(E) = \hat{A}(E)$ and $\mathcal{B}(E) = \hat{B}(E)$.

Proceeding the same way as in Ref. [6], the matrices $\mathcal{A}(E)$ and $\mathcal{B}(E)$ are comprised of entire functions in E and can therefore be expanded in Taylor series around an arbitrary energy, E_0, within the domain of analyticity. This domain is not the entire complex plane, though, since $\mathcal{A}(E)$ and $\mathcal{B}(E)$ are defined when $r\to\infty$ for $\tilde{A}(E,r)$ and $\tilde{B}(E,r)$, which are analytic for finite r only. The expansions are only accurate within a circle around E_0 in the complex plane.

The matrices $\mathcal{A}(E)$ and $\mathcal{B}(E)$ are approximated by a finite number of terms of the

Taylor series:

$$\mathcal{A}(E) \approx \sum_{i=0}^{M} \alpha_i(E_0)(E-E_0)^i, \tag{3.32}$$

$$\mathcal{B}(E) \approx \sum_{i=0}^{M} \beta_i(E_0)(E-E_0)^i. \tag{3.33}$$

For multi-channel scattering, α_i and β_i are $N \times N$ matrices. The elements of these matrices are the adjustable parameters in the procedure for fitting experimental cross-sections [4].

As indicated in Ref. [6], the expansion coefficients must be real for real E_0. The value, M determines the number of fitting parameters. For single-channel fittings, if $M = 2$ for example, there will be six fitting parameters: three each for the expansion of $\mathcal{A}(E)$ and $\mathcal{B}(E)$. If $M = 2$ for multi-channel scattering with the number of channels $N = 3$, the fitting parameters will be six 3×3 matrices; there will then be 54 fitting parameters in total. In principle, the fittings can be done around complex E_0, but this would double the number of fitting parameters (since there is a real and an imaginary part to each parameter), which becomes computationally expensive. For all the fittings performed for this thesis, real E_0 are chosen and the value M for the fitting is indicated. In general, the number of fitting parameters is given by $2(M+1)N^2$.

When $\mathcal{A}(E)$ and $\mathcal{B}(E)$ are obtained from the appropriate fitting of data (which will be covered in the next section), bound and resonance states can be determined from the resulting Jost matrices. When locating spectral points of the S-matrix, it can be determined whether these are on the physical or unphysical sheet of the Riemann surface by explicitly controlling the sign of the channel momenta, k_n. Correct bound and resonance states will then be determined by ensuring that they are located on the correct sheet of the Riemann surface.

It should also be mentioned that complications may arise for scattering involving attractive Coulomb interactions, as indicated in Ref. [6]. Such problems typically

arise in atomic physics, where the attractive interactions between protons and electrons play a large part in bound and resonance states of molecular systems. Only nuclear interactions, where the long-ranged Coulomb part is always repulsive, are considered in this thesis. Therefore, such complications can safely be ignored.

3.3 Fitting procedure

Data may be available for all possible channels in a scattering problem, or only for a limited number of channels. The channel data is typically given by the channel cross-sections at specific energies:

$$\sigma_{mn}(E_i^{mn}) \pm \delta_i^{mn}, \qquad i = 1,2,...,N^{(mn)}, \tag{3.34}$$

where the number of available cross-sections for the different channels, $N^{(mn)}$, as well as the corresponding energy values may differ. The experimental error for each channel cross-section at an energy, E_i^{mn}, is given by δ_i^{mn}. The energy, E_0, around which the matrices $\mathcal{A}(E)$ and $\mathcal{B}(E)$ are expanded in Eq. (3.32) and (3.33), can be chosen somewhere within the interval covered by these collision energies, where a resonance is expected to be found. The optimal values of the fitting parameters are found by minimising the following χ^2 function:

$$\begin{aligned}\chi^2 = \sum_i^{N^{mn}} \left[\frac{\sigma_{mn}(E_i^{mn}) - \sigma_{mn}^{\text{fit}}(E_i^{mn})}{\delta_i^{mn}}\right]^2 \\ + \sum_j^{N^{m'n'}} \left[\frac{\sigma_{mn}(E_j^{m'n'}) - \sigma_{m'n'}^{\text{fit}}(E_j^{m'n'})}{\delta_j^{m'n'}}\right]^2 \\ + \cdots + \sum_{m>n,i} |S_{mn}(E_i^{mn}) - S_{mn}(E_i^{mn})|^2,\end{aligned} \tag{3.35}$$

where the fitting cross-sections, $\sigma_{mn}(E)$, are determined with Eq. (1.150):

$$\sigma_{mn} = \frac{\pi}{k_m^2}(2\ell_m + 1)\,|S_{mn}(E) - \delta_{mn}|^2,$$

with $S(E) = f^{(\text{out})}[f^{(\text{in})}]^{-1}$ and the Jost matrices in the semi-analytic form of Eq. (3.28). The scattering is clearly also limited to systems with zero spin. The matrices $\mathcal{A}(E)$ and $\mathcal{B}(E)$ are expanded in Taylor series and the elements of $\alpha_i(E)$ and $\beta_i(E)$ are the fitting parameters, indicated before.

The summations of the χ^2 function represent the fitting of the data of each available channel. The last term is somewhat different, though. It ensures the symmetry of the S-matrix in accordance with the detailed balance theorem, which arises from the time-reversal invariance [24]. This does not, however, hold for the scattering of particles with non-zero spin, and will thus be omitted in the fittings performed in Chapter 6.

The minimisation is done using the MINUIT code [33] in Fortran, due to its capacity for handling large amounts of data speedily. A random initial set of values for the fitting parameters are generated, and the minimisation is performed. The parameters obtained from the minimisation are stored, together with the value obtained for χ^2. A new set of random initial values for the fitting parameters are generated, and the minimisation is repeated. If a better minimum for χ^2 is obtained, the corresponding parameters replace the previous values. This process is repeated many thousands of times to obtain the best possible fitting.

When a suitable fitting is obtained, the spectral points are determined by finding the energy values $\mathcal{E}_i$ such that $\det\left[f^{(\text{in})}(\mathcal{E}_i)\right] = 0$, on the appropriate sheet of the Riemann surface for bound and resonance states. The Runga-Kutta method, among other methods, is mostly used to determine these zeros numerically. The fittings are then repeated for different E_0 and M and the spectral points for these fitting are determined. If the spectral points do not appear for fittings around different E_0 that are near each other, they are not true spectral points and are discarded.

3.4 Fitting example

The model potential

In order to demonstrate the efficiency of the proposed method, a model two-channel problem is considered, where the parameters of the resonances can be determined exactly. This model is used in Ref. [4], where artificial data points with a typical distribution of errors are generated. In addition to the error-bar for each pseudo-data point, a random shift (up or down) from the exact cross-section for each energy is introduced. This is how a typical value for experimental "noise" is simulated. Using these points, fittings are performed and resonance parameters are determined. These are compared with the exact values.

The artificial data points are generated using the following two-channel reduced potential, which includes Coulomb interactions:

$$V(r) = \begin{pmatrix} -1.0 & -7.5 \\ -7.5 & +7.5 \end{pmatrix} r^2 e^{-r} + \begin{pmatrix} 1 & 0 \\ 0 & 1 \end{pmatrix} \frac{1}{r}. \tag{3.36}$$

The short-range term in this potential is the same as in the well-known Noro–Taylor model [34]. The units are chosen such that $\mu_1 = \mu_2 = 1$ with $\hbar c = 1$ and $\ell_1 = \ell_2 = 0$. The channel threshold energies are $E_1 = 0$, as usual, and $E_2 = 0.1$. The Coulomb term is clearly repulsive, with $2k_n\eta_n = 1$. This potential does not represent a physical system, but is chosen due to its richness in sharp, well-defined resonances.

Theses resonances and the channel cross-sections can be determined exactly by calculating the matrices $A(E,r)$ and $B(E,r)$ from the system of differential equations (2.37) and (2.38), with boundary conditions (2.39) on page 60. The method of complex rotation is also implemented when determining $A(E,r)$ and $B(E,r)$, which is discussed in detail in Ref. [17]. The matrices $\mathcal{F}^{(\text{in/out})}(E,r)$ can then be determined with Eq. (2.43), thus the Jost matrices can be determined with Eq. (2.54). The exact Jost matrices then allow the exact resonance parameters and cross-sections to be determined. The first six of these resonances for the potential (3.36) are given in Table

Resonance	E_r	Γ	Γ_1	Γ_2
1	6.278042551	0.036866729	0.006898807	0.029967922
2	8.038507867	2.563111275	0.617710684	1.945400591
3	8.861433400	7.883809113	1.949506410	5.934302704
4	9.020824224	14.07907263	3.591961102	10.48711153
5	8.566130944	20.75266055	5.414178669	15.33848188
6	7.548492959	27.69926473	7.328979882	20.37028485

Table 3.1: The exact resonance energies and widths generated by the potential (3.36) [4].

3.1, including the partial widths calculated with Eq. (1.101) on page 34.

The data and results

For the elastic channels $(1 \to 1)$ and $(2 \to 2)$, 30 data points in the energy interval, $6 < E < 11$, are generated. These data points are exact. In any scattering experiment, it is impossible to obtain exact scattering cross-sections. In order to make these cross-section values more like experimental values, they are shifted around the exact values by using a Gaussian distribution. To be precise, the exact values, $\sigma_{mn}(E_i^{mn})$, are replaced as follows:

$$\sigma_{mn}(E_i^{mn}) \to G_i\, \sigma_{mn}(E_i^{mn}), \tag{3.37}$$

where G_i is a number from a normal distribution with a mean of 1 and a standard deviation of Δ. Smaller values of Δ therefore simulates smaller experimental noise and larger values result in greater experimental noise. To test the stability of the fitting method, three values of Δ are used: 0.01, 0.05 and 0.10. As well as the simulated noise, typical values for the experimental error for the generated data are also introduced.

The center of expansion is chosen to be $E_0 = 8$ for all the fittings. In the case of low experimental noise ($\Delta = 0.01$), a value of $M = 5$ is chosen in the expansions (3.32) and (3.33). For this two-channel scattering problem, there are 48 fitting parameters. For greater experimental noise ($\Delta = 0.05$ and $\Delta = 0.10$), a value of $M = 3$ is chosen

and then there are 32 fitting parameters. The reason for the different choice in M is that, for large M, the fitting curve tries to pass through almost all the data points and so does noisy zigzags, which result in a loss of overall accuracy [4].

Figures 3.3 and 3.4 show the two-channel fittings of the artificially generated data with $\Delta = 0.01$ of the elastic channels, $(1 \to 1)$ and $(2 \to 2)$, respectively. Figures 3.5 and 3.6 show the fittings for $\Delta = 0.05$ and Figures 3.7 and 3.8 show the fittings for $\Delta = 0.10$.

All matrix elements of the Jost matrices are involved in the two-channel fitting of the data points in the elastic channels $(1 \to 1)$ and $(2 \to 2)$. The corresponding diagonal elements of the S-matrix, which are related to the elastic channels, will be accurate for a good fitting. Yet the off-diagonal elements of the S-matrix should also be close to the correct values. This implies that, even if no data points for the inelastic channels $(1 \to 2)$ and $(2 \to 1)$ are available, reasonably accurate cross-sections, $\sigma_{21}(E)$ and $\sigma_{12}(E)$ should be obtained. Figure 3.9 shows the exact cross-section for the inelastic channel $(1 \to 2)$ and the predicted curves obtained for $\Delta = 0.01, 0.05$, and 0.10. Of course, as one would expect, the greater the accuracy of the experimental data, the more accurate the prediction for the cross-section in the channel where no data points are available.

When adequate fittings are obtained, the corresponding fitting parameters are used to construct the Jost matrices. Roots of $\det\left[f^{(\mathrm{in})}(\mathcal{E}_i)\right]$ on the unphysical sheet of the Riemann surface of the energy are then determined. For this sheet, the signs in $k_n = \pm\sqrt{2\mu_n(E-E_n)/\hbar^2}$ are chosen such that both channel momenta k_1 and k_2 have negative imaginary parts. These roots are then resonance spectral points, and are given in Table 3.2 for the fittings with experimental noise simulated by $\Delta = 0.01, 0.05$, and 0.10.

3.5 Remarks

As expected, with less "noise", the resonance parameters obtained from the fitting correspond considerably better to the exact values. Yet even with very high experimental noise ($\Delta = 0.10$), the first, narrow resonance is still obtained with a reasonable accuracy. Not only are the energy and total width reproduced, but the partial widths as well. For a wide resonance (the second resonance), reasonable parameters are still obtained where there is high experimental noise. Even for an extremely wide resonance (the third), the energy obtained is not far from the exact value.

One of the advantages of the proposed method is that the fitting procedure involves all matrix elements of the Jost matrices and therefore all elements of the S-matrix, even if experimental data for only some of the channels are available. The S-matrix resulting from the fitting should therefore be correct in all channels. In principle, this means that by fitting accurately measured data in one or two channels, a reasonable estimate for the cross-sections in the other channels, where the measurements are difficult or impossible, could be obtained.

These results, which are the principal findings from Ref. [4], show that the model based on the semi-analytic structure of the Jost matrices is accurate and robust for fittings of experimental data, even if the data has a great amount of experimental noise. A more detailed discussion follows in the final chapter, but this fitting method will first be applied to real experimental data in Chapters 5 and 6. The method has also effectively been applied to locate two-channel resonances in the nuclei ^{5}He [35] and ^{8}B [36].

Before considering the physical systems in Chapters 5 and 6, which are applicable in astrophysics, some introductory concepts in astrophysics will be discussed in the next chapter.

Resonance	Δ	E_r	Γ	Γ_1	Γ_2
1	exact	6.278042552	0.036866729	0.006898807	0.029967922
	0.01	6.277997424	0.036731019	0.006721542	0.030009477
	0.05	6.278563562	0.035568397	0.006497720	0.029070677
	0.10	6.278669302	0.036236713	0.006638945	0.029597768
2	exact	8.038507867	2.563111275	0.617710684	1.945400591
	0.01	7.998939904	2.096675299	0.623726003	1.472949296
	0.05	7.676616089	2.502856671	0.792088450	1.710768220
	0.10	7.968634195	1.662113407	0.231505793	1.430607614
3	exact	8.861433400	7.883809114	1.949506410	5.934302704
	0.01	11.21325906	3.204531546	0.031776330	3.172755216
	0.05	9.188805831	2.549030291	0.364986606	2.184043685
	0.10	9.259323135	2.226793463	1.232709401	0.994084062

Table 3.2: The resonance parameters obtained from fitting the model data with different degrees of experimental noise [4].

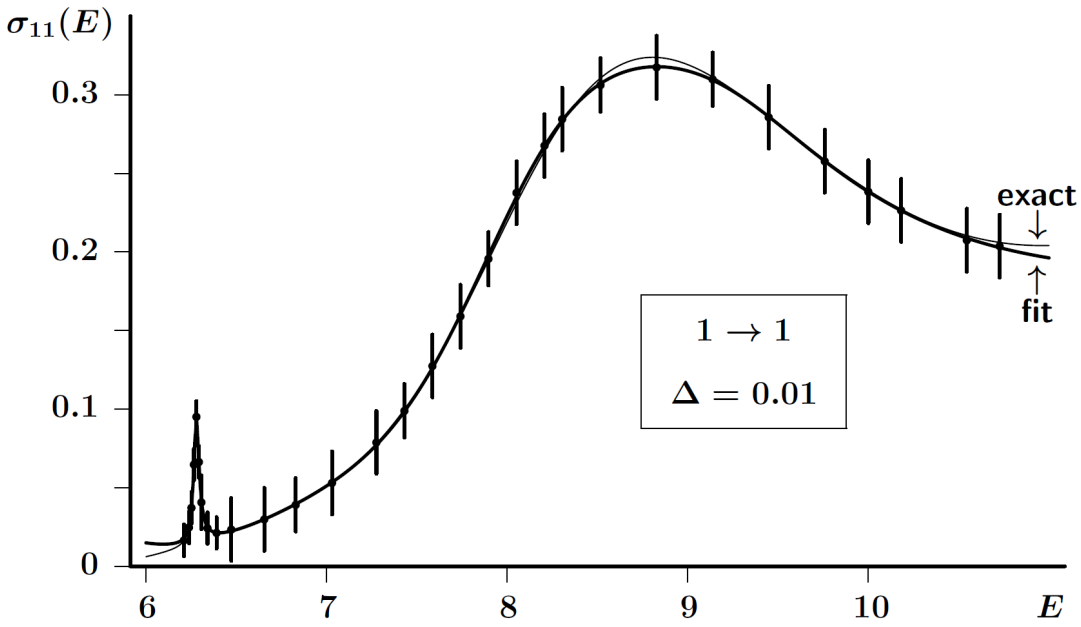

Figure 3.3: The data points for the elastic channel, $(1 \to 1)$ together with the curves showing the exact and fitted cross-sections. The experimental noise for the points has the normal distribution with the standard deviation $\Delta = 0.01$ [4].

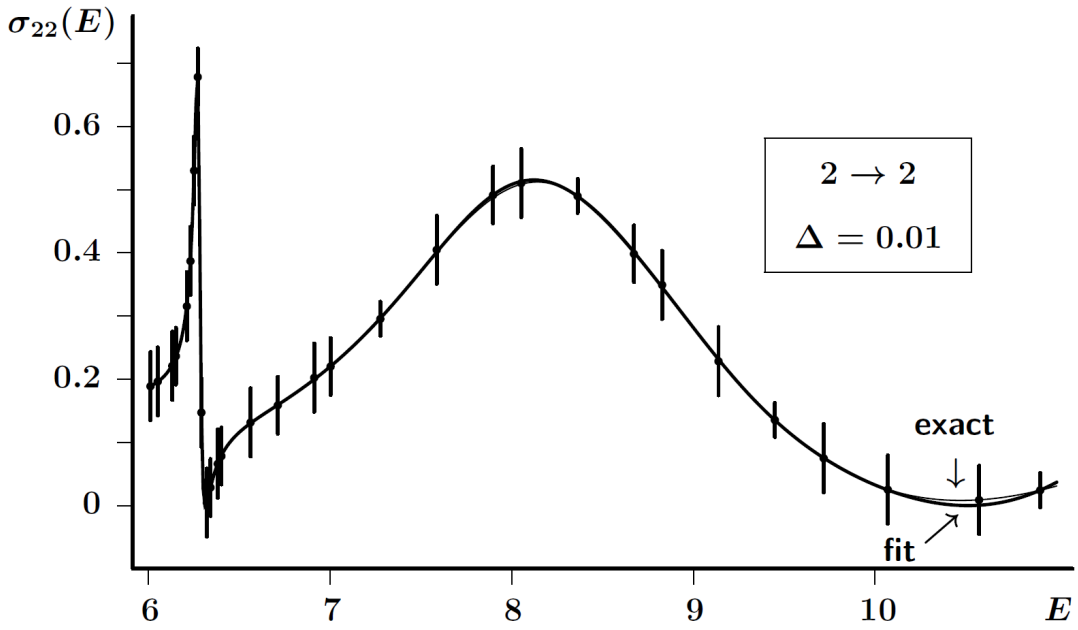

Figure 3.4: The data points for the elastic channel, $(2 \to 2)$ together with the curves showing the exact and fitted cross-sections. The experimental noise for the points has the normal distribution with the standard deviation $\Delta = 0.01$ [4].

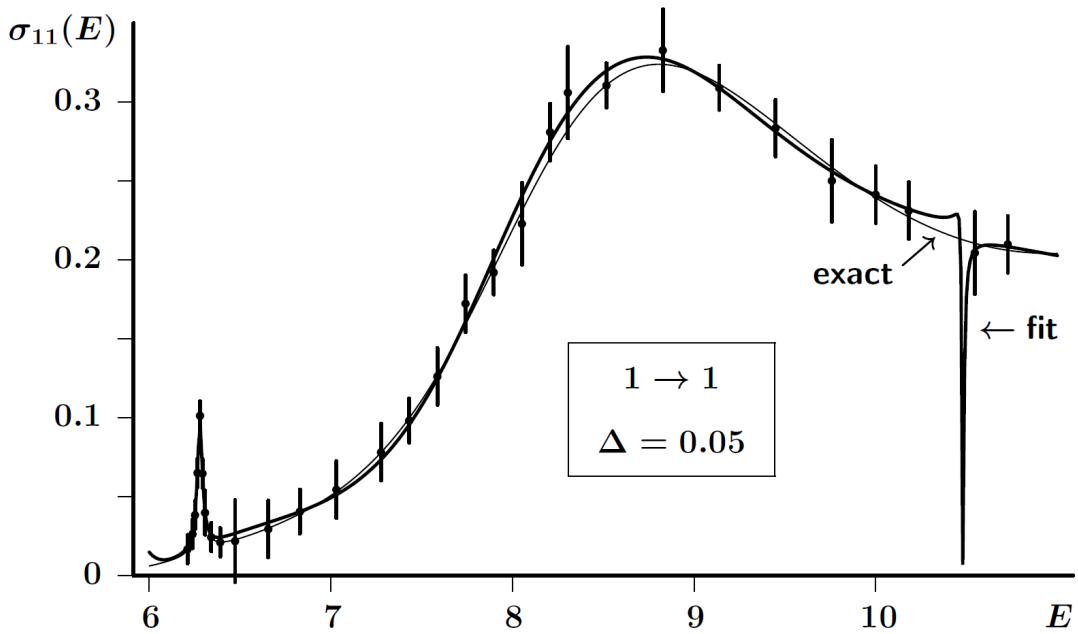

Figure 3.5: The data points for the elastic channel, $(1 \to 1)$ together with the curves showing the exact and fitted cross-sections. The experimental noise for the points has the normal distribution with the standard deviation $\Delta = 0.05$ [4].

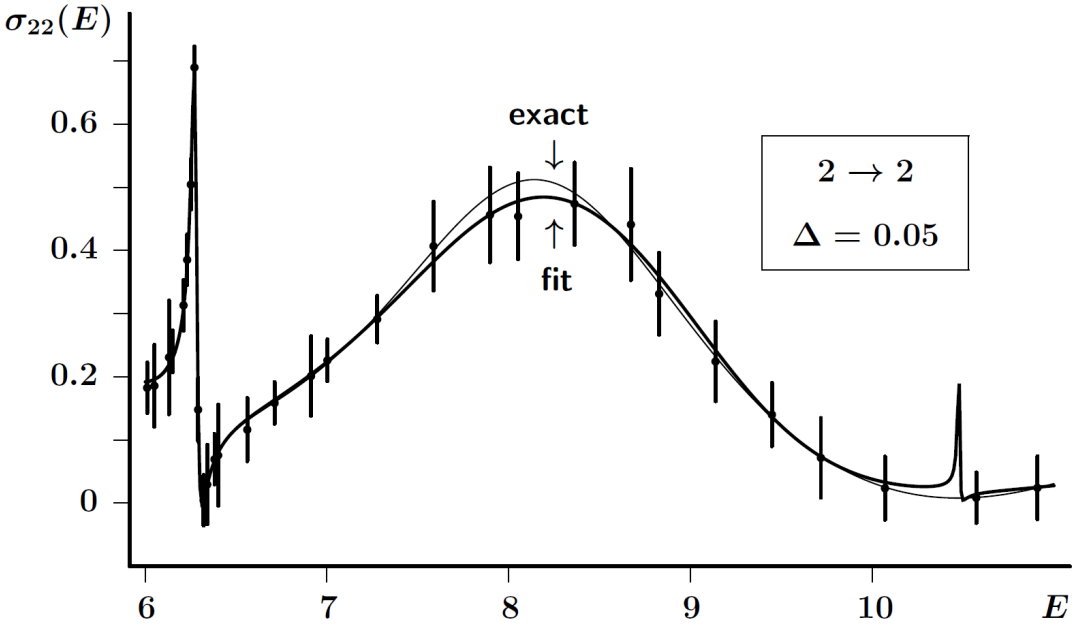

Figure 3.6: The data points for the elastic channel, $(2 \to 2)$ together with the curves showing the exact and fitted cross-sections. The experimental noise for the points has the normal distribution with the standard deviation $\Delta = 0.05$ [4].

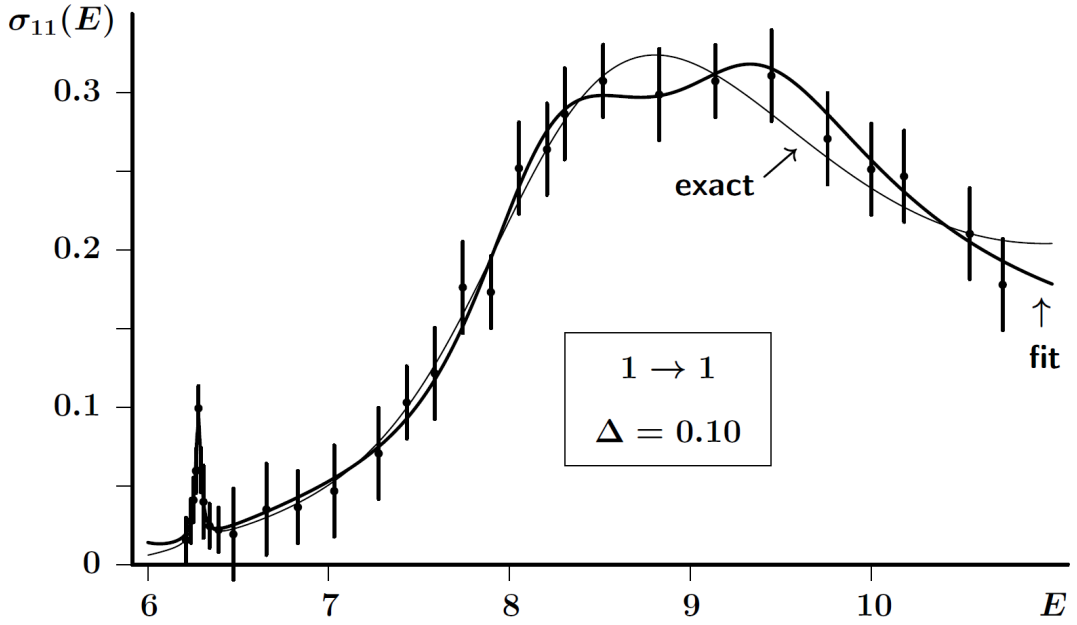

Figure 3.7: The data points for the elastic channel, $(1 \to 1)$ together with the curves showing the exact and fitted cross-sections. The experimental noise for the points has the normal distribution with the standard deviation $\Delta = 0.10$ [4].

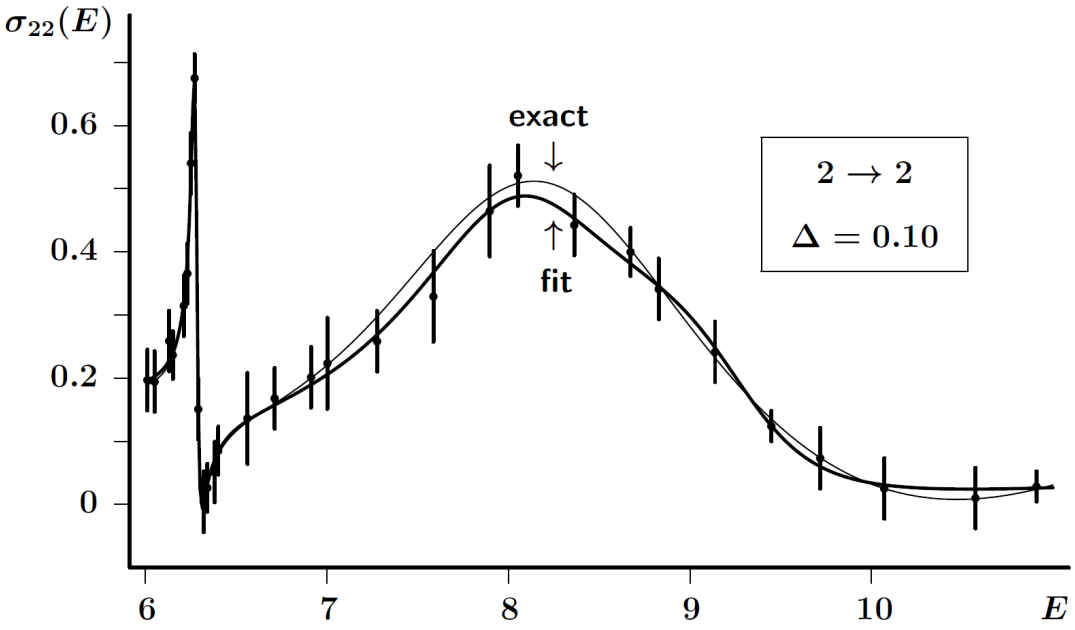

Figure 3.8: The data points for the elastic channel, $(2 \to 2)$ together with the curves showing the exact and fitted cross-sections. The experimental noise for the points has the normal distribution with the standard deviation $\Delta = 0.10$ [4].

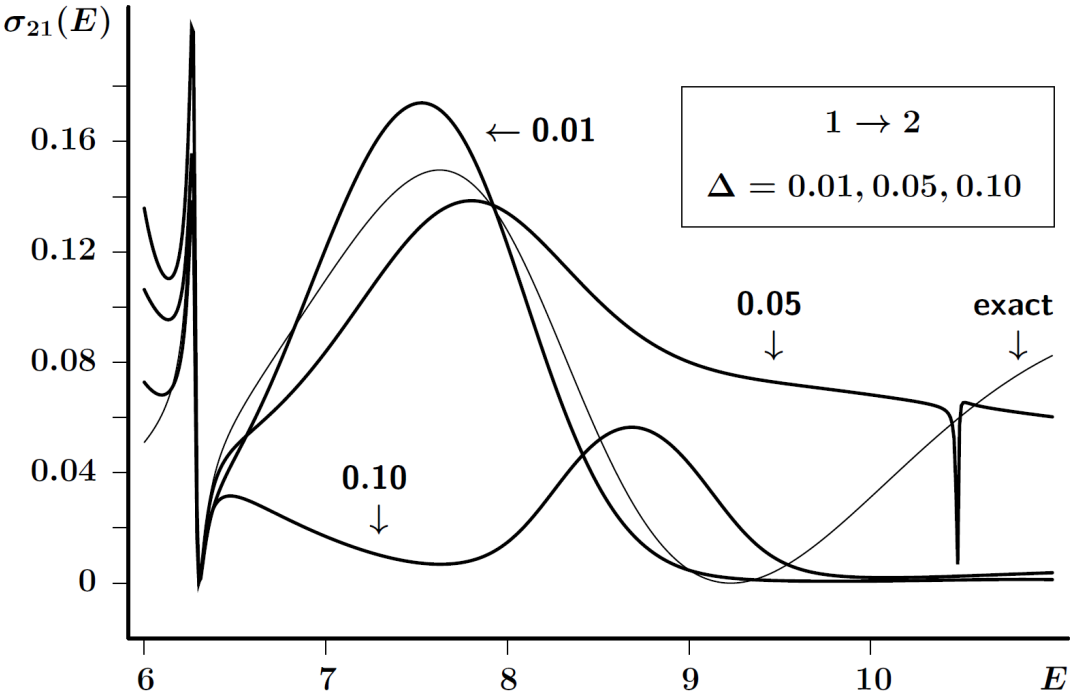

Figure 3.9: Exact inelastic cross-section (thin curve) for the inelastic transition channel, $(1 \to 2)$ and the approximate curves obtained after fitting the data in the elastic channels with the experimental noise determined by the standard deviations $\Delta = 0.01$, 0.05, and 0.10 [4].

Chapter 4

Astrophysics and the ANC

This chapter introduces some concepts and models in astrophysics. In particular, the Asymptotic Normalisation Coefficient (ANC) for bound and resonance states is defined, which is related to the astrophysical $\mathcal{S}$-factor of radiative capture reactions.

The $\mathcal{S}$-factor, in turn, allows reaction rates in stars, star lifetimes and isotope abundances to be determined, among other things. It is beyond the scope of this thesis to use calculated ANC values to determine star lifetimes, for example, but the general theory will be outlined. The goal is to illustrate the practical use and importance of the ANC.

The relationship between the S-matrix residue and the ANC will be derived explicitly. This does form a cardinal part of this thesis, since such a derivation for scattering involving Coulomb interactions does not readily appear in the literature. This relationship is used in Chapter 5 in the Jost function analysis of α^{12}C scattering data, where the ANC values for the resonances of ^{16}O in the reaction, $^{12}\mathrm{C}(\alpha,\gamma)^{16}\mathrm{O}$, are obtained. In Chapter 6, ANC values for the bound and resonance states of ^{6}Li in the reaction $\alpha(d,\gamma)^{6}\mathrm{Li}$ are obtained from a Jost matrix analysis.

Both reactions, $^{12}\mathrm{C}(\alpha,\gamma)^{16}\mathrm{O}$ and $\alpha(d,\gamma)^{6}\mathrm{Li}$, occur in stars. A brief introduction to the current understanding of the evolution of the universe and a discussion on nuclear fusion reactions in stars follows.

4.1 Evolution of the Universe

In recent years there has been a renewed interest in certain nuclear processes, such as the reactions $^{12}C(\alpha,\gamma)^{16}O$ and $\alpha(d,\gamma)^{6}Li$, due to their relevance in astrophysics. While many of these processes have been studied since the golden years of nuclear physics in the 1950s and 1960s, certain scattering parameters for these reactions (such as the ANC) have not been determined to satisfaction. There has also been considerable improvement in the models used for analysing experimental data, not to mention the advances in computing power to perform fittings of said data.

Of particular interest are the nuclear fusion reactions in stars that are responsible for the creation of the heavier elements. Due to the limited nature of the data available from stars, namely measurements of radiation, many aspects of heavy-element synthesis remain a mystery. In fact, one of the eleven most important physics questions in our century is:

"How and where are the heavy elements produced?" [37].

To begin answering this question, the origin of matter and in particular the origin of the lighter atomic isotopes, will be considered in the context of the origin of the universe.

The most commonly accepted model for the origin of the universe is, of course, the *Big Bang Theory*. According to this model, soon after the *Big Bang*, the universe cooled over time in such a way that its temperature can be approximated by $T \approx \frac{15\times10^{9}}{\sqrt{t}}$ K, which is equivalent to a thermal energy of $E \approx \frac{1.3}{\sqrt{t}}$ MeV [37].
The available thermal energy determines the nature of matter during this time-evolution: see Figure 4.1.

For very early times; $t < 1\ \mu$s, the universe consisted of a deconfined soup of quarks and gluons; the quark-gluon plasma. The phase diagram for this plasma is the focus of many modern studies in particle physics, since the specifics of how the plasma forms baryons, in particular the proton, is not yet well-understood.

For times; $1\ \mu\text{s} < t < 1$ s, protons and neutrons did exist, but the available en-

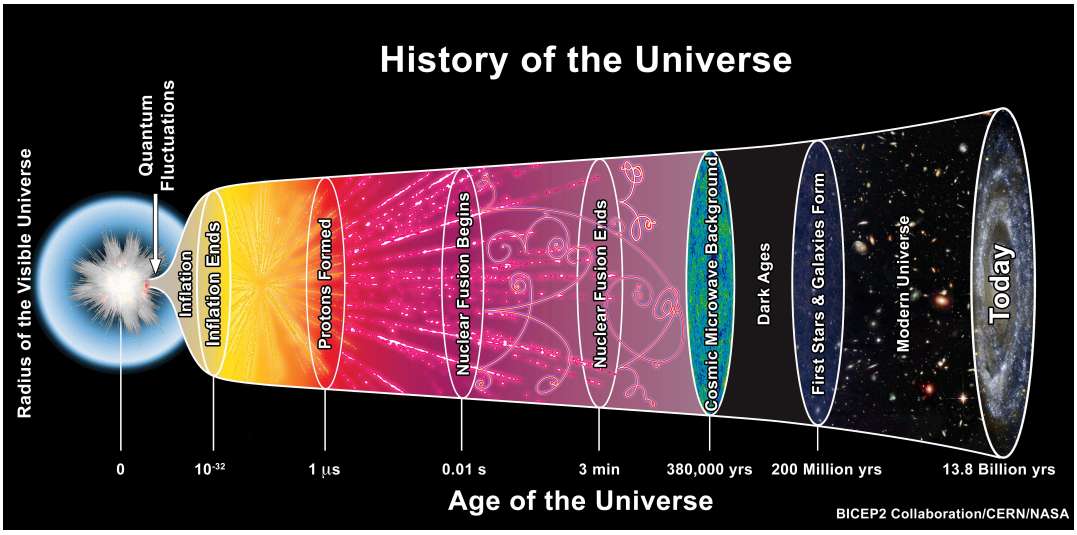

Figure 4.1: Evolution of the universe from the Big Bang.

ergy was still larger than the difference in rest masses of the neutron and proton: $(m_n - m_p)c^2 = 1.24$ MeV. Enough radiative energy was therefore available for the conversion of protons to neutrons and neutrons to protons via the weak interaction. Spontaneous pairs of electron-positron pairs were also formed [37].

Only for $t > 1$ *s* were neutrons and protons really stable enough to bind to form light nuclei. The period: 0.01 s $< t <$ 3 min, where this cosmic nuclear fusion took place, is known as the *Era of Nucleosynthesis* [37]. Most of the hydrogen and helium isotopes currently in existence were formed in this period. It was thought that most of the lithium isotopes currently in existence were also formed in this period, but there is a significant discrepancy with the theoretical predictions and the observed abundance of lithium [38]: this is the so-called *Lithium Discrepancy*, which is an important problem in nuclear astrophysics. The results from the study of ^{6}Li resonances, which is the focus of Chapter 6, can assist in solving this problem.

Returning to the evolution of the universe: after the *Era of Nucleosynthesis*, in the period; 3 min $< t <$ 380000 years, the light nuclei (mostly protons) combined with free electrons to form hydrogen and helium atoms. This is known as the *recombination* period. The recombination had an important repercussion: thermal radiation could no longer be scattered from these neutral atoms (as opposed to the charged

nuclei and electrons), which meant that these photons started to move freely though the universe. The photons existed mostly in the order of microwaves and can still be detected as radio-waves today (the grey-noise between radio stations, for example): this is some of the best evidence for the *Big Bang Theory*.

After *recombination*, photons were no longer backscattered and stars had not yet formed: the universe was completely dark. This period, 380000 years $< t <$ 200 million years, is appropriately named the *Dark Ages*.

For reasons that are still unknown (although many models have been proposed), 200 million years after the *Big Bang*, massive concentrations of hydrogen and helium atoms were formed, assisted by gravity, resulting in the spontaneous fusion of the nuclei of these atoms. These were the first stars.

The fusion of the hydrogen and helium isotopes provide sufficient energy for the fusion of their products, as well as preventing the implosion of stars due to gravity. The "ashes" from the initial reactions provide the fuel for higher-order fusion reactions. It is thus within stars that most of the heavier elements are formed, at least up to iron, which has the most tightly bound nucleus of all elements.

When a massive star collapses, a so-called supernova ensues. The shock-wave from this explosion results in a drastic increase in the temperature of the star, which provides the energy for the formation of elements heavier than iron.

The universe, in its current state, is then comprised of first- and second generation stars (which came to be because of the implosion of first generation stars). These stars are grouped in numerous galaxies, which, like the stars, only formed late in the evolution of the universe. How the universe will continue to evolve is still somewhat uncertain. While numerous likely models exist, certain important parameters, such as dark matter and dark energy, remain illusive. This, however, is not important for this thesis and is merely mentioned to give a broader perspective.

This section is just a short summary of the current understanding of the evolution of the universe. It is important, though, since the application of the results of this thesis are then better understood within the context of particle physics, astrophysics and

cosmology. One of the cardinal reactions in stars, radiative capture, is the focus of the next section.

4.2 Stellar nucleosynthesis and radiative capture

The Hydrogen isotope comprised of a single proton is the most abundant element in the universe [37]. The proton is then the main fuel-source of stars. Apart from the Helium produced during the *Era of Nucleosynthesis*, it is further produced in stars in a sequence of nuclear reactions involving the fusion of protons, which result in the formation of ^{4}He (the α-particle) in particular. This occurs either via the proton-proton chain in smaller stars (smaller than 1.3 times the mass of the sun) or via the CNO cycle in larger stars (larger than 1.3 times the mass of the sun) [39]. Both reaction chains can occur in all stars, but the proton-proton chain is much more prominent in smaller stars. The CNO cycle, which is an abbreviation for the carbon-nitrogen-oxygen cycle, occurs at greater energies and requires the presence of the ^{12}C isotope, which acts as a catalyst.

Various factors influence the production of the heavier elements, most particularly the available thermal energy in a star. Other reaction chains govern this production, for example the triple-helium process, which results in the production of ^{12}C from the reaction of three alpha particles [37]. This process occurs later in a star's lifetime, when its hydrogen has been depleted. This causes a rise in temperature in the core, which provides sufficient energy for the triple-helium process to commence. A by-product of this process is the reaction of the produced ^{12}C with excess alpha particles to form ^{16}O. It is this reaction which is considered in Chapter 5.

The available thermal energy in even the hottest star is of the order $E \approx 10$MeV. Furthermore, when supernovae occur for massive stars, the temperature (and thermal energy) will not increase more than 50%. All nuclear reactions that occur in stars and supernovae can therefore be considered non-relativistically, and the derivations of the previous chapters are applicable to nuclear reactions that occur via scattering

processes in stars.

Many of these reactions in stars and supernovae explosions occur through sub-threshold bound states or low-energy resonance states. This is the main mode of element production in stars and supernovae, since the Coulomb barrier in the scattering of nuclei suppresses the direct reaction near the threshold energy [40]. This type of reaction, known as radiative capture, is then responsible for much of the radiation from stars and supernovae.

Radiative capture can be described as the two-body scattering of nucleus A by nucleus B which results in an excited state of the product nucleus C, which then enters the ground state by ejecting a photon: $A+B \rightarrow C^* \rightarrow C+\gamma$ [37]. Although this is clearly two-channel scattering, such radiative capture reactions can be studied by considering elastic $A+B$ scattering, which can result in bound and resonance states of C.

Experimental data of the elastic $A+B \rightarrow A+B$ scattering can then be analysed with the method outlined in Chapter 3, which is exactly what is done in Chapters 5 for α^{12}C scattering and for $d\alpha$ scattering in Chapter 6.

4.3 The $\mathcal{S}$-factor

One of the main goals of astrophysicists in general is to determine the reaction rates of radiative capture reactions, which can be used to determine stellar energy production, time-scales of the nuclear burning process (and so stellar lifetimes) as well as the abundance of heavier elements (beyond hydrogen and helium). The astrophysical $\mathcal{S}$-factor for radiative capture at low energies, can be used to determine these quantities. The $\mathcal{S}$-factor is defined as follows:

$$\mathcal{S}(E) = Ee^{2\pi\eta}\sigma_\gamma(E), \tag{4.1}$$

where $\sigma_\gamma(E)$ is the radiative capture cross-section. The $\mathcal{S}$-factor is effectively a re-scaling of this scattering cross-section to limit the strong energy dependence, which

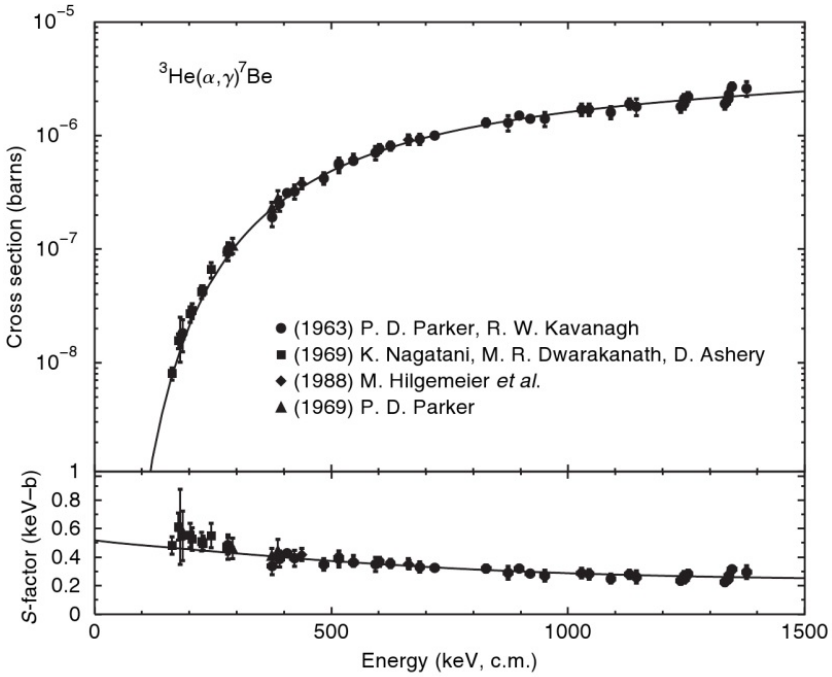

Figure 4.2: Dependence of cross-section and $\mathcal{S}$-factor on energy, for the reaction ^{3}He(^{4}He, γ)^{7}Be [37].

is mainly due to the repulsive Coulomb interaction at lower energies; hence the exponential factor containing the Sommerfeld parameter, η. The Coulomb interaction will always be repulsive for nuclear reactions in stars, since all nuclei are positive. Due to the re-scaling, for certain energy ranges, the $\mathcal{S}$-factor is well-approximated by a constant and is the preferred quantity in astrophysics (rather than scattering cross-section or phase-shift). See, for example, Figure 4.2, obtained from Ref. [37], which shows the total scattering cross-section and corresponding $\mathcal{S}$-factor for the radiative capture reaction, ^{3}He(^{4}He, γ)^{7}Be in the energy range $0\,\text{MeV} < E_{cm} < 1.5\,\text{MeV}$. There is a rapid decrease in cross-section at energies lower than the Coulomb barrier energy, which is not reflected in the $\mathcal{S}$-factor, which is almost constant. The $\mathcal{S}$-factor can often be used to extrapolate to lower energies where physical measurements are impossible. Furthermore, there is a direct dependence of the $\mathcal{S}$-factor on the reaction rate, as will be shown.

For the two-body scattering of particle 1 by particle 2, the average reaction rate per

particle pair, r_{12}, is given by [37],

$$r_{12} = \frac{1}{1+\delta_{12}} n_1 n_2 \langle \sigma v \rangle, \tag{4.2}$$

with

$$\langle \sigma v \rangle = \int_0^\infty \sigma(E)\phi(v)dv. \tag{4.3}$$

The number densities for the particles are represented by n_1 and n_2. The distribution of relative velocities in the plasma, $\phi(v)$, is given by the Maxwell-Boltzmann distribution at non-relativistic energies for a system at thermal equilibrium. This is a reasonable approximation for most stellar systems, as indicated before.

This average reaction rate is directly related to timescales of nuclear burning processes in stars, approximations for star lifetimes, stellar energy production as well as models for determining particle abundance: see Ref. [37] for further details. It can be shown that the average reaction rate is related to the $\mathcal{S}$-factor by the following:

$$\langle \sigma v \rangle = \sqrt{\frac{8}{\pi\mu(k_B T)^3}} \int_0^\infty \mathcal{S}(E)\, e^{\left(-\frac{E}{k_B T} - \sqrt{\frac{E_G}{E}}\right)} dE, \tag{4.4}$$

with

$$E_G = 4\pi^2 \eta^2 E. \tag{4.5}$$

The exponent in the above expression is known as the Gamow distribution, which has a peak at:

$$E_p = \left(\frac{1}{4} E_G k_B^2 T^2\right)^{\frac{1}{3}}, \tag{4.6}$$

which is known as the effective burning energy and is typically very small - much smaller than experimentally measurable energies. Often the $\mathcal{S}$-factor is approximately constant and the integral can easily be approximated. Even if the $\mathcal{S}$-factor varies significantly around the Gamow peak, it can be expanded in a Taylor series around $E = 0$ to obtain an effective $\mathcal{S}$-factor.

The $\mathcal{S}$-factor for radiative capture at low energies then needs to be determined. This is often impossible to do directly from the cross-section by Eq. (4.1) since radiative

capture cross-sections cannot accurately be measured at low energies, nor are extrapolations of these cross-sections reliable. The $\mathcal{S}$-factor at low energies can, however, be approximated from relevant ANC values.

4.4 The Asymptotic Normalisation Coefficient

The Asymptotic Normalisation Coefficient (ANC) for a bound or resonance state physical radial wave-function in a specific channel is the amplitude of the corresponding outgoing spherical wave. In numerous texts, this outgoing wave is represented by the Whittaker function, $W_{-\eta_n,\ell_n+\frac{1}{2}}(-2ik_nr)$. Ref. [37] defines the ANC with the following, for example:

$$u_n(\mathcal{E}_i,r) \xrightarrow[r\to\infty]{} \mathcal{A}_n W_{-i\eta_n,\ell_n+\frac{1}{2}}(-2ik_nr), \tag{4.7}$$

where $u_n(\mathcal{E}_i)$ is the bound or resonance state wave-function at spectral energy $\mathcal{E}_i$. The ANC for the channel n, is given by $\mathcal{A}_n$. Recall that the channel may be uniquely determined by its threshold energy, E_n, as well as the quantum numbers ℓ, s and J. For the single-channel scattering of particles with zero spin, the ANC is just given by $\mathcal{A}_\ell$, since it is uniquely defined by the angular momentum quantum number, ℓ.

The Whittaker functions and $H_\ell^{(\pm)}(\eta,kr)$, given as a linear combination of the Regular and Irregular Coulomb functions in Eq. (2.23) with asymptotic behaviour given by Eq. (2.24), differ by an energy dependent factor as follows [14]:

$$H_\ell^{(\pm)}(\eta,kr) = (\mp i)^{\ell+1} e^{\pi\eta/2} e^{\pm i\delta_\ell^c} W_{\mp i\eta_n,\ell_n+\frac{1}{2}}(\mp 2ik_nr). \tag{4.8}$$

Eq. (4.7) can then be written as follows:

$$\begin{aligned} u_n(\mathcal{E}_i,r) &\xrightarrow[r\to\infty]{} \mathcal{A}_n i^{\ell_n+1} e^{-\pi\eta_n/2} e^{-i\delta_{\ell_n}^c} H_{\ell_n}^{(+)}(\eta_n,k_nr) \\ &\xrightarrow[r\to\infty]{} e^{-\pi\eta_n/2}\mathcal{A}_n e^{ik_nr - i\eta_n\ln(2k_nr)}. \end{aligned} \tag{4.9}$$

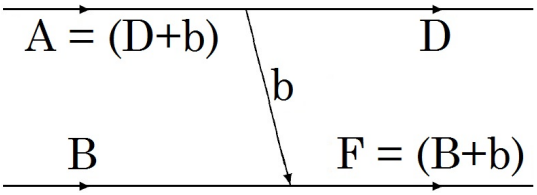

Figure 4.3: Diagram illustrating transfer reaction, $A+B \rightarrow D+F$.

This definition agrees with articles such as Ref. [41]. However, certain authors use relations for the ANC which is equivalent to a definition where the factor $e^{-\pi\eta_n/2}$ is omitted. For this reason, the ANC will be defined by the following asymptotic behaviour of the physical channel radial wave-functions:

$$u_n(\mathcal{E}_i, r) \xrightarrow[r\to\infty]{} a\mathcal{A}_n e^{ik_n r - i\eta_n \ln 2k_n r}, \tag{4.10}$$

where the factor a is chosen to be $e^{-\pi\eta/2}$ or 1. Depending on the strength of the Coulomb interaction, this choice has a small impact on the calculated ANC values. This definition is applicable to bound states as well as resonances.

It should be noted that this is the single-particle ANC for the bound or resonance states obtained from the scattering of two particles: the scattering of A and B to form C via radiative capture. Eq. (4.10) represents the wave-function of particle C, either in the ground state or in an excited state.

Another important nuclear reaction is the transfer reaction, $A+B \rightarrow D+F$, where A and F are composite particles with a common constituent, b: $A = D+a$ and $F = B+a$. The particle b is then *transferred* from one nucleus to the other, hence the name. The transfer reaction is illustrated in Figure 4.3.

An identical expression to 4.10 is used to define the ANC for the overlap wave-function of A and B: see Ref [41], for example. This wave-function and its ANC is related to the transfer reaction. There is a useful relation between the overlap wave-function ANC and the single particle ANC, which allows one value to be calculated if the other is known: see Refs. [37] or [41] for details. As an example given by Ref. [37], calculation of the ANC for the overlap function in the transfer reaction

^{48}Ca$(d,p)^{49}$Ca has lead to considerable insight into the radiative-capture reaction, ^{48}Ca$(n,\gamma)^{49}$Ca, which is difficult to analyse directly due to experimental limitations. The single-particle ANC values for radiative capture reactions will be determined in this thesis, but these values are relevant to certain transfer reactions as well.

To summarise, the ANC describes the strength of the exponential tail of the bound state and resonance wave-functions. Therefore, radiative capture reactions as well as transfer reactions at low physical energies directly depend on the ANC values [37]. A review and summary of various definitions of the ANC can be found in Refs. [41,42].

As mentioned in the previous section, the radiative capture reaction given by $A(B,\gamma)C$ is a two-channel reaction, where the transition channel $A+B \rightarrow C+\gamma$ is of particular interest. It is the cross-section and corresponding $\mathcal{S}$-factor of this channel which is of particular interest to astrophysicists, since stellar reaction rates depend on the $\mathcal{S}$-factor of this channel.

An expression for the $\mathcal{S}$-factor at low energies for the inelastic channel of the $A(B,\gamma)C$ reaction for a sub-threshold bound state of particle C, is given in terms of the corresponding ANC in Ref. [41], Eq. (38). This expression is only applicable to the scattering of particles with zero spin. A similar expression can be obtained for particles with non-zero spin. Furthermore, similar expressions also exist for resonances.

If the ANC values for bound and resonance states of radiative capture reactions can then be determined, the $\mathcal{S}$-factor can be determined, which allows the average reaction rate of radiative capture to be calculated. This will be left to the astrophysicists. Accurately determining the ANC values is the concern of this thesis.

The next section shows how the ANC for a bound or resonance state is related to the corresponding S-matrix residue. The S-matrix residues can, in turn, be determined with the Jost matrices.

4.5 ANC and *S*-matrix residue

The single-channel relation between the ANC and the *S*-matrix residue for bound states is well known for the scattering of neutral particles, where there are no Coulomb interactions. It is given by [42]:

$$\mathrm{Res}\,[S_\ell, k] = i(-1)^{\ell+1}\mathcal{A}_\ell^2\,. \tag{4.11}$$

Refs. [41, 42] also give the bound state expression for the scattering of charged particles, where there are short-range and Coulomb interactions. The corresponding relation for resonances was further suggested in Refs. [43, 44].

In this section, an alternative derivation for bound and resonance states is given, from the Appendix of Ref. [7]. For simplicity, the derivation of the relationship between the ANC and the *S*-matrix residue at spectral energies is done for single-channel scattering only, as only the single-channel relation is necessary for this thesis. The result can be extended to multi-channel scattering.

Firstly, the so-called Jost solutions, $\chi_\ell^{(\pm)}(E,r)$, of the single-channel radial Schrödinger equation (1.37) are introduced. For the scattering of neutral particles, they are usually defined by the following boundary conditions at infinity [3]:

$$\chi_\ell^{(\pm)}(E,r) \underset{r\to\infty}{\longrightarrow} h_\ell^{(\pm)}(kr) \underset{r\to\infty}{\longrightarrow} (\mp i)^{\ell+1}e^{\pm ikr}\,, \qquad \eta = 0\,. \tag{4.12}$$

For the scattering of charged particles, they are solutions of a single channel of Eq. (2.7) and the definition is generalised as follows:

$$\chi_\ell^{(\pm)}(E,r) \underset{r\to\infty}{\longrightarrow} H_\ell^{(\pm)}(\eta,kr)e^{\mp i\delta_\ell^c} \underset{r\to\infty}{\longrightarrow} (\mp i)^{\ell+1}e^{\pm i[kr-\eta\ln(2kr)]}\,. \tag{4.13}$$

The single-channel Jost functions for the scattering of charged particles are defined by the regular solution Eq. (2.49), or equivalently, (2.50):

$$\phi(E,r) \underset{r\to\infty}{\longrightarrow} H_\ell^{(-)}(\eta,kr)e^{+i\delta^c}f_\ell^{(\mathrm{in})}(E) + H_\ell^{(-)}(\eta,kr)e^{-i\delta^c}f_\ell^{(\mathrm{out})}(E),$$

which can then be written in terms of the Jost solution:

$$\phi(E,r) \xrightarrow[r\to\infty]{} \chi_\ell^{(-)}(E,r) f_\ell^{(\mathrm{in})}(E) + \chi_\ell^{(+)}(E,r) f_\ell^{(\mathrm{out})}(E). \tag{4.14}$$

The Wronskian of any two solutions for a single-channel of the radial Schrödinger equation (2.7) is independent of r, thus it can be determined at any r, in particular where $r \to \infty$. The Jost functions can then be given in terms of the Wronskian as follows:

$$f_\ell^{(\mathrm{in/out})}(E) = \pm \frac{i}{2k} W\left[\chi_\ell^{(\pm)}, \phi_\ell\right] , \tag{4.15}$$

where $W[f,g] = fg' - f'g$ is the Wronskian of two functions. Using the Wronskian of the Regular and Irregular Coulomb functions (see Ref. [14]) and Eq. (2.23), the definition of $H_\ell^{(\pm)}(\eta, kr)$, the following Wronskian can be obtained:

$$W[H_\ell^{(-)}(\eta,kr), H_\ell^{(+)}(\eta,kr)] = 2ik \, .$$

To simplify the notation, the energy derivative of a function will be denoted by the dot over the function, as before. The energy derivative of Eq. (4.15) for the incoming Jost function then gives:

$$\dot{f}_\ell^{(\mathrm{in})}(E) = \frac{i}{2k}\left[W(\chi_\ell^{(+)}, \dot{\phi}_\ell) + W(\dot{\chi}_\ell^{(+)}, \phi_\ell)\right] + W(\chi_\ell^{(+)}, \phi_\ell)\frac{d}{dE}\left(\frac{i}{2k}\right) . \tag{4.16}$$

At a resonance or a bound state energy $\mathcal{E}_i$, it is known that $f_\ell^{(\mathrm{in})}(\mathcal{E}_i) = 0$. Using Eq. (4.14) this implies:

$$\phi(\mathcal{E}_i, r) \xrightarrow[r\to\infty]{} \chi_\ell^{(+)}(\mathcal{E}_i, r) f_\ell^{(\mathrm{out})}(\mathcal{E}_i), \tag{4.17}$$

and so

$$W(\chi_\ell^{(+)}(\mathcal{E}_i, r), \phi_\ell(\mathcal{E}_i, r)) = W(\phi_\ell(\mathcal{E}_i, r), \chi_\ell^{(+)}(\mathcal{E}_i, r)) = 0. \tag{4.18}$$

At a spectral energy, Eq. (4.16) then becomes:

$$\dot{f}_\ell^{(\mathrm{in})}(\mathcal{E}_i) = \frac{i}{2k}\left\{W\left[\chi_\ell^{(+)}(\mathcal{E}_i, r), \dot{\phi}_\ell(\mathcal{E}_i, r)\right] + W\left[\dot{\chi}_\ell^{(+)}(\mathcal{E}_i, r), \phi_\ell(\mathcal{E}_i, r)\right]\right\} . \tag{4.19}$$

Let $\mathcal{V}(r)$ represent the sum of the short-ranged ($V(r)$) and Coulomb reduced potentials:

$$\mathcal{V}(r) = V(r) + \frac{2k\eta}{r}. \tag{4.20}$$

Then the radial Schrödinger equations for the functions ϕ_ℓ and $\chi_\ell^{(+)}$ at two different energies, E and $\tilde{E}$, read as follows:

$$\begin{aligned}\left[\frac{d^2}{dr^2} + k^2 - \frac{\ell(\ell+1)}{r^2} - \mathcal{V}(r)\right]\phi_\ell(E,r) &= 0\,,\\ \left[\frac{d^2}{dr^2} + \tilde{k}^2 - \frac{\ell(\ell+1)}{r^2} - \mathcal{V}(r)\right]\chi_\ell^{(+)}(\tilde{E},r) &= 0\,.\end{aligned}$$

Multiplying the first equation by by $\chi_\ell^{(+)}(\tilde{E},r)$, the second by $\phi_\ell(E,r)$ and subtracting the second from the first, the following is obtained:

$$\phi_\ell''(E,r)\chi_\ell^{(+)}(\tilde{E},r) - \phi_\ell(E,r)\chi_\ell^{''(+)}(\tilde{E},r) + (k^2-\tilde{k}^2)\phi_\ell(E,r)\chi_\ell^{(+)}(\tilde{E},r) = 0\,,$$

which is equivalent to

$$\frac{d}{dr}W\left[\chi_\ell^{(+)}(\tilde{E},r), \phi_\ell(E,r)\right] = (\tilde{k}^2-k^2)\phi_\ell(E,r)\chi_\ell^{(+)}(\tilde{E},r)\,. \tag{4.21}$$

Taking the derivative over E, the following is obtained:

$$\begin{aligned}\frac{d}{dr}W\left[\chi_\ell^{(+)}(\tilde{E},r), \dot{\phi}_\ell(E,r)\right] &= \\ &-\frac{2\mu}{\hbar^2}\phi_\ell(E,r)\chi_\ell^{(+)}(\tilde{E},r) + (\tilde{k}^2-k^2)\dot{\phi}_\ell(E,r)\chi_\ell^{(+)}(\tilde{E},r)\,.\end{aligned}$$

Substituting $E = \tilde{E} = \mathcal{E}_i$, which gives $k^2 - \tilde{k}^2 = 0$, then results in the following:

$$\frac{d}{dr}W\left[\chi_\ell^{(+)}(\mathcal{E}_i,r), \dot{\phi}_\ell(\mathcal{E}_i,r)\right] = -\frac{2\mu}{\hbar^2}\phi_\ell(\mathcal{E}_i,r)\chi_\ell^{(+)}(\mathcal{E}_i,r)\,. \tag{4.22}$$

Similarly, by differentiating Eq. (4.21) over $\tilde{E}$ and substituting $E = \tilde{E} = \mathcal{E}_i$, the radial

derivative of the second term in Eq. (4.19) is obtained:

$$\frac{d}{dr}W\left[\dot{\chi}_\ell^{(+)}(\mathcal{E}_i,r),\phi_\ell(\mathcal{E}_i,r)\right]=\frac{2\mu}{\hbar^2}\phi_\ell(\mathcal{E}_i,r)\chi_\ell^{(+)}(\mathcal{E}_i,r)\ . \tag{4.23}$$

Notice that the sum of Eq. (4.22) and Eq. (4.23) is zero, as expected when considering the derivative over r of Eq. (4.19).

Integrating Eq. (4.22) from 0 to r and Eq. (4.23) from r to ∞, the following is obtained:

$$\begin{aligned}W\left[\chi_\ell^{(+)}(\mathcal{E}_i,r),\dot{\phi}_\ell(\mathcal{E}_i,r)\right]-W\left[\chi_\ell^{(+)}(\mathcal{E}_i,0),\dot{\phi}_\ell(\mathcal{E}_i,0)\right]\\ =-\frac{2\mu}{\hbar^2}\int_0^r\phi_\ell(\mathcal{E}_i,r')\chi_\ell^{(+)}(\mathcal{E}_i,r')dr'\ ,\end{aligned} \tag{4.24}$$

$$\begin{aligned}W\left[\dot{\chi}_\ell^{(+)}(\mathcal{E}_i,\infty),\phi_\ell(\mathcal{E}_i,\infty)\right]-W\left[\dot{\chi}_\ell^{(+)}(\mathcal{E}_i,r),\phi_\ell(\mathcal{E}_i,r)\right]\\ =\frac{2\mu}{\hbar^2}\int_r^\infty\phi_\ell(\mathcal{E}_i,r')\chi_\ell^{(+)}(\mathcal{E}_i,r')dr'\ .\end{aligned} \tag{4.25}$$

It can be shown that, at a spectral point, the following terms in these equations vanish:

$$W\left[\chi_\ell^{(+)}(\mathcal{E}_i,0),\dot{\phi}_\ell(\mathcal{E}_i,0)\right]=0\ , \tag{4.26}$$

$$W\left[\dot{\chi}_\ell^{(+)}(\mathcal{E}_i,\infty),\phi_\ell(\mathcal{E}_i,\infty)\right]=0\ . \tag{4.27}$$

Indeed, at a spectral point the functions ϕ_ℓ and $\chi_\ell^{(+)}$ at large distances only differ by an energy-dependent normalisation coefficient, as can be seen from Eq. (4.17). Since the Schrödinger equation is homogeneous, this implies that ϕ_ℓ and $\chi_\ell^{(+)}$ are linearly-dependent. Therefore, also at short distances they can only differ by an energy-dependent coefficient, while the r- dependence, namely, $\sim r^{\ell+1}$, is the same. When ϕ_ℓ is differentiated with respect to E near the point $r=0$, the r-dependence is not affected. In other words, $\chi_\ell^{(+)}(\mathcal{E}_i,r)$ and $\dot{\phi}_\ell(\mathcal{E}_i,r)$ are also linearly-dependent when $r\to 0$, which implies Eq. (4.26).

Concerning Eq. (4.27), notice that for a bound state, $\phi_\ell(\mathcal{E}_i,\infty)=0$, due to its exponential dependence on ikr and the fact that $k=i|k|$. The Jost solution $\chi_\ell^{(+)}(\mathcal{E}_i,r)$ also has this exponential dependence on ikr. After its differentiation over the energy, this exponential factor is also present in $\dot{\chi}_\ell^{(+)}(\mathcal{E}_i,r)$, and so at large r, Eq. (4.27) holds for a bound state.

As far as a resonance is concerned, consider the corresponding wave-function along a complex radius $r=|r|\exp(i\theta)$, with a rotation angle θ such that $\mathrm{Im}(kr)>0$. With such a complex rotation of the coordinate, it is possible to uniquely normalise a resonance wave-function [45]. Furthermore, without a reasonable and clearly defined recipe for the normalisation, it would be meaningless to consider the ANC for resonance states. Therefore, when $r\to\infty$ along a complex path, a resonance can be treated in exactly the same way as a bound state and the reasoning for bound states becomes applicable.

Now proceed by substituting Eq. (4.24) and Eq. (4.25) into Eq. (4.19), to obtain the following:

$$\begin{aligned}\dot{f}_\ell^{(\mathrm{in})}(\mathcal{E}_i) &= \frac{\mu}{i\hbar^2 k}\int_0^\infty \phi_\ell(\mathcal{E}_i,r)\chi_\ell^{(+)}(\mathcal{E}_i,r)dr \\ &= \frac{\mu}{i\hbar^2 k} f_\ell^{(\mathrm{out})}(\mathcal{E}_i)\int_0^\infty \left[\chi_\ell^{(+)}(\mathcal{E}_i,r)\right]^2 dr\,, \end{aligned} \tag{4.28}$$

where the last equality follows from Eq. (4.17). The integral can now be expressed in terms of the ANC. In order to do this, consider the properly normalised wave-function, $u_\ell(\mathcal{E}_i,r)$, of the discrete state: a function that is proportional to $\chi_\ell^{(+)}(\mathcal{E}_i,r)$ and obeys the condition:

$$\int_0^\infty [u_\ell(\mathcal{E}_i,r)]^2\,dr = 1\,. \tag{4.29}$$

When dealing with a resonance, the integration should naturally be done along a complex path. For both bound or resonance states, the norm can be defined as the integral of the square of the wave-function. Indeed, a bound state wave-function can always be made real and therefore $|u_\ell|^2=u_\ell^2$. For a resonance state, the norm is also introduced via integration of the square of the wave-function (see, for example,

Refs. [46, 47]).

Comparing Eq. (4.10), by which the ANC is defined, with Eq. (4.13), the following is obtained:

$$u_\ell(\mathcal{E}_i,r) = i^{\ell+1} a \mathcal{A}_\ell \chi_\ell^{(+)}(\mathcal{E}_i,r) \; . \tag{4.30}$$

Substituting $\chi_\ell^{(+)}(\mathcal{E}_i,r)$ from this equation to the integral in (4.28) and taking into account the normalisation condition (4.29), the following is obtained:

$$\text{Res}\,[S_\ell,E] = \frac{f_\ell^{(\text{out})}(\mathcal{E}_i)}{\dot{f}_\ell^{(\text{in})}(\mathcal{E}_i)} = i(-1)^{\ell+1}\frac{\hbar^2 k}{\mu} a^2 \mathcal{A}_\ell^2 \; , \tag{4.31}$$

where the relation between the S-matrix residue and the Jost functions, Eq. (1.119) is also used.

The residues of the S-matrix residues over the variables k and E are easily related. The derivative in Eq. (1.119) is simply replaced with,

$$\frac{d}{dE} = \frac{dk}{dE}\frac{d}{dk} = \frac{\mu}{\hbar^2 k}\frac{d}{dk}, \tag{4.32}$$

which gives:

$$\text{Res}\,[S_\ell(E),E] = \frac{\hbar^2 k}{\mu}\text{Res}\,[S_\ell(k),k] \, . \tag{4.33}$$

This then results in:

$$\text{Res}\,[S_\ell,k] = i(-1)^{\ell+1} a^2 \mathcal{A}_\ell^2 \; . \tag{4.34}$$

If $a = e^{-\pi\eta/2}$ is chosen, this equations corresponds exactly to Eq. (12) in [41] for bound states. If $a = 1$ is chosen, the expression corresponds exactly to the expression for the scattering of neutral particles, Eq. (4.11) (see, for example, the Appendix of Refs. [48] or [42]). For this reason, it is the preferred choice. It then also corresponds exactly to Eq. (1.104) on page 35 of Chapter 1.

Furthermore, for $a = 1$, the relation becomes equivalent to the expressions used in Refs. [40, 49]. For $a = e^{-\pi\eta/2}$, the relation becomes equivalent to the expressions used in Ref. [50]. This will be shown explicitly in the next section. The equivalence

with the expression in these references in particular are highlighted, since the results of Chapters 5 and 6 will be compared with the results of these references.

4.6 Equivalence with other expressions

Rather than using the S-matrix residue, many texts introduce the *renormalised Coulomb-nuclear partial amplitude*. It is the Coulomb-nuclear partial amplitude of Eq. (2.67) for a singe channel, which can be written in terms of the phase-shift as follows:

$$\mathrm{f}_{\ell}^{cn} = \frac{e^{2i\delta_{\ell}^{c}}(e^{2i\delta_{\ell}}-1)}{2ik},$$

which is then adjusted by a Coulomb correction factor:

$$\frac{(\ell!)^2 e^{\pi\eta}}{[\Gamma(\ell+1+i\eta)]^2}.$$

It is given by Refs. [40, 49, 50] as follows:

$$\tilde{\mathrm{f}}_{\ell}^{cn} = \frac{e^{2i\delta_{\ell}^{c}}(e^{2i\delta_{\ell}}-1)}{2ik}\frac{(\ell!)^2 e^{\pi\eta}}{[\Gamma(\ell+1+i\eta)]^2}. \tag{4.35}$$

Recall that the single-channel scattering S-matrix can be given in terms of the phase-sifts by Eq. (2.75) and (2.76):

$$S_{\ell}(k) = e^{2i\delta_{\ell}^{c}} e^{2i\delta_{\ell}} \tag{4.36}$$

Using this relation, multiplying equation (4.35) with $(k-k_s)$ and taking the limit as $k \to k_s$ on both sides, gives the following relationship between the single-channel S-matrix residue and the renormalised Coulomb-nuclear partial amplitude residue at momentum pole k_s:

$$\mathrm{Res}\left[\tilde{\mathrm{f}}_{\ell}^{N}(k), k_s\right] = \frac{\mathrm{Res}\left[S_{\ell}(k), k_s\right](\ell!)^2 e^{\pi\eta_s}}{2ik_s[\Gamma(\ell+1+i\eta_s)]^2}, \tag{4.37}$$

where the momentum pole k_s corresponds with a spectral energy $\mathcal{E}_i$, so that $k_s = \sqrt{2\mu\mathcal{E}_i/\hbar^2}$.

The Nuclear Vertex Constant (NVC or $\tilde{G}_\ell$) is defined in terms of the renormalised Coulomb-nuclear partial amplitude residue. There are, however, differences in the definition. It can be written as follows:

$$\text{Res}\left[\tilde{\text{f}}^N_\ell(k), k_s\right] = -b^2 \frac{\mu^2}{2\pi k_s} \tilde{G}^2_\ell. \tag{4.38}$$

with $b = 1$ in Refs. [40, 49] and $b = i^\ell$ in Ref. [50].

The NVC, in turn, is related to the Asymptotic Normalisation Coefficient. Again, there are differences in the relation used. It is given by:

$$\mathcal{A}_\ell = \frac{b}{a} i^{-\ell} e^{-\pi\eta/2} \frac{\mu}{\sqrt{\pi}} \frac{\Gamma(\ell+1+i\eta_s)}{\ell!} \tilde{G}_\ell, \tag{4.39}$$

with $a = 1$ in Refs. [40, 49]. In Ref. [50], $a = e^{-\pi\eta/2}$. Thus it can be shown that the relationship between the ANC and S-matrix residue at momentum pole k_s is given by the following:

$$\text{Res}\left[S_\ell(k), k_s\right] = a^2 i(-1)^{\ell+1} \mathcal{A}^2_\ell. \tag{4.40}$$

This expression corresponds exactly with Eq. (4.34). With the appropriate choice of the arbitrary factor a, the results of this thesis can be compared with those of other studies.

The renormalised Coulomb-nuclear partial amplitude is used by numerous authors in fitting data, since its analytic structure is well-understood and it relates directly to the effective-range expansion and the NVC and ANC. For methods based on the effective range expansions, however, there are (as mentioned) complications for multi-channel scattering. For this reason, the fitting method given in Chapter 3 is preferable.

The necessary background in scattering theory has been discussed in Chapters 1 and 2 and the Jost matrix method of analysis has been introduced in Chapter 3. This chapter has outlined the importance of certain nuclear processes in stars and shown

how the ANC values can give much-needed insight into problems in astrophysics. The means of calculating the ANC from the Jost matrices have also been determined. Experimental nuclear scattering data is analysed with the outlined method in the next chapters.

Chapter 5

Analysis of α^{12}C scattering data

This chapter gives the results of Ref. [7], which is the second of the three articles that this thesis is based on. The fitting method described in Chapter 3 is used to analyse elastic, single-channel α^{12}C cross-sections, which are calculated from the phase-shifts obtained from the available R-matrix analysis of raw experimental data. The Jost functions are constructed from the fittings and the resonance parameters for the states $J^{\pi} = 0^{+}$, 1^{-}, 2^{+}, 3^{-}, and 4^{+} are determined. The corresponding S-matrix residues for these resonances are determined, which allows the calculation of the ANC values.

5.1 Purpose of the study

The isotope, ^{16}O, is one of three stable isotopes of oxygen (with ^{17}O and ^{18}O) and is by far the most abundant of these isotopes in nature ($\sim 99.76\%$). It is, of course, very important in biological systems, specifically in respiration and photosynthesis.

It is also important in nuclear astrophysics, as mentioned in the previous chapter. It is produced mostly by reactions involving the α-particle, which is produced in stars as the result of hydrogen burning. These α-particles are further burned (mainly in red giants, where the enegy is sufficient) via the formation of α-clustered nuclei [51].

Firstly, triple-α collisions form the carbon isotope ^{12}C: this is the triple-helium pro-

cess referred to in the previous chapter. The α-particles and ^{12}C are then consumed via the radiative capture process, $^{12}\mathrm{C}(\alpha,\gamma)^{16}\mathrm{O}$. It is this reaction that determines the carbon-oxygen abundance in the universe [51].

This radiative transition occurs via a sequence of α^{12}C resonances, the spectrum of which is rich and well-studied [9]. However, the Asymptotic Normalisation Coefficients for these resonances, which are important parameters in the radiative capture $^{12}\mathrm{C}(\alpha,\gamma)^{16}\mathrm{O}$ reaction, are still not firmly established. For more information, see, for example, Ref. [52].

This $^{12}\mathrm{C}(\alpha,\gamma)^{16}\mathrm{O}$ reaction at the energies relevant to astrophysics (which are small) can be studied by analysing the single-channel α^{12}C scattering process, since the other channels, namely, ^{11}C+^{5}He and ^{13}C+^{3}He open at much higher threshold energies. Also recall from the discussion of Section 1.1 that the ^{16}O nucleus, even in an excited state, can be considered as a two-body system comprised of the ^{12}C and ^{4}He clusters.

Furthermore, adequate experimental data for single-channel α^{12}C scattering is available, so that a reliable Jost-function analysis can be performed. Using this analysis, resonance parameters for states defined by the quantum numbers $J^{\pi} = 0^{+},1^{-},2^{+},3^{-},4^{+}$ are determined, as well as the corresponding S-matrix residues and the ANC values for these resonance states.

The quantum number, J, represents the total angular momentum quantum number, as usual. Since both the α-particle and ^{12}C have zero spin, $J = \ell$ for this scattering problem. The π refers to the parity quantum number, which is a measure of the spacial symmetry of the wave-function in a scattering experiment. It can be symmetrical ($\pi = +1$) or anti-symmetrical ($\pi = -1$). In atomic and nuclear systems, it is determined by the quantum number ℓ [11], with

$$\pi = (-1)^{\ell}. \tag{5.1}$$

Previous studies using different fitting methods will briefly be discussed in the next section.

5.2 Previous studies and data

In Refs. [53–55], the R-matrix analysis of α^{12}C scattering data in the energy range from $E \sim 2\,\text{MeV}$ to $E \sim 5\,\text{MeV}$ was used to determine the partial wave scattering phase-shifts and α^{12}C resonance parameters.

The phase-shifts from Refs. [54, 55] were also analysed in Refs. [40, 49], where various methods, including the S-matrix pole method (SMP, also used in Ref [56]) were employed to determine the resonance parameters for the 0^+, 1^-, 2^+, and 3^- states. As far as the authors of Ref. [7] are aware, Ref. [49] is the only other article where the ANC values for several α^{12}C resonances are reported. The results of Ref. [7] will specifically be compared with Ref. [49].

Such a comparison of ANC values is complicated by the fact that, when it comes to the collision of charged particles, there is no generally accepted definition of the ANC. As indicated in Chapter 4, there is no general convention of a in Eq. (4.10), given by the following for single-channel scattering:

$$u(\mathcal{E}_i, r) \xrightarrow[r\to\infty]{} a\mathcal{A}_\ell e^{ikr - i\eta \ln 2kr}. \tag{5.2}$$

However, in all cases, $\mathcal{A}_\ell$ is related to the residue of the S-matrix at the corresponding pole: see Eq. (4.31). Since the residue is defined uniquely, it is preferable to report the main results of this analysis in terms of the residues rather than the ANC. Yet for the purpose of comparison with the few ANC values available in Ref. [49], the ANC values calculated for $a = 1$ in Eq. (5.2) are presented. It was shown in Chapter 4 how the relevant formulae in Ref. [49] are equivalent to Eq. (4.31) for such a choice of a, which is then given by:

$$\text{Res}\,[S_\ell, E] = i(-1)^{\ell+1}\frac{\hbar^2 k}{\mu}\mathcal{A}_\ell^2\,. \tag{5.3}$$

The derivation of this relation in other articles is usually done for a bound state pole (see, for example, Ref. [41]). Despite this, it is assumed that the same relation should also be valid for a resonance pole. This logic relies on the fact that the bound and res-

onance states transform into each other when the depth of the attractive part of the potential is gradually changing, which was briefly mentioned in Chapter 1. Since everything should change continuously, it would be peculiar if the relation between the residue and the asymptotic behaviour of the wave-function was changing abruptly.

Before the ANC values are calculated, the resonance parameters need to be determined from the fitting of data. The Jost-function analysis of the same data from Refs. [54, 55] will be used here. The novelty of the Jost method arises from exploiting the analytic structure of the Jost functions to parameterise the available scattering data and then to analytically continue the appropriate Jost function to complex energies in search of resonances, as indicated in Chapter 3.

In principle, the Jost fitting method of Chapter 3 can be used to fit raw experimental data. However, such a procedure would require dealing with too many free fitting parameters. The available R-matrix fits of Refs. [54, 55] give phase-shifts for each partial wave, which can be fitted separately. This reduces the number of fitting parameters considerably.

R-matrix fittings are often used as an initial fitting of experimental data, since the number of fitting parameters are manageable and accurate phase-shifts in the partial wave decomposition can be obtained at experimental energies. The analytic continuation to complex energies can, however, lead to inaccuracies, hence the need for methods such as the Jost function analysis.

A brief summary of the basic principle of the R-matrix theory from Ref. [57] follows. The configuration space in the R-matrix method is divided into two arbitrary regions, with the division occurring at a point known as the channel radius, r_c. In the external region, $r > r_c$, far from the source of the interaction potential, scattering properties can be satisfied. In the internal region, $r < r_c$, near the source of the interaction potential, the wave-function is approximated by a square-integrable basis. This basis is chosen to be energy independent, which results in a simple R-matrix structure with real energy-independent fitting parameters. The R-matrix is, in turn, related to the

S-matrix and so also to the partial wave phase-shifts.

For example, for the single-channel scattering of charged particles with zero spin, the partial wave *R*-matrix is given by the following:

$$R_\ell(E) = \sum_{i=1} \frac{\gamma_{\ell i}^2}{\mathcal{E}_{\ell i} - E}, \tag{5.4}$$

where $\gamma_{\ell i}$ is known as the reduced width and $\mathcal{E}_{\ell i}$ are energy poles corresponding to bound and resonance states. In general, only a limited number of these poles influence low-energy phase-shifts. The number of relevant poles then determines the number of terms in the summation. The Coulomb-nuclear phase-shift can then be determined with:

$$\tan \delta_\ell^{\text{cn}} = -\frac{F_\ell(\eta, kr_c) - kr_c R_\ell(E) \partial_r F_\ell(\eta, kr_c)}{G_\ell(\eta, kr_c) - kr_c R_\ell(E) \partial_r G_\ell(\eta, kr_c)}. \tag{5.5}$$

The reduced width, $\gamma_{\ell i}$, then serves as the fitting parameter. Various complications with this fitting procedure can arise, especially with overlapping resonances. It is beyond the scope of this thesis to perform *R*-matrix fittings and the results of the analysis performed in Refs. [54, 55] will be used in the Jost-function fittings.

Although the Jost-functions can be fitted to the Coulomb-nuclear phase-shifts of [54, 55] directly, it is preferable to perform the fittings with the scattering cross-sections. The Coulomb-nuclear partial-width phase-shifts of Ref. [54, 55] allow the calculation of the *S*-matrix by Eq. (2.75) and (2.76): $S_\ell(E) = e^{2i\delta_\ell^{\text{cn}} + 2i\delta_\ell^{\text{c}}}$, thus the "experimental" partial wave cross-sections can be determined with Eq. (1.151) on page 50:

$$\sigma_\ell^{\text{exp}} = \frac{\pi}{k^2}(2\ell+1)\left|e^{2i(\delta_\ell + \delta_\ell^c)} - 1\right|^2. \tag{5.6}$$

The fitting of these cross-sections are then performed in the way described in Chapter 3. The main points will be summarised for single-channel scattering in the next section.

5.3 Fitting procedure and calculations

The Jost functions (and therefore the S-matrix) are not single-valued functions of the energy variable, E. They are defined on a Riemann surface with an infinite number of sheets, where $E = 0$ is the square-root as well as the logarithmic branching point. Since the fitting of data occurs at real, positive E, there is a danger of incorrect analytic continuation to complex energies to determine resonance states, if a simplified formula (without the correct branching) is used in the fitting.

In order to safeguard the analytic continuation, the representations of the single-channel Jost functions are used in the form of Eq. (3.31) on page 97:

$$f_\ell^{(\text{in/out})}(E) = \frac{e^{\pi\eta/2}\ell!}{\Gamma(\ell+1\pm i\eta)}\left\{\mathcal{A}_\ell(E) - \left[\frac{2\eta h(\eta)}{C_0^2(\eta)} \pm i\right] C_\ell^2(\eta) k^{2\ell+1}\mathcal{B}_\ell(E)\right\},$$

where $\mathcal{A}_\ell(E)$ and $\mathcal{B}_\ell(E)$ are analytic and single-valued functions of E. If they are approximated by finite Taylor series, the analytic structure of the Jost functions is not affected, i.e. the correct branching properties are kept intact.

The functions $\mathcal{A}(E)$ and $\mathcal{B}(E)$ are approximated by Eq. (3.32) and (3.33). To indicate the dependence of the expansions on ℓ for a specific partial wave, these equations will be given explicitly for a single-channel fitting as follows:

$$\mathcal{A}_\ell(E) \approx \sum_{i=0}^{M} \alpha_i(\ell, E_0)(E - E_0)^i \,, \tag{5.7}$$

$$\mathcal{B}_\ell(E) \approx \sum_{i=0}^{M} \beta_i(\ell, E_0)(E - E_0)^i \,. \tag{5.8}$$

The fitting parameters are the unknown expansion coefficients α_i and β_i. The corresponding values of $\sigma_\ell^{\text{fit}}(E_i)$ are determined with Eq. (1.151), which is written as follows when using the expression for the S-matrix in terms of the Jost functions:

$$\sigma_\ell = \frac{\pi}{k^2}(2\ell+1)\left|\frac{f_\ell^{(\text{out})}(E)}{f_\ell^{(\text{in})}(E)} - 1\right|^2 . \tag{5.9}$$

The following function is then minimised using the MINUIT program developed in CERN [33]:

$$\chi^2 = \sum_{i=1}^{N} \left[\sigma_\ell^{\exp}(E_i) - \sigma_\ell^{\text{fit}}(E_i) \right]^2 , \tag{5.10}$$

where N is the number of the data points at the collision energies E_i. The experimental errors are assumed to be the same for all the data points (this is why they do not appear in the denominator of the χ^2-function).

The energies E_0 around which the expansions in Eq. (5.7) and (5.8) are done, are chosen near peaks in the data. As before, the larger the number of parameters in the expansions, M, the larger the circle in the complex plane around E_0 where the expansion is reliable. The number M should be chosen large enough so that the resonance energy falls within this circle. Values between $M = 5$ and $M = 9$ are chosen for the fittings in this study. If E_0 is chosen near a resonance energy, fewer terms are sufficient.

The accuracy of the analysis can be estimated by locating the same resonance with different values of E_0. The average values of the resonance parameters determined with different choices of E_0 and the corresponding standard deviations are calculated, which serve as the error estimate. It should be emphasised that these standard deviations have nothing to do with the experimental errors: they simply show the stability of the calculations and give the corresponding reliability intervals.

After fitting the data, the Jost functions of Eq. (3.31) are determined and are used to locate resonances. These correspond to complex energies, $\mathcal{E}_i = E_r + \frac{i}{2}\Gamma$, on the unphysical sheet of the Riemann surface such that $f_\ell^{(\text{in})}(\mathcal{E}_i) = 0$. It is easy to choose the correct sheet by taking the sign of k such that $\text{Im}(k) < 0$ and taking the value of the principal branch for the logarithmic term, $\ln(k)$.

The corresponding residues of the S-matrix for each $\mathcal{E}_i$ can then be determined using Eq. (1.119) on page 40:

$$\text{Res}\left[S, \mathcal{E}_i\right] = \frac{f^{(\text{out})}(\mathcal{E}_i)}{\dot{f}_\ell^{(\text{in})}(\mathcal{E}_i)}.$$

In principle, the derivative in the denominator can be found analytically. It is, how-

ever, simpler to calculate it numerically using the central-difference approximation,

$$\dot{f}_\ell^{(\mathrm{in})}(E) \approx \frac{f_\ell^{(\mathrm{in})}(E+\varepsilon) - f_\ell^{(\mathrm{in})}(E-\varepsilon)}{2\varepsilon} , \tag{5.11}$$

since the equation (3.31) has a complicated E dependence. A value of $\varepsilon = 10^{-6}$ MeV is used in the numerical calculations, which gives an accuracy of at least 5 digits.

When the residues are determined, the ANC values are calculated with Eq. (5.3). It should be noted that, since the phase of the wave-function can be chosen arbitrarily, the value of the ANC can always be made real. This means that it is sufficient to know its absolute value, $|\mathcal{A}_\ell|$, which is reported here.

It is further noted that in other works (see, for example, Ref. [41]) the poles and the residues of the S-matrix are usually found on the k-plane rather than on the E-surface. There is an obvious advantage in such a choice, since the S-matrix is a single-valued function of k (if for $\ln(k)$ the principal branch is taken). However, the use of the wave number is only convenient in a single-channel problem. When the number of channels is greater than one, there is no single momentum, but the energy variable, E, remains common for all the channels. Since the method used in this thesis is designed for an arbitrary number of channels, it is preferable to work with the variable E even in the single-channel case. Moreover, the representations (3.31) are constructed in such a way that the unknown functions $\mathcal{A}_\ell(E)$ and $\mathcal{B}_\ell(E)$ depend on E. Actually, the power-series expansions of these functions generalise the well-known effective-range expansion (which is done with $E_0 = 0$ and over the even powers of k, i.e. over the powers of E). The relation between the residues of the S-matrix over the variables k and E is given by Eq. (4.33) .

5.4 Results

The α^{12}C system is considered in the following five partial waves: 0^+, 1^-, 2^+, 3^-, and 4^+. For each, $N \sim 100$ data points were fitted with eight to twelve different E_0.

For every choice of E_0, the resonance parameters were determined. Ideally, these parameters should not depend on E_0. Such a dependence does exist, however, due to the approximations (5.7) and (5.8). Therefore, the average values (over different E_0) of the resonance parameters and the corresponding standard deviations are presented as the final results. These standard deviations are calculated under the assumption that the values obtained with different E_0 are statistically independent. Such standard deviations can only characterise the accuracy of these calculations and have nothing to do with experimental errors.

The calculations were done with the parameters for the model (N, M, E_0) listed in Table 5.1. For each fitting, the number of terms, M in the expansions, (5.7) and (5.8), were increased until the results with at least five stable digits were obtained. An example of such a convergence is shown in Table 5.2 for the 4^+ resonances. For $m = 0$, only the second resonances could be found in this fitting.

The final results are given in Table 5.3. For the purpose of comparison, the corresponding values reported in other studies are also shown, where available. The values from Ref. [49] are the average values obtained from the various methods applied in that work, where the error is the standard deviation.

Two resonances were located in the 2^+ state, as well as in the 4^+ state. Each of the other states has only one resonance in the considered energy range.

The quality of the fitting of the data points can be seen from the examples shown in Figures 5.1-5.5. The plots only show the fittings around the resonance structures, but the entire energy range of available data points, $1.9 - 5.0$ MeV, were fitted for all ℓ.

As seen from the plots, the fitted curves correctly reflect all the patterns in the distributions of the data points. However, at some instances the curves deviate from the data. A possible reason for these deviations is the fact that the α^{12}C system is treated as a two-body one. The representations (3.31) of the Jost functions have the correct two-body structure. On the other hand, the experimental data correspond to actual many-body collisions.

The resonance energies, E_r, and corresponding widths, Γ, for the located resonances

are in a good agreement with the accepted values. In addition to these two parameters, which characterises a resonance, the residues of the S-matrix at the resonance poles were also determined. These residues are needed for calculating the ANC values for the resonance wave-functions, which in turn are needed in various calculations related to nuclear astrophysics, as described in Chapter 4. In the few instances where the ANC values were previously determined, the calculations of Ref. [7] given in this chapter, produce compatible results. This is an assurance that all the results are sufficiently reliable.

5.5 Remarks

Despite its simplified two-body character, the advantage of the Jost method lies in using the special representations of the Jost functions with the correct analytic structure. This allows a reliable analytic continuation of the Jost functions to complex energies. They are continued from the real axis, where the fittings are performed, to the complex domain where resonances are located.

The focus of the present work is to obtain the low-energy resonances generated in the α^{12}C collision. Apart from the resonances, there are sub-threshold bound states that also play an important role in astrophysical processes involving these nuclei. These lie just below the corresponding threshold energy.

In principle, the method used here can also be applied for extracting the characteristics of these bound states. However, since the lowest collision energy (1.9 MeV) at which the data is available is quite far from the threshold, the direct application of this method would not be sufficiently accurate. There are various options to address this: to wait for new measurements at lower energies, for example, or to use a more complicated multi-step procedure for the analytic continuation. This will be based on the methods described, for example, in Ref. [2]. Such a study will not be considered in this thesis. Other avenues will also be discussed in Chapter 7.

J^π	N	M	E_0 [MeV]
0^+	154	9	4.4, 4.5, 4.6, 4.8, 4.9, 5.2, 5.3
1^-	354	9	0.1, 2.0, 2.1, 2.2, 2.3, 2.5, 2.6, 2.7, 2.8
2^+	354	9	2.3, 2.4, 2.5, 2.6, 2.7, 2.8, 2.9, 3.0, 3.1
3^-	354	9	3.7, 3.8, 3.9, 4.0, 4.1, 4.2, 4.3, 4.4, 4.5
4^+	120	5	3.4, 3.5, 3.6, 3.7, 3.8, 3.9, 4.0, 4.1, 4.2

Table 5.1: Each of the found resonances was located using N data points, M terms in the expansions (5.7, 5.8), and with a set of the central points E_0 over which the statistical averaging was done [7].

4^+	First resonance			Second resonance		
M	E_r [MeV]	Γ [keV]	Res$[S_\ell, E_r - \frac{i}{2}\Gamma]$ [keV]	E_r [MeV]	Γ [keV]	Res$[S_\ell, E_r - \frac{i}{2}\Gamma]$ [keV]
0	-	-	-	3.911	6.639	$-6.257 - i2.173$
1	3.220	2.1	$-1.4 - i1.6$	3.940	0.775	$-0.737 - i0.239$
2	3.192	33.5	$-19.3 - i26.6$	3.940	0.579	$-0.558 - i0.155$
3	3.203	16.9	$-11.5 - i12.1$	3.940	0.785	$-0.745 - i0.246$
4	3.199	21.2	$-14.2 - i15.4$	3.940	0.619	$-0.595 - i0.172$
5	3.197	24.5	$-16.0 - i18.3$	3.940	0.604	$-0.581 - i0.165$
6	3.197	23.6	$-15.6 - i17.3$	3.940	0.606	$-0.583 - i0.166$

Table 5.2: Convergence of the parameters of the two 4^+ resonances with an increasing number of terms M and with fixed $E_0 = 3.8$ MeV [7].

J^π	E_r [MeV]	Γ [keV]	Res $\left[S_\ell, E_r - \frac{i}{2}\Gamma\right]$ [keV]	$\lvert\mathcal{A}_\ell\rvert \times 10^3$ [fm$^{-1/2}$]	Ref.
0^+	4.892 ± 0.001	1.382 ± 0.096	$(-1.357 \pm 0.095) - i(0.261 \pm 0.021)$	10.87 ± 0.38	this work and [7]
	4.887 ± 0.002	2.4 ± 1.1		14.0 ± 3.5	[49]
	4.887 ± 0.002	1.5 ± 0.5			[9]
1^-	2.362 ± 0.009	361.9 ± 4.9	$(271 \pm 20) + i(96 \pm 16)$	188.1 ± 4.8	this work and [7]
	2.317 ± 0.071	333 ± 17		179.8 ± 3.6	[49]
	2.423 ± 0.011	420 ± 20			[9]
2^+	2.685 ± 0.001	0.842 ± 0.015	$(-0.656 \pm 0.013) + i(0.527 \pm 0.009)$	9.862 ± 0.090	this work and [7]
	2.61 ± 0.16	0.65 ± 0.11		8.68 ± 0.75	[49]
	2.6826 ± 0.5	0.625 ± 0.100			[9]
2^+	4.348 ± 0.003	76.8 ± 2.3	$(26.8 \pm 8.9) + i(69.9 \pm 5.4)$	82.7 ± 1.3	this work and [7]
	4.369 ± 0.017	77.8 ± 2.8		83.3 ± 1.6	[49]
	4.358 ± 0.004	71 ± 3			[9]
3^-	4.241 ± 0.011	796 ± 20	$(-160 \pm 47) + i(539 \pm 43)$	227.4 ± 8.2	this work and [7]
	4.275 ± 0.052	811 ± 15		236.0 ± 4.3	[49]
	4.44 ± 0.20	800 ± 100			[9]
4^+	3.197 ± 0.001	23.6 ± 1.9	$(-15.7 \pm 1.1) - i(17.3 \pm 1.7)$	49.7 ± 2.0	this work and [7]
	3.195	25.9			[54, 55]
	3.194 ± 3	26 ± 3			[9]
4^+	3.940 ± 0.001	0.607 ± 0.012	$(-0.584 \pm 0.011) - i(0.166 \pm 0.006)$	7.61 ± 0.08	this work and [7]
	3.936	0.42			[54, 55]
	3.9348 ± 0.0016	0.28 ± 0.05			[9]

Table 5.3: Parameters of the seven resonances that were found in the α^{12}C system and the available values of the corresponding parameters from Refs. [9, 49, 54, 55].

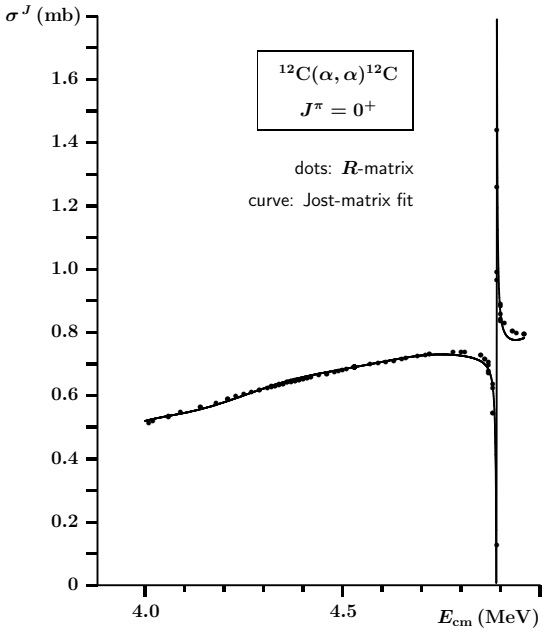

Figure 5.1: Fit of the data points for the 0^+ partial cross-section with $E_0 = 4.6\,\text{MeV}$ and $M = 9$ in the expansions (5.7, 5.8) [7].

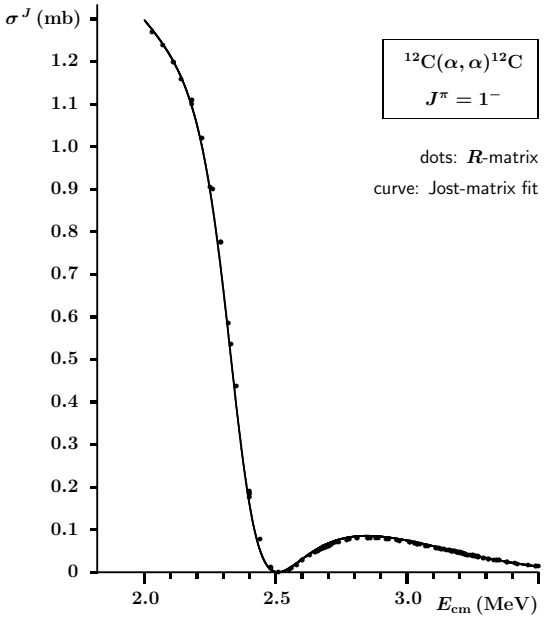

Figure 5.2: Fit of the data points for the 1^- partial cross-section with $E_0 = 2.5\,\text{MeV}$ and $M = 9$ in the expansions (5.7, 5.8) [7].

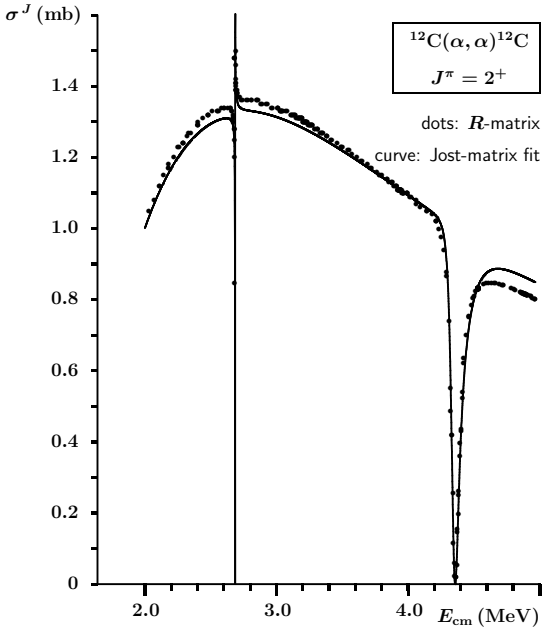

Figure 5.3: Fit of the data points for the 2^+ partial cross-section with $E_0 = 3.1\,\text{MeV}$ and $M = 9$ in the expansions (5.7, 5.8) [7].

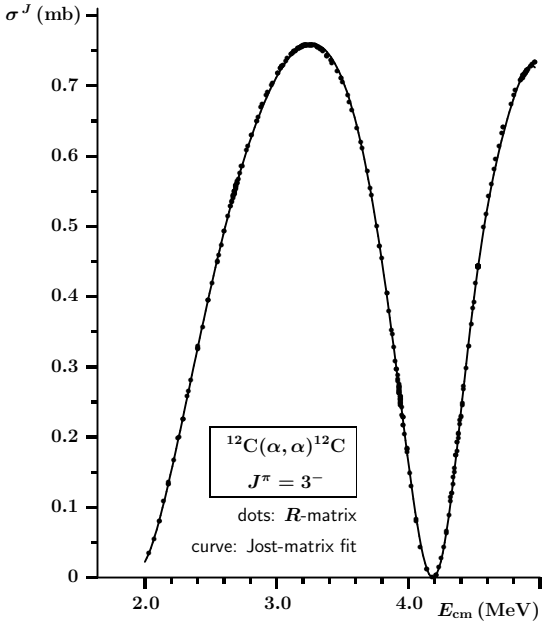

Figure 5.4: Fit of the data points for the 3^- partial cross-section with $E_0 = 3.9\,\text{MeV}$ and $M = 9$ in the expansions (5.7, 5.8) [7].

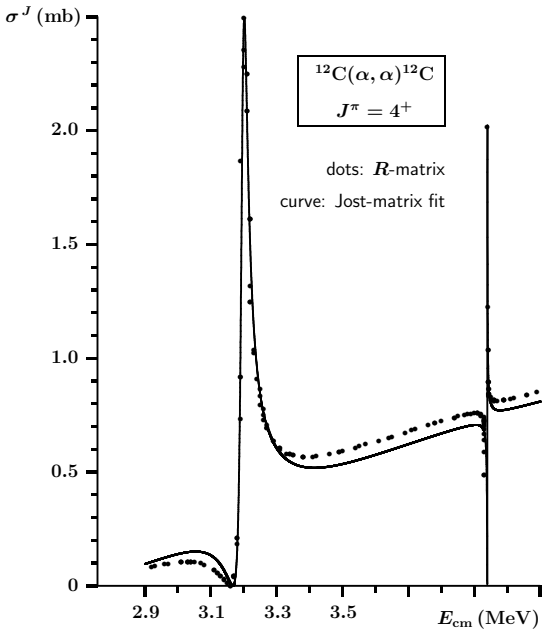

Figure 5.5: Fit of the data points for the 4^+ partial cross-section with $E_0 = 3.4\,\mathrm{MeV}$ and $M = 5$ in the expansions (5.7, 5.8) [7].

Chapter 6

Analysis of $d\alpha$ scattering data

In this chapter, the same Jost matrix fitting method described in Chapter 3 is used to fit $d\alpha$ scattering data. The results are from Ref. [8], which is the third and final article this thesis is based on.

To determine the parameters of the bound and resonance states of the ^{6}Li nuclear system with quantum numbers 1^+, 2^+, 3^+, 2^-, and 3^-, two different sets of data for $d\alpha$ scattering are analysed using the Jost matrices. The $d\alpha$ cross-sections are fitted by both a single-channel and a two-channel S-matrix, written in terms of the semi-analytic Jost matrices given in Chapter 3.

The Jost matrices obtained from the fitting are used at complex energies to locate resonances and the bound state, as well as to determine the corresponding S-matrix residues and ANC values. The scattering parameters determined in this analysis, which is based on an S-matrix with the correct analytic structure, correspond well with parameters determined by other authors.

6.1 The ^{6}Li isotope

The ^{6}Li isotope is one of the lighter nuclei and consequently has a relatively simple spectrum, consisting of less than a dozen well distinguished levels [58]. The abundance of this isotope is very small ($\sim 7.6\%$) as compared to that of ^{7}Li ($\sim 92.4\%$),

but its importance in thermonuclear dt-fusion motivated numerous experimental and theoretical studies of ^{6}Li.

In dt-fusion, the deuterium nucleus (^{2}H or d) and tritium nucleus (^{3}H or t) undergo fusion, which produces energy as well as a neutron (n) and ^{4}He, the α-particle. This fusion process, $d+t \rightarrow n+\alpha+energy$, takes place when boosted-fission nuclear weapons are detonated. It was also seen as a practically viable source of energy - there are even some modern fusion reactors in development that make use of dt-fusion. Tritium is unstable, however, with a half-life of 12.32 years. Consequently, natural tritium is very rare, and is mostly produced in the atmosphere by the interaction of atmospheric gasses with cosmic rays. An example of such a reaction is the interaction of ^{3}He with a fast (sufficiently energetic) neutron: $^3\text{He}+n \rightarrow {}^1\text{H}+t$.

A means of producing tritium for dt-fusion is therefore required. The neutron"ignition" of ^{6}Li, given by $n+{}^6\text{Li} \rightarrow t+\alpha$, is one of the few practically viable options. The ^{6}Li nucleus then serves as a stable source of tritium for dt-fusion. The production of tritium for military purposes has drastically declined since the end of the Cold War.

The nucleus ^{6}Li is also of importance in astrophysics, especially in connection with the puzzle associated with its abundance. This is the *Lithium Discrepancy* referred to in Chapter 4. It is believed that the synthesis of ^{6}Li via the radiative capture reaction $\alpha(d,\gamma)^6$Li was the main process by which the isotope was produced during the primordial nucleosynthesis as well as subsequently in stars [59]. Therefore, further studies of ^{6}Li are important.

Many collision processes, and in particular the radiative capture $\alpha(d,\gamma)^6$Li, may go via the intermediate formation of resonances. For this reason, accurate knowledge of these resonances parameters are essential. Among the parameters of interest are, of course, the ANC values, which determine the behaviour of the resonance wavefunctions at large distances. This is where the radiative capture mainly happens, due to the Coulomb repulsion between the colliding nuclei at close distances. Thus far, the ANC values for several among many known excited states of ^{6}Li have been

calculated (see, for example, Ref. [50]). One of the goals of this study is to determine the ANC values for several more states of ^{6}Li and to confirm the values of previous studies, or to improve the accuracy of the known parameters.

In its ground state the nucleus ^{6}Li can be viewed as a bound state of the α-particle and deuteron [60]. The α-particle is the most tightly bound of any nuclear complex and has a binding energy of ~ 28 MeV. A configuration of the nucleus of ^{6}Li where the α-particle cluster is present should then exist for excitation energies at least up to ~ 20 MeV. The deuteron cluster, in contrast, "dissolves" and becomes the *pn* pair at much lower energies. This implies that, in a theoretical consideration of the excited states of ^{6}Li, one has to deal with the three-body system, αpn, at least.

When analysing experimental scattering data, however, only the initial and final channels need to be considered. The constituents of the intermediate collision complex are something of a "black box". If an *S*-matrix that correctly describes the observed transitions among the channels can be constructed, it does not matter what kind of configurations are formed in that "black box". The poles of such an *S*-matrix should be at the correct (complex) resonance energies. Such an *S*-matrix will of course not reproduce all possible resonances, but only those that are reachable from the channels taken into account.

The analysis of elastic, two-body $d\alpha$ scattering is performed in this study. Since the isospins of both d and α are zero, only resonances of ^{6}Li with total isospin, $T = 0$ can be found. Yet in the spectrum of ^{6}Li, states with $T = 1$ do exist [58]. Most of the low-lying levels of ^{6}Li have zero isospin and decay into the $d\alpha$ channel, though. This makes the analysis of Ref. [8], reported here, reasonable and substantiated.

6.2 Fittings of channel data

The channels consider here may only differ by the orbital angular momentum quantum number, ℓ. All channels then have the same threshold and are thus degenerate in the energy. The states are defined by total angular momentum, J, and the

J^π	coupled $d\alpha$-channels
0^-	P_0
1^+	$S_1 - D_1$
1^-	P_1
2^+	D_2
2^-	$P_2 - F_2$
3^+	$D_3 - G_3$
3^-	F_3
4^-	$F_4 - H_4$

Table 6.1: Coupled partial waves in the $d\alpha$-collision for several lowest values of the total angular momentum J [8].

parity, π. The spins of the deuteron and the α-particle are 1 and 0, respectively. The total spin of the $d\alpha$ system is then $s = 1$. Since π is conserving, the maximum number of coupled partial waves for a given J is two. The channels under consideration are given in Table 6.1.

For each state with definite J^π, the S-matrix at the energy E is, as usual, written in terms of the Jost matrices by Eq. (2.121) on page 81:

$$S(E) = f^{(\mathrm{out})}(E)\left[f^{(\mathrm{in})}(E)\right]^{-1} .$$

The symbols J and π can be included to distinguish between the S-matrix for the different states, but to simplify the notation they are omitted. The exact semi-analytic expressions for the Jost matrices, given by Eq. (3.28) in Chapter 3, are written as follows:

$$\begin{aligned} f^{(\mathrm{in/out})}_{\ell'\ell}(E) &= \frac{e^{\pi\eta/2}\ell'!}{\Gamma(\ell'+1\pm i\eta)}\left\{\frac{C_\ell(\eta)k^{\ell-\ell'}}{C_{\ell'}(\eta)}\mathcal{A}_{\ell'\ell}(E)\right. \\ &- \left.\left[\frac{2\eta h(\eta)}{C_0^2(\eta)}\pm i\right]C_{\ell'}(\eta)C_\ell(\eta)k^{\ell'+\ell+1}\mathcal{B}_{\ell'\ell}(E)\right\} . \end{aligned} \tag{6.1}$$

The channels are here distinguished by ℓ, therefore the matrix elements are specifically indicated by ℓ and ℓ'. For a single channel, $\ell = \ell'$. The wave momentum, k, is common for all the channels, since they have the same thresholds and the same

reduced mass, μ. It is given by: $k = \pm\sqrt{2\mu E/\hbar^2}$. Similarly, the Sommerfeld parameter is the same for all channels: $\eta = \frac{\mu e^2 Z_1 Z_2}{k\hbar^2}$. As usual, the matrices $\mathcal{A}_{\ell\ell'}$ and $\mathcal{B}_{\ell\ell'}$ in Eq. (6.1) are unknown and are determined by the dynamics of the physical system [8]. They are again approximated by several terms of their Taylor expansions around E_0, with the expansion coefficients serving as fitting parameters:

$$\mathcal{A}_{\ell\ell'}(E) \approx \alpha^{(0)}_{\ell\ell'} + \alpha^{(1)}_{\ell\ell'}(E-E_0) + \alpha^{(2)}_{\ell\ell'}(E-E_0)^2 + \cdots + \alpha^{(M)}_{\ell\ell'}(E-E_0)^M \,, \quad (6.2)$$

$$\mathcal{B}_{\ell\ell'}(E) \approx \beta^{(0)}_{\ell\ell'} + \beta^{(1)}_{\ell\ell'}(E-E_0) + \beta^{(2)}_{\ell\ell'}(E-E_0)^2 + \cdots + \beta^{(M)}_{\ell\ell'}(E-E_0)^M \,. \quad (6.3)$$

For each experimental data point, $\sigma^{\text{exp}}_{\ell\ell'}(E)$, the corresponding fitting cross-section from Eq. (2.142) of Chapter 2 is calculated, given by:

$$\sigma^{\text{fit}}_{\ell\ell'}(E) = \frac{\pi}{k^2}\frac{2J+1}{2s+1}|S_{\ell\ell'}(E) - 1|^2 \,, \quad (6.4)$$

since the scattered particles for this system have non-zero spin. As will be discussed in the next section, experimental values for the transition cross-sections are not available. The following function is then minimised:

$$\chi^2 = \sum_{i=1}^{N_1}\left[\sigma^{\text{exp}}_{\ell_1}(E_i) - \sigma^{\text{fit}}_{\ell_1}(E_i)\right]^2 + \sum_{i=1}^{N_2}\left[\sigma^{\text{exp}}_{\ell_2}(E_i) - \sigma^{\text{fit}}_{\ell_2}(E_i)\right]^2 \,, \quad (6.5)$$

where the first sum takes the deviations of the fitted points from the experimental ones in the first channel into account, and the second sum runs over the data points in the second channel (if it exists for a given J, as shown in Table 6.1). The values N_1 and N_2 are the numbers of data points in the fitting, in the first and the second channels, respectively. The minimisation was again done using the MINUIT code [33].

It should be highlighted that the diagonal matrix element, $S_{\ell\ell}$, obtained from (6.1), depends on all the elements of the matrices $f^{(\text{in/out})}$ (diagonal and off-diagonal). This means it depends on all the elements of the matrices $\alpha^{(n)}$ and $\beta^{(n)}$, hence the coupling of the channels is always present in the fitting procedure used here and it is correctly taken into account. When performing a two-channel fitting of data

from only some available channels, all the fitting parameters are involved in such a fit. The resulting S-matrix should therefore correctly describe the other channels as well. This was previously demonstrated in the model scattering problem of Chapter 3, as well as in Ref. [6].

When the Jost matrices are obtained from the fitting, the bound and resonance state energies, $\mathcal{E}_i$, can be determined with $\det[f^{(\text{in/out})}(\mathcal{E}_i)] = 0$ on the appropriate sheets of the Riemann surface. The S-matrix residues at these spectral energies, as well as the ANC values for the corresponding bound and resonance states, can then be determined.

Only the ANC values of the elastic channels will be determined, so the single-channel Eq. (4.31) on page 125 with $a = e^{-\pi\eta/2}$ can be used:

$$\text{Res}\,[S_{\ell\ell}, \mathcal{E}_i] = i(-1)^{\ell+1}\frac{\hbar^2 k}{\mu}e^{-\pi\eta}\,\mathcal{A}_\ell^2\,. \tag{6.6}$$

This choice of a is used since the calculations of this chapter (and of Ref. [8]) then correspond to the relevant equations of Ref. [50], as shown in Chapter 4.

6.3 Experimental data

The $d\alpha$ data used for these fitting are the combined data of two different sets of scattering cross-sections, denoted further as the sets A and B. They cover adjacent intervals of the collision energy and therefore complement each other.

Data set A consists of the $d\alpha$ cross-sections obtained from the corresponding phase-shifts of Ref. [61], where an energy independent analysis of 3900 raw experimental data points was done, with channel coupling included. These phase-shifts cover the centre-of-mass (C.M.) energy range from 4 MeV to 30 MeV. There are roughly 20 data points available for each of the partial waves with $\ell = 0,1,2,3,4,5$.

Data set B comprises the $d\alpha$ cross-sections which were derived from the Padé

approximation of the S-matrix, obtained in Ref. [62] by fitting energy-dependent single-channel experimental data in the C.M. energy interval from 0.5 MeV to 3.5 MeV. Channel coupling was not taken into account by the authors of Ref. [62]. Since the S-matrix of [62] is given in an explicit form, a sequence of data points convenient for this analysis can be generated from it, even outside the original energy-interval. Using this freedom, 40 points in each channel were generated. This evenly covers the C.M. energies from 0.4 MeV to 4.0 MeV. Due to the existence of certain resonance structures at higher energies, generated points with $E > 4.0$ MeV may deviate from actual experimental values. The data set A covers the higher energy range more accurately.

Therefore, combining the sets A and B, 40 points between 0.4 MeV and 4 MeV, and 20 points between 4 MeV and 30 MeV for each channel are obtained. The sets A and B match smoothly around 4 MeV and are thus consistent.

The same data sets were used in Ref. [50], where a method similar to the effective-range expansion, was applied for extracting the information about the discrete states of the $d\alpha$-system. The authors of Ref. [50] analysed the data sets A and B separately, though. Following the suggestion of Ref. [62], the two sets are combined and treated as a single one here.

A brief description of how the phase-shifts of set B are obtained from the Padé parameters of Ref. [62] will follow. The Padé approximations are polynomials given by the following, where a_i and b_j are the fitting parameters:

$$P_N(E) = \sum_{i=0}^{N} a_i E^i, \qquad Q_M(E) = 1 + \sum_{j=1}^{M} b_j E^j. \tag{6.7}$$

The Coulomb-nuclear phase-shifts, δ_ℓ^{cn}, are then determined from the following approximation [62]:

$$\frac{P_N(E)}{Q_M(E)} \approx k^{2\ell+1}\tilde{C}_\ell^2 \left[\cot(\delta_\ell^{\mathrm{N}}) - i + \frac{2\eta H(\eta)}{\tilde{C}_0^2}\right], \tag{6.8}$$

with

$$\tilde{C}_0^2 = C_0^2 = 2\pi\eta/(e^{2\pi\eta}-1), \qquad \tilde{C}_\ell^2 = \tilde{C}_{\ell-1}^2(1+\eta^2/\ell^2), \tag{6.9}$$

and

$$H(\eta) = \psi(i\eta) + \frac{1}{2i\eta} - \ln\left[-i\eta\ \mathrm{sgn}(-Z_1Z_2)\right], \tag{6.10}$$

with $\psi(z)$ representing the digamma function, as before.

The nuclear phase-shifts for each channel are then combined with the nuclear phase-shifts from Data set A. The points from Data set B are smoother than those from Data set A, but this is of course because they are generated from Padé fittings.

The total experimental scattering cross-sections to be fitted, $\sigma_{\ell\ell'}^{\mathrm{exp}}(E)$, are then obtained with Eq. (6.4) via the S-matrix. Only the elastic scattering phase-shifts are available. The S-matrix main diagonal elements are then determined by Eq. (2.75) on 69:

$$S_{\ell\ell}(E) = e^{2i(\delta_\ell^N+\delta_\ell^c)}. \tag{6.11}$$

Before giving the results from the fitting of the data generated in this way, the Padé-expansions (6.7), will be compared with the expansions of the Jost functions.

6.4 The Padé and Jost methods

The discussion will be limited to single-channel scattering. The semi-analytic representation for the S-matrix (where functions of the energy-branching variables k and η are factorised) is given in Ref. [6] by (6.1), where the S-matrix is again the "ratio" of Jost functions. For single-channel scattering, it can be written as follows:

$$S_\ell(E) = e^{2i\delta_\ell^c}\frac{\mathcal{A}(E) - [\frac{2\eta h(\eta)}{C_0^2} - i]C_\ell^2 k^{2\ell+1}\mathcal{B}(E)}{\mathcal{A}(E) - [\frac{2\eta h(\eta)}{C_0^2} + i]C_\ell^2 k^{2\ell+1}\mathcal{B}(E)}. \tag{6.12}$$

The single-channel S-matrix for scattering involving Coulomb interactions in terms of the Padé functions $P_N(E)$ and $Q_M(E)$ given in Ref. [62] can be derived from the

S-matrix in terms of the phase-shift, Eq. (6.11) and Eq. (6.8):

$$S_\ell(E) = e^{2i\delta_\ell^c} \frac{P_N(E) - k^{2\ell+1}\tilde{C}_\ell^2 \left[\frac{2\eta\tilde{H}(\eta)}{\tilde{C}_0^2} - 2i\right] Q_M(E)}{P_N(E) - k^{2\ell+1}\tilde{C}_\ell^2 \frac{2\eta\tilde{H}(\eta)}{\tilde{C}_0^2} Q_M(E)}. \tag{6.13}$$

The following relations between the various functions of k and η from Refs. [6] and [62] hold, which can be shown from Eq. (2.15), (3.9), (6.9) and (6.10):

$$\tilde{C}_\ell(\eta) = \frac{(2\ell+1)!}{2^\ell \ell!} C_\ell(\eta), \tag{6.14}$$

$$H(\eta) = h(\eta) + i\pi \left(\frac{1}{e^{2\pi\eta} - 1}\right). \tag{6.15}$$

Eq. (6.13) then becomes the following:

$$S_\ell(E) = e^{2i\delta_\ell^c} \frac{\tilde{L}^2 P_N(E) - \left[\frac{2\eta h(\eta)}{C_0^2} - i\right] C_\ell^2 k^{2\ell+1} Q_M(E)}{\tilde{L}^2 P_N(E) - \left[\frac{2\eta h(\eta)}{C_0^2} + i\right] C_\ell^2 k^{2\ell+1} Q_M(E)}, \tag{6.16}$$

with

$$\tilde{L} = \frac{2^\ell \ell!}{(2\ell+1)!} \tag{6.17}$$

This is of a similar form to (6.12), apart from the factor $\tilde{L}^2$. The Padé functions $P_N(E)$ and $Q_M(E)$ are therefore similar to the single-channel form of the functions expanded in the Taylor series, $\mathcal{A}(E)$ and $\mathcal{B}(E)$ (given in Eq. (6.2) and (6.3)), but the factor L^2 is encapsulated in the coefficients a_j of Eq. (6.7).

The Padé functions $P_N(E)$ and $Q_M(E)$ are, in fact, Taylor expansions around $E_0 = 0$, with some of the parameters (like $b_0 = 1$) already fixed, and a fixed, differing number of terms for each of the functions which are expanded ($N \neq M$).

The advantage of using the Padé expansions, $P_N(E)$ and $Q_M(E)$, for an initial single-channel fitting is in the small number of fitting parameters and the fact that extrapolation of data to higher and lower energies is stable. The Taylor expansion can be unstable at the endpoints for a small number of data points to be fitted.

The benefit of using the Taylor expansions of $\mathcal{A}(E)$ and $\mathcal{B}(E)$ in the Jost method lies in the reliable analytic continuation to complex energies, since the expansions can be done around any E_0 with an arbitrary number of terms in the expansion. Furthermore, the analytic properties of the S-matrix in the Jost method for a multi-channel fitting are also rigorously derived, which means the Jost method can reliably be implemented in a multi-channel fitting, as is done in this study.

6.5 Results

When fitting the data, several different central points, E_0 and different numbers, M, in the expansions, (6.2 and 6.3), were used. The choice of these parameters is determined by the choice of the energy domain where a resonance may be found. It is obvious that the closer E_0 is to a resonance, the more accurately it can be located. By repeating the calculations for the same resonance with different E_0 or M, the accuracy achieved can be checked, similar to what was done in the previous chapter. In this chapter, the averages of these fittings around different E_0 will not be determined, however.

Ideally, the resonance parameters should not depend on such a choice of E_0 or M. Therefore all the digits in their values that remain the same with different E_0, can be considered as accurate.

Consider the coupled S_1 and D_1 partial waves in the state 1^+. The results of the analysis of these states is given in Table 6.2. For the corresponding fitting, $E_0 = -1.45\,\text{MeV}$ and $M = 1$. The quality of the fit is clear in Figures 6.1 and 6.2. The bound state energy from these calculations agrees well with the value that is considered as accepted in the compilation, Ref. [58]. The ANC determined here for the S_1 partial wave is somewhat larger than the values from Ref. [50], though. The ANC from the D_1 partial wave agrees with one of the two values reported in Ref. [50], where it was supposed that the $S_1 - D_1$ coupling was weak, since the D_1-ANC was small compared to S_1-ANC. However, the comparison of these values is not a decis-

E_r [MeV]	Γ [MeV]	Res$[S_{00},E]$ [MeV]	Res$[S_{22},E]$ [MeV]	$\lvert\mathcal{A}_0\rvert$ [fm$^{1/2}$]	$\lvert\mathcal{A}_2\rvert$ [fm$^{1/2}$]	Ref.
-1.4691		29.588 $+i42.904$	0.00603 $-i0.00079$	2.3330	0.0252	this work and [8]
				1.960	0.093	[50] (v. 1)
				1.900	0.025	[50] (v. 2)
-1.4743						[58] (accepted)
3.8858	2.6324	0.00196 $+i0.00087$	-1.7743 $-i1.0906$	0.0153	0.4768	this work and [8]
3.900	2.347			0.028	0.455	[50] (v. 1)
3.872	1.860			0.018	0.392	[50] (v. 2)
4.18 ± 0.05	1.5 ± 0.2					[58] (accepted)

Table 6.2: Parameters of the bound and resonance states of ^{6}Li with $J^\pi = 1^+$, obtained from a two-channel fit of the elastic cross-sections for the S_1 and D_1 partial waves of the d-α scattering [8]. The corresponding parameters from Refs. [50, 58] are given here for the purpose of comparison.

ive argument for such a conclusion. A reasonable judgement on the strength of the coupling between any two channels can be made, if the cross-section of the transition between them is considered. As mentioned before, the method of analysis used here has an advantage that the same fitting parameters describe all the elastic and inelastic processes. Thus, after fitting the S_1 and D_1 channels, the correct transition cross-section is automatically obtained, which is shown in Figure 6.3. The values are three orders of magnitude smaller than both the elastic cross sections, given in Figures 6.1 and 6.2. This implies that the $S_1 - D_1$ coupling is indeed weak.

Now consider the 1^+ resonance in the coupled $S_1 - D_1$ channels. The weak coupling between the two partial waves results in the absence of any visible irregularities around the resonance energy, $E \sim 3.9$ MeV, in the S_1 cross-section. The 1^+ resonance at this energy is thus completely dominated by the D_1 wave. The results from the Jost matrix analysis agree well with those from Ref. [50]. This can be said not only about the resonance energy and width, but also about the ANC values. However, the width is somewhat larger than the value accepted in the compilation, Ref. [58].

A possible explanation can be that a potential barrier is needed to sustain this resonance, and in the state with $\ell = 2$ there exists a centrifugal barrier for that purpose. After this resonance is formed in the D_1 wave, it can decay back to the same wave,

J^π	ℓ_J	E_r [MeV]	Γ [MeV]	Res$[S_\ell, E_r - \frac{i}{2}\Gamma]$ [MeV]	$\lvert\mathcal{A}_\ell\rvert$ [fm$^{1/2}$]	Ref.
2^+	D_2	2.8448	1.3229	$-1.0387 - i0.7135$	0.4262	this work and [8]
		2.960	0.995		0.349	[50] (set A fit)
		2.802	1.178		0.384	[50] (set B fit)
		2.838 ± 0.022	1.30 ± 0.1			[58] (accepted)
3^+	D_3	0.7135	0.0219	$0.0141 - i0.0166$	0.1124	this work and [8]
		0.690	0.024		0.119	[50] (set A fit)
		0.704	0.025		0.121	[50] (set B fit)
		0.712 ± 0.002	0.024 ± 0.002			[58] (accepted)
3^+	D_3	9.1632	8.2023	$0.7411 - i1.1532$	0.2793	this work and [8]
		14.326	17.8			[61]
2^-	F_2	20.906	29.034	$-20.743 - i0.8508$	0.8043	this work and [8]
		25.526	22			[61] (Sol. A)
		19.526	30			[61] (Sol. C)
3^-	F_3	10.305	16.724	$-7.3697 + i4.7254$	0.5403	this work and [8]
		22.526	16			[61]

Table 6.3: Parameters of ^{6}Li resonances in the states with 2^+, 3^+, 2^-, and 3^- obtained from fittings of the corresponding cross-sections of $d\alpha$ scattering [8]. The available values of the corresponding parameters from Refs. [50, 58, 61] are given for comparison.

or to the S_1 wave. However, because of the weak coupling between them, the probability of decaying into the S_1 wave is very small. Nonetheless, it is nonzero and contributes something to the total width. This is why the total width determined here is a bit bigger than the value of Ref. [50], where the coupling was completely ignored.

The next state considered here is the partial wave D_2 ($J^\pi = 2^+$), which is not coupled to any other waves. The data points for this state and the corresponding cross-section from the fitting with $E_0 = 2.6$ MeV and $M = 3$, are shown in Figure 6.4. In this channel, one resonance at the energy $E = (2.8448 - \frac{i}{2}1.3229)$ MeV was found, which practically coincides with the value accepted in the compilation, Ref. [58]. The S-matrix residue and the corresponding ANC are given in Table 6.3.

Next are two quantum states $2^-(P_2 - F_2)$ and $3^+(D_3 - G_3)$, which are both mixtures of two partial waves. However, similar to the $(S_1 - D_1)$ case, the cross-sections for the transitions $P_2 \leftrightarrow F_2$ and $D_3 \leftrightarrow G_3$ were calculated to be several orders of magnitude smaller than the corresponding elastic cross-sections. This implies that

the couplings in these pairs of partial waves are extremely weak and therefore the resonances (if any) are dominated by a single wave in both states.

Both two-channel fittings for the pairs $(P_2 - F_2)$, $(D_3 - G_3)$ and single-channel fittings for each of the waves P_2, F_2, D_3, and G_3 were attempted separately. The single-channel fits reveal resonances only in the waves F_2 and D_3. The two-channel fittings give the 2^- and 3^+ resonances with the same parameters obtained via the single-channel fittings. In this way, one resonance in the state 2^- is found and two resonances in the state 3^+ are found. Their parameters are given in Table 6.3, where only the dominant partial waves are shown. The corresponding fittings of the cross sections are shown in Figures 6.5 and 6.6. These fittings were done with $E_0 = 1.0\,\text{MeV}$ and $M = 5$ for D_3 and with $E_0 = 30\,\text{MeV}$ and $M = 2$ for F_2.

The last resonance that was found is in the state $3^-(F_3)$, which involves only one partial wave. Its parameters are also shown in Table 6.3. The cross-section for this state, together with the fitted curve ($E_0 = 15\,\text{MeV}$, $M = 2$), are shown in Figure 6.7.

6.6 Remarks

It should be noted that the resonances found in the partial waves F_2, F_3, and the second resonance in D_3, were not included in the accepted list of Ref. [58]. They are very wide and are therefore difficult to find with any method. The only work where the resonances in these states were reported, was the older work, Ref. [61]. As is seen from Table 6.3, the findings of this chapter (and Ref. [8]) only roughly corresponds with the findings of Ref. [61]. This means that an independent confirmation is needed before these resonances can be considered as firmly established. It is seen from Figures 6.5 and 6.7 that there is much experimental uncertainty in the available data for the partial waves F_2 and F_3 and therefore deducing reliable resonance parameters for these channels is difficult.

In the initial fitting attempts, where the data sets A and B were considered separately, vastly different results were obtained. This indicates the importance of using a larger

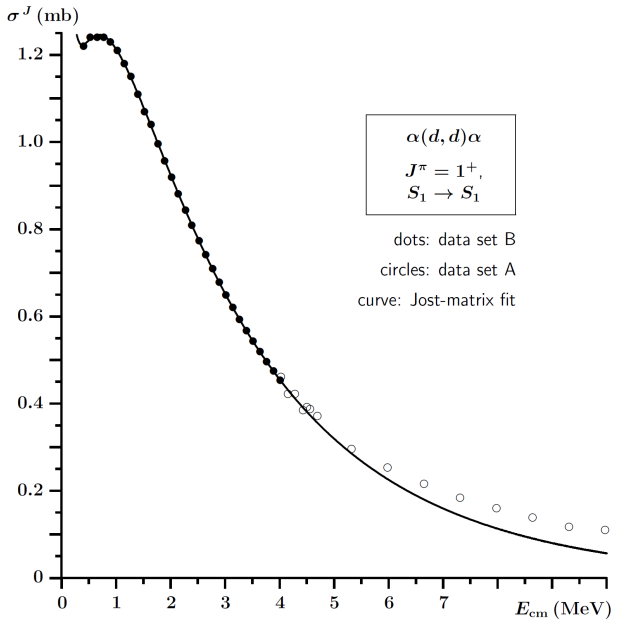

Figure 6.1: Fit of the data points in the partial wave S_1 [8].

energy range in performing fittings to obtain parameters for wide resonances.

Lastly, it should be mentioned that no resonances were found, as was expected, in the other states listed in Table 6.1.

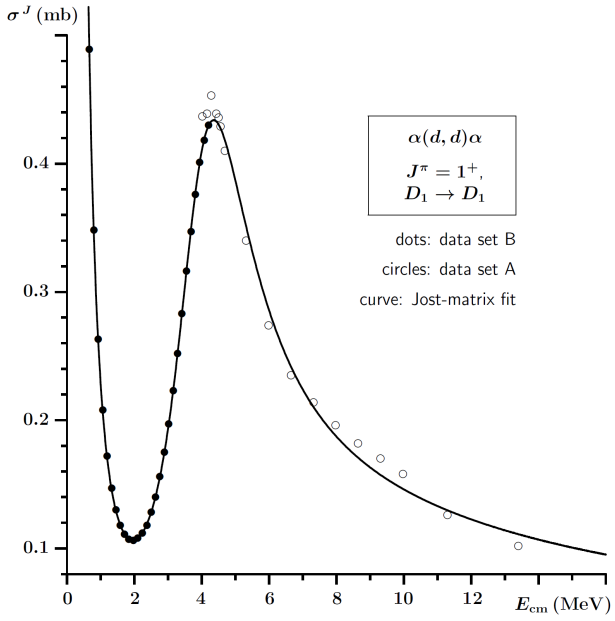

Figure 6.2: Fit of the data points in the partial wave D_1 [8].

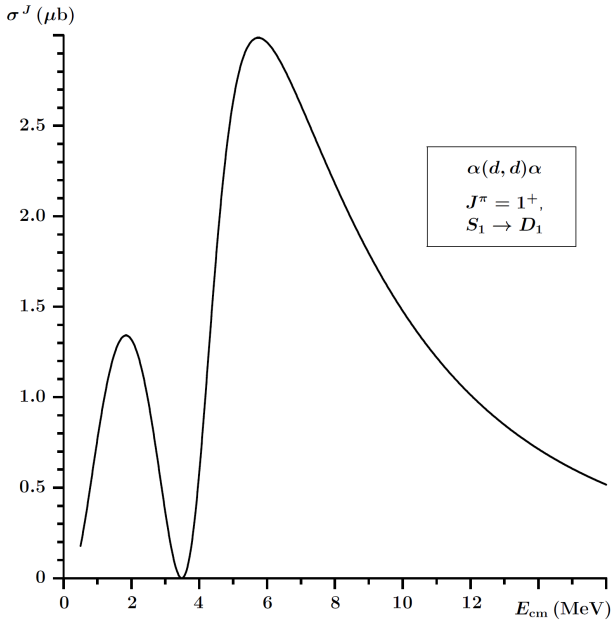

Figure 6.3: Cross-section for the transition between the partial waves S_1 and D_1 [8].

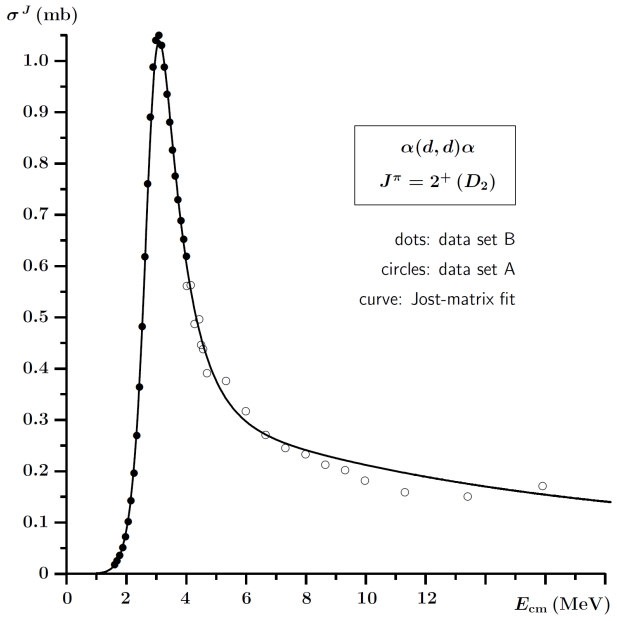

Figure 6.4: Fit of the data points in the partial wave D_2 [8].

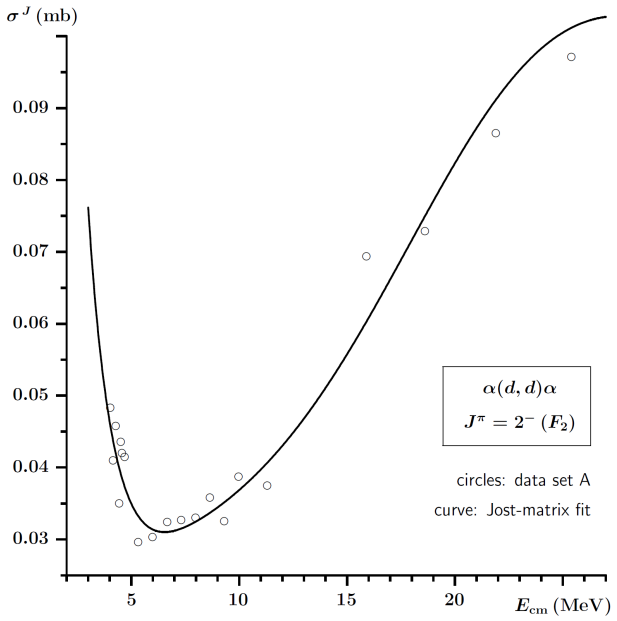

Figure 6.5: Fit of the data points in the partial wave F_2 [8].

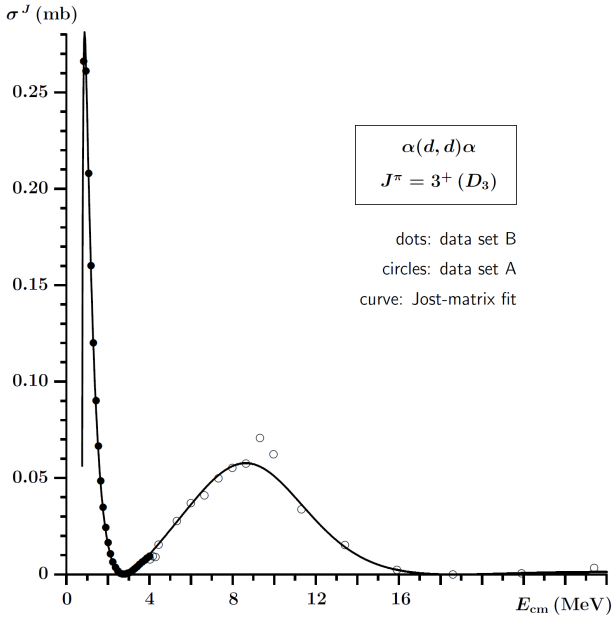

Figure 6.6: Fit of the data points in the partial wave D_3 [8].

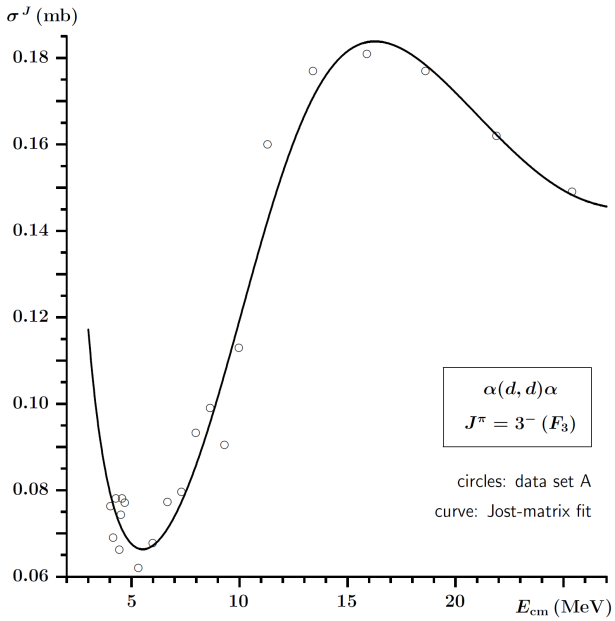

Figure 6.7: Fit of the data points in the partial wave F_3 [8].

Chapter 7

Conclusion

In this chapter, the advantages of using the Jost matrix method of analysis are highlighted. The main results of the study are then summarised and possible future work using the Jost matrix method is discussed.

7.1 Discussion

The Jost matrix method allows bound and resonance states to be located from the same fitting. Methods like the Breit-Wigner parameterisation, however, are limited to determining resonance parameters, and usually only for sharp resonances. Due to the exact relationship between the S-matrix residue and the Jost matrices, scattering parameters such as the ANC can also be determined.

Methods based on the effective-range expansion, which contributed to the development of the Jost method, also allows bound and resonance state parameters, as well as the corresponding ANC values, to be determined. In fact, the results from Ref. [49] for α^{12}C scattering in Chapter 5 as well as the results for $d\alpha$ scattering in Ref. [50], given in Chapter 6, depend directly on parameterising data with effective-range-like functions. The results from the calculations of this thesis (as well as the articles it is based on) are compared with the results from these articles.

Effective-range methods are, however, generally only accurate for small energy-

values. Multi-channel effective range methods are also complicated and cumbersome, as discussed in Chapter 3. Using the Jost method, the extension to multi-channel scattering simply requires certain quantities to become matrices. In fact, while only two-channel problems were considered in the calculations for this thesis, the theory is applicable to scattering in any number of channels. The Jost matrices can furthermore be expanded around any complex energy, which means the Jost method is accurate at large energies as well as low energies, depending on the choice of E_0.

If the Jost matrices can be determined from fitting experimental data by using a suitable expansion, the corresponding S-matrix, phase-shift, scattering cross-section or any other quantity of importance can be determined. However, the Jost matrices cannot be expanded in a Taylor series (or any other expansion) directly, nor can other quantities describing quantum scattering processes, such as the scattering amplitude and S-matrix. These quantities are not analytic and single-valued function of E, but multi-valued functions defined on a complicated Riemann surface of the energy with the number of branch points equal to the number of channels, as discussed in Chapter 3.

This difficulty is addressed by using the semi-analytic expression for the multi-channel Jost matrices derived in Ref. [6], where all the factors responsible for the branching of the Riemann surface are given explicitly. The remaining, unknown functions are analytic and single-valued, defined on a simple energy plane, which makes them considerably easier to approximate with an expansion. Since the factors responsible for the branching of the Riemann surface are isolated and can be manipulated directly, the analytic continuation of the Jost matrices onto any sheet of the Riemann surface can be performed with certainty. This semi-analytic expression for the Jost matrices also explicitly includes Coulomb interactions.

A similar semi-analytic expression has been used for the fitting of scattering data for neutral particles in Ref. [24]. This expression, pertaining to the scattering of particles with short-range interactions only, is recovered if the Coulomb interaction is "switched off" by setting $\eta_n = 0$. Similar to the simple effective-range theory,

the presence of the Coulomb potential makes the explicit factors in the semi-analytic expression for the Jost matrix very complicated. Yet the remaining functions of E are still smooth and can be approximated by just a few terms of the Taylor series. This is demonstrated for a model two-channel scattering problem in Ref. [4], reported in Chapter 3, where the proposed method is shown to be accurate and stable.

It is shown that the energy, total width as well as the partial widths for narrow resonances can be calculated, even for experimental data with considerable experimental noise. For such data points with large deviations from the exact values, the energy and total width of wider resonances could accurately be reproduced and for very wide resonances, at the very least the resonance energy was determined.

It is also shown in Chapter 3 that a multi-channel fitting of experimental data from a limited number of channels can be used to accurately generate cross-sections for the unknown channels. Cross-sections for transition channels, which are often unknown, can be obtained in particular. The strength of the coupling determines the relative magnitude of the transition cross-sections. In Chapter 6, the transition cross-sections for the coupled channels of $d\alpha$ are determined to show that the relevant coupling is weak.

In general, the calculations of Chapter 6 (and Ref. [8]) reasonably reproduce, or confirm, the parameters of the bound state of ^{6}Li as well as the parameters of all the resonances with isospin zero, given in Ref. [58]. Some of the resonances not included in the compilation [58], but found in Ref. [61] are also approximately confirmed. It can then be claimed that the parameters published in Ref. [8] given in Chapter 6 are reliable, as much as the data from which they were deduced is accurate. The same is true for the results of Ref. [7], reported in Chapter 5. Here the resonances of ^{12}O are confirmed, given in Ref. [9].

Furthermore, the Asymptotic Normalisation Coefficients are determined for the located discrete states of both nuclear scattering systems. These values are relevant to the study of the radiative capture reactions $\alpha(d,\gamma)^6$Li and ^{12}C$(\alpha,\gamma)^{16}$O in astrophysics, as discussed in Chapter 4.

7.2 Future work

As mentioned in Chapter 3, the Jost method of analysis has successfully been used in locating two-channel resonances in the nuclei ^{5}He [35] and ^{8}B [36]. The application of this method has certainly not been exhausted, though. Almost 80 years of non-relativistic experimental scattering data is available for analysis. In many instances, scattering parameters already determined from the available data must be verified. Other parameters, such as the ANC, has not yet been determined for numerous scattering experiments relevant to astrophysics. The multi-channel analysis of single-channel data from certain strongly coupled systems will also be attempted to gain insight into the channels for which no data is available. This would be impossible using most other methods. The method can also be applied to simulated data, similar to what is done in Chapter 3. Such fittings would be used to gain insight into the potentials that generated the data.

The analysis of the α^{12}C data is also by no means complete. As mentioned in Chapter 5, certain subthreshold bound states exist for such a scattering process. Values for the corresponding ANC values have been determined in Ref. [28] and Ref. [40] using effective-range-like and other functions, but there is still disagreement on these results. Due to the insufficient data at low energies, two avenues, other than the ones mentioned in Chapter 5, will be pursued to locate these subthreshold bound states and to determine the corresponding ANC values from the fitting of the data. Firstly, the unknown functions in the semi-analytic Jost matrices are usually expanded in Taylor series. This can lead to fitted functions with large fluctuations at the endpoints, especially if the experimental data points are few. Other, more stable expansions will be attempted. The second avenue requires a two-channel analysis of the α^{12}C system, where the data for the second channel is generated from a suitable potential, if no experimental data is available. I am optimistic that both avenues may yield promising results.

There are also numerous new non-relativistic experiments being conducted, that require theoretical support. Much work must be done to extend the theory further,

so that it is generally applicable to a broader spectrum of scattering problems. In particular, the relation with R-matrix methods of Ref. [57] will be explored.

It should be stressed that the Jost matrix method used in this thesis is nonrelativistic. It cannot, therefore, be used directly in analysing high-energy physics scattering data, although such an analysis is possible. There are, however, a wide range of further problems in atomic and low-energy nuclear physics, where it could find applications.

In principle, one can attempt the same parameterisation for high energies if the relativistic relation between the energy and momentum, $E = \sqrt{\hbar^2 k^2 c^2 + \mu^2 c^4}$, is used in all the formulae. Such an inclusion of relativistic kinematics into nonrelativistic operators is common for various initial parameterisations of scattering data in particle physics. Mathematical rigour and substantiation is, however, lost.

In conclusion: the Jost matrix method is a robust and accurate way to determine scattering parameters from analysing scattering data. It is mathematically rigorous, easy to conceptualise and relatively simple to implement. It can give insight into numerous nuclear and atomic systems. Devoting more time to the study of Jost matrices in scattering theory, in particular in fitting experimental data, would certainly be worthwhile.

Bibliography

[1] G. Breit and E. Wigner, Phys. Rev. **49** 519, (1936)

[2] V. I. Kukulin, V. M. Krasnopol'sky, and J. Horáček, *Theory of Resonances: Principles and Applications* (Academia, Praha, 1989)

[3] J.R. Taylor, *Scattering Theory: The Quantum Theory of Nonrelativistic Collisions* (Dover Publications, Inc., New York, 2000)

[4] P. Vaandrager and S. A. Rakityansky, *"Extracting the resonance parameters from experimental data on scattering of charged particles"*, Int. J. Mod. Phys. E **25**, 1650014 (2016)

[5] A. Švarc, M. Hadžimehmedović, H. Osmanović, J. Stahov, L. Tiator and R. L. Workman, *"Introducing the Pietarinen expansion method into the single-channel pole extraction problem"*, Phys. Rev. C **88** 035206, (2013)

[6] S. A. Rakityansky and N. Elander, *"Analytic structure of the multichannel Jost matrix for potentials with Coulombic tails"*, J. Math. Phys. **54**, 122112(2013)

[7] P. Vaandrager, S.A. Rakityansky, "*Residues of the S-matrix for several* $\alpha^{12}C$ *resonances from the Jost function analysis*", Nucl. Phys. A **992**, 121627 (2019)

[8] P. Vaandrager and S. A. Rakityansky, *"Jost-matrix analysis of experimental data on* d^4He *scattering"*, Nucl. Phys. A **1000**, 121799 (2020)

[9] D.R. Tilley, H.R. Weller and C.M. Cheves, *Energy Levels of Light Nuclei* $A =$ $16 - 17$, Nucl. Phys. A, **564**, pp. 1-183 (1993)

[10] V. B. Belyaev, S.A. Rakityansky and W. Sandhas, *"Three-body resonances Λnn and ΛΛn"*, Nucl. Phys. A **803**, pp 210-226 (2008)

[11] N. Zettili, *Quantum Mechanics: Concepts and Applications* (2nd edition, Wiley, Chichester, 2009)

[12] L. Narici, E. Beckenstein, *Topological Vector Spaces* (2nd edition, CRC Press, New York, 2010)

[13] S. A. Rakityansky and N. Elander, *"Multi-channel analog of the effective-range expansion"*, J. Phys. A **44**, 115303 (2011)

[14] M. Abramowitz and A. Stegun, *Handbook of mathematical functions* (Dover, New York, 1965).

[15] R. Jost, *" Uber die falschen Nullstellen der Eigenwerte der S-Matrix"*, Helv. Phys. Acta, v. XX, pp. 256-266 (1947)

[16] K. Chadan, R. Kobayashi and T. Kobayashi, *"The absolute definition of the phase-shift in potential scattering"*, J. Math. Phys **42**(9), 4031(2001)

[17] S. A. Rakityansky and N. Elander, *"Analyzing the contribution of individual resonance poles of the S-matrix to two-channel scattering"*, Int. J. Quant. Chem. **106**, 1105-1129 (2006)

[18] S. A. Rakityansky *"Partial widths of a multi-channel resonance"*, J. Phys.: Conf. Ser **915**, 012008 (2017)

[19] S. A. Rakityansky and N. Elander, *"Analytic Structure and Power-Series Expansion of the Jost Matrix"*, Few-Body Syst. **54**, pp. 673–683 (2012)

[20] G. Strang, *Linear algebra and its applications* (Harcourt, Brace and Jovanovich Publishers; San Diego, 1988)

[21] R. Mehrem, *"The plane-wave expansion, infinite integrals and identities involving Spherical Bessel functions"*, Appl. Math. and Comput. **217**(12), pp 5360-5365 (2011)

[22] A. Messiah, *Quantum Mechanics* (Dover Publications, Inc., New York, 1999)

[23] J.L. Walsh, *"Interpolation and approximation by rational functions in the complex domain"*, American Mathematical Society Colloquium Publications, vol. XX, (1960)

[24] S. A. Rakityansky and N. Elander, *"A method for extracting the resonance parameters from experimental cross section"*, Int. J. Mod. Phys. E **22**, 1350032(2013)

[25] M. H. Ross and G. L. Shaw, *"Scattering length and effective range theory for multi-channel processes"*, Ann. Phys. **9**, pp. 391–415 (1960)

[26] L. Rosenberg, *"Multichannel effective-range theory with long-range interactions"*, Phys. Rev. A **57**(3), pp. 1862–1869 (1998).

[27] D. Gaspard and J.M. Sparenberg *"Effective-range function methods for charged particle collisions"*, Phys. Rev. C **97**, 044003 (2018).

[28] J.M. Sparenberg, P. Capel, and D. Baye, *"Influence of low energy scattering on loosely bound states"*, Phys. Rev. C **81**, 011601 (2010).

[29] R. H. Dalitz and S. Tuan, *"The phenomenological representation of K-nucleon scattering and reaction amplitudes"*, Ann. Phys. (N.Y.) **10**, pp. 307–351 (1960).

[30] J. Humblet, *"Analytical structure and properties of Coulomb wave functions for real and complex energies"*, Ann. Physics **155**, pp. 461-493(1984)

[31] E. Lambert, *"Fonction de portée effective et déplacement en énergie des états liés en présence d'un potentiel coulombien modifié"*, Helv. Phys. Acta **42**, pp. 667-677(1969)

[32] H. Poincaré, *""Sur les groupes des équations linéaires"*, Acta Math. **4**, pp. 201–311 (1884).

[33] F. James and M. Roos, *"Minuit - a system for function minimization and analysis of the parameter errors and correlations"*, Comp. Phys. Comm. 10 (1975) 343-367; http://hep.fi.infn.it/minuit.pdf

[34] T. Noro and H. S. Taylor, *""Resonance partial widths and partial photodetachment rate using the rotated-coordinate method"*, J. Phys. B: Atom. Mol. Phys. **13**, L377 (1980)

[35] S.A. Rakityansky and S.N. Ershov, *Jost-matrix analysis of the resonance* ^{5}He$^*(\frac{3}{2}^+)$ *near the dt-threshold*, Int. J. Mod. Phys. E **28**(8), 1950064 (37 pages) (2019)

[36] S.A. Rakityansky, S.N. Ershov and T.J. Tshipi, *Resonance states* 0^+ *of the Boron isotope* ^{8}B *from the Jost-matrix analysis of experimental data*, Int. J. Mod. Phys. E **28**(8), 1950083 (21 pages) (2019)

[37] I.J. Thompson and F.M. Nunes, *Nuclear Reactions for Astrophysics* (Cambridge University Press, Cambridge, 2009.)

[38] D. N. Schramm and R. V. Wagoner, "*Element Production in the Early Universe*", Annu. Rev. Nucl. Sci. **27**, pp. 37-74 (1977)

[39] S. Maurizio and C. Santi, *Evolution of Stars and Stellar Populations* (John Wiley and Sons, New Jersey, 2005).

[40] Yu. V. Orlov, B. F. Irgaziev, and L. I. Nikitina, *"Asymptotic normalization coefficients of resonant and bound states from the phase shifts for* $\alpha-\alpha$ *and* $\alpha-C^{12}$ *scattering"*, Phys. Rev. C **93**, 014612(2016)

[41] A. M. Mukhamedzhanov and R. E. Tribble, *"Connection between asymptotic normalization coefficients, subthreshold bound states, and resonances"*, Phys. Rev. C **59**, 3418(1999)

[42] A. Baz', Y. Zel'dovich, and A. Perelomov, *Scattering, Reactions and Decay in Nonrelativistic Quantum Mechanics* (PST, Jerusalem, 1969), Translated from Russian by Z. Lerman

[43] E.I. Dolinskii and A.M. Mukhamedzhanov, *Relation of deduction in S-matrix pole to proportional coefficient in wave-function asymptotics*, Izv. Akad. Nauk SSSR, Ser. Fiz. 41, 2055 (1977)

[44] E.I. Dolinskii and A.M. Mukhamedzhanov, Bull. Acad. Sci. USSR, Phys. Ser. 41, 55 (1977)

[45] T.N. Rescigno and C.W. McCurdy, *"Normalization of resonance wave functions and the calculation of resonance widths"*, Phys. Rev., **A34**, 1882-1887 (1986)

[46] T. Berggren, *"On the use of resonant states in eigenfunction expansions of scattering and reaction amplitudes"*, Nucl.Phys., **A109**, 265-287 (1968)

[47] M. Castagnino, R. Id. Betan, R. Laura and R.J. Liotta, *"Quantum decay processes and Gamov states"*, Journal of Phys. **A35**, pp. 6055-6074 (2002)

[48] S. A. Rakityansky and I.M. Gopane, *"Effective-range parameters and vertex constants for* Λ*-nuclear systems"*, Int. J. Mod. Phys. E **26**(4), 1750014 (2017)

[49] B. F. Irgaziev and Yu. V. Orlov, *"Resonance properties including asymptotic normalization coefficients deduced from phase-shift data without the effective-range function"*, Phys. Rev. C **98**, 015803(2018)

[50] L. D. Blokhintsev , L. I. Nikitina, Yu. V. Orlov, D. A. Savin, "*Characteristics of* $d+\alpha$ *Bound and Resonant States from Analytic Continuation of the Effective-Range Expansion*", Few-Body Syst. **55**, pp. 1009-2012 (2013)

[51] Claus E. Rolfs and William S. Rodney, *Cauldrons in the Cosmos*, (The University of Chicago Press, Chicago and London, 1988).

[52] C. A. Gagliardi, A. Azhari, V. Burjan, F. Carstoiu, V. Kroha, A. M. Mukhamedzhanov, A. Sattarov, X. Tang, L. Trach, and R. E. Tribble, *"Asymptotic normalization coefficients in nuclear astrophysics and structure"*, Eur. Phys. J. A **15**, pp. 69-73(2002)

[53] R. Plaga, H. Becker, A. Redder, C. Rolfs, and H. Trautvetter, *"The Scattering of Alpha particles from* ^{12}C *and the* $^{12}C(\alpha,\gamma)^{16}O$ *stellar reaction rate"*, Nucl. Phys. A **465**, pp. 291-316 (1987)

[54] P. Tischhauser *et al.*, *"Elastic* $\alpha - ^{12}C$ *Scattering and the* $^{12}C(\alpha,\gamma)^{16}O$ *E2 S Factor"*, Phys. Rev. Lett. **88**, 072501 (2002)

[55] P. Tischhauser *et al.*, *"Measurement of elastic* $^{12}C + \alpha$ *scattering: Details of the experiment, analysis, and discussion of phase shifts"*, Phys. Rev. C **79**, 055803 (2009)

[56] A. M. Mukhamedzhanov, B. F. Irgaziev, V. Z. Goldberg, Yu. V. Orlov, and I. Qazi, *"Bound, virtual, and resonance S-matrix poles from the Schrödinger equation"*, Phys. Rev. C **81**, 054314 (2010)

[57] P. Descouvemont and D. Baye, "*The R-matrix theory*", Rep. Prog. Phys. **73**, 036301 (2010)

[58] D.R. Tilley, C.M. Cheves, J.L. Goldwin, G.M. Hale, H.M. Hofmann, J.H. Kelley, C.G. Sheu, H.R. Weller, "*Energy levels of light nuclei* $A = 5,6,7$", Nucl. Phys. A **708**, pp. 3-163 (2002)

[59] F.E. Cecil, J.S. Yan, C.S. Galovich, "*The reaction* $d(\alpha,\gamma)^6$Li *at low energies and the primordial nucleosynthesis of* ^{6}Li", Phys. Rev. C **53**(4), pp. 1967-1970, 1996

[60] S. Satsuka and W. Horiuchi, "*Emergence of nuclear clustering in electric-dipole excitations of* ^{6}Li", Phys. Rev. **C 100**, 024334 (2019)

[61] B. Jenny, W. Grüebler, V. König, P. A. Schmelzbach, C. Schweizer, "*Phase-Shift Analysis of* $d\alpha$ *Elastic Scattering Between 3 and 43 Mev*", Nuc. Phys. A **397**, pp. 61-101 (1983)

[62] V. M. Krasnopol'sky, V. I. Kukulin, E. V. Kuznetsova, "*Energy-dependent phase-shift analysis of* $^2\mathrm{H} + ^4\mathrm{He}$ *scattering in the energy range* $0.87 < E_d < 5.24$ *MeV*", Phys. Rev. C **43**(2), pp. 822-834 (1991)